**TECHNISCHE
UNIVERSITÄT
WIEN**

**VIENNA
UNIVERSITY OF
TECHNOLOGY**

DISSERTATION

Development of an Online Flow-Through System to Determine the Arterial Input Function for Compartment Modeling

Ausgeführt zum Zwecke der Erlangung des akademischen
Grades eines Doktors der technischen Wissenschaften

eingereicht an der Fakultät für Physik
der Technischen Universität Wien

unter der Anleitung von

Ao.Univ.Prof. Dipl.-Ing. Dr.techn. Helmuth Böck,
Atominstitut, Technische Universität Wien

und

Priv.Doz. Dipl.-Ing. Dr.techn. Claudia Kuntner,
Medizinische Universität Wien

durch

Dipl.-Ing. Friedrich Röhrbacher
Matrikelnummer: 9626764
Lindauergasse 28/9, 1160 Wien

28. März 2012

_____
Unterschrift

Contents

Kurzfassung

Untersuchungen mit PET Scannern liefern Informationen über das räumliche und zeitliche Verhalten von Positronen emittierenden Nukliden. Dadurch kann unter anderem das Verhalten von neu entwickelten Medikamenten, die mit einem solchen Nuklid markiert sind, in präklinischen Studien analysiert werden. Um detaillierte Aussagen über die Verteilung der Substanzen zu erhalten, wird eine pharmakokinetische Kompartmentanalyse durchgeführt. Dabei handelt es sich um ein Rechenmodell, bei dem die Verteilung der markierten Substanz im Körper in einem oder mehreren Kompartments dargestellt wird. Dazu benötigt man die Konzentration der Substanz im arteriellen Blut über die Zeit. Infolge der radioaktiven Markierung entspricht diese Menge jedoch auch der Aktivität. Somit kann mittels Bestimmung der Aktivität im Blut und der Analyse des PET Bildes eine genaue Aussage über die Pharmakokinetik getroffen werden.

Diese Dissertation beschreibt die Entwicklung, den Aufbau und die Eigenschaften eines Online-Durchfluss-Systems, welches die Aktivitäts-konzentration als Funktion der Zeit in arteriellem Blut von Versuchstieren bei präklinischen Studien aufzeichnet. Dem Tier werden zwei Katheder gesetzt, welche mit einem Schlauch über einen arterio-venösen shunt verbunden sind. Dieser Schlauch wird in einer definierten Geometrie durch das Messvolumen des Gerätes geführt. Das Messsystem arbeitet im Koinzidenz-modus und besteht aus zwei baugleichen und gegenüberliegend angeordneten Detektoren, zwischen denen sich das Messvolumen befindet. Dabei werden die Annihilations-Photonen gemessen, die unmittelbar nach der Emission des Positrons entstehen. Die Anzahl der so gemessenen Ereignisse, der Kalibrierfaktor und das Blutvolumen im Messsystem liefern die genaue Zeit-Aktivitäts-Kurve. Eine eigens für diese Anwendung entwickelte Software sorgt für eine optimierte Verarbeitung der Messdaten, stellt diese zeitgleich mit der Messung grafisch dar und speichert die Daten in geeigneter Art und Weise.

Für diese Studie wurden die ^{18}F Tracer [^{18}F]Fluordesoxyglucose (FDG) und [^{18}F]Ciprofloxacin sowie die ^{11}C Tracer [^{11}C]Verapamil, [^{11}C]Tariquidar, [^{11}C]Mephobarbital und [^{11}C]MC113 verwendet. Die injizierten Aktivitäten reichten von 5,5 bis 100 MBq. Das Online-Durchfluss-System wurde mittels manueller Probennahme und anschließender Messung in einem Gam-

macounter (Referenzsystem) evaluiert. Die Ergebnisse zeigten eine sehr gute Übereinstimmung für alle Tracer sowie für verschiedene Messzeiten von 40 bis 100 Minuten. Die durchschnittlichen Abweichungen der Ergebnisse des Online-Durchfluss-Systems gegenüber dem Referenzsystem betragen $0,9\pm7,1\%$ für den Maximalwert in der Zeitaktivitäts-Kurve und $-7,9\pm8,0\%$ für das Integral über die Messdauer.

Abstract

Investigations with PET scanners offer spatial and time related information about the behaviour of a positron emitting nuclide. One application of this technology is the investigation of the behaviour of new pharmaceuticals labeled with such a nuclide in pre-clinical studies. Detailed understanding and description of this behaviour can be acquired by pharmacokinetic compartment modeling. This mathematical model requires the determination of the time activity curve (TAC) and area under the curve (AUC) of the arterial blood as input functions. Consequently, the analysis of PET data together with the time activity curve of the arterial blood provides detailed information on the kinetic behaviour of the new pharmaceutical.

This thesis describes the development, configuration and characteristics of an online flow-through system to determine the TAC from arterial blood (also called input function) of rodents in pre-clinical studies. The measurement of the input function is carried out by an arterio-venous shunt which consists of a tubing system. This tubing system is placed partly in the measurement volume of the detector system. The detector system works in coincidence mode and consists of two identical scintillation detectors that are mounted oppositely with the measurement volume between them. Because a positron annihilates immediately after emission it can be detected by measuring both 511 keV annihilation photons. To make sure no error counts are recorded the detectors are shielded and the signals are filtered for their energy and timing coincidence. The number of true coincident events together with the measurement volume and calibration factor provides the activity concentration. A software especially developed for this application controls the measurement and provides the correct input function.

For this study the ^{18}F tracers [^{18}F]fluordesoxyglucose (FDG) and [^{18}F]ciprofloxacin as well as the ^{11}C tracers [^{11}C]verapamil, [^{11}C]tariquidar, [^{11}C]mephobarbital and [^{11}C]MC113 were used. The administered activities ranged from 5.5 to 100 MBq. To evaluate this online flow-through system the results were compared to those recorded by manual sampling. The online flow through system showed excellent correlation for all tracers, the activity range and different measurement periods varying between 40 and 100 min. The mean differences between flow-through system and manual sampling (reference system) are $0.9\pm7.1\%$ for the peak values of the TAC and $-7.9\pm8.0\%$ for the AUC values.

List of Abbreviations

AIF	Arterial Input Function
BGO	Bismuth Germanium Oxide
CFD	Constant Fraction Discriminator
CFX	Ciprofloxacin
COBALT	Coincidence Online Blood Activity Level Tool
DLL	Dynamic Link Library
FDG	Fluordesoxyglucose
GUI	Graphical User Interface
HLC	Half-Life Correction
LaB	Lanthanum Bromine
LaCl	Lanthanum Chlorine
LLD	Low Level Discriminator
LSO	Lutetium Silicon Oxide
LYSO	Lutetium Yttrium Silicon Oxide
MBB	Mephobarbital
NaI	Sodium Iodine
NIM	National Instruments Module
PET	Positron Emission Tomography
PMT	Photo Multiplier Tube
TAC	Time Activity Curve
TQD	Tariquidar
ULD	Upper Level Discriminator
VIT	Variable Integration Time
VPM	Verapamil

Acknowledgements

I would like to thank all those who gave me the opportunity to complete this thesis. In particular I would like to thank ...

... Seibersdorf-Laboratories for financial support and providing equipment as well as laboratories which have been the base for this project,

... Thales Schröttner and Claudia Kuntner for local mentoring during the project,

... Helmuth Böck and Karin Poljanc for their mentoring at the Vienna University of Technology,

... Otmar Putz for his explanations and advices in matters of electronics and electric supply,

... Anton Vyvadil for his contribution to all kind of manual labour,

... Markus Kraus for his workshop drawings and his help in manual labour.

... Elisabeth Magerl for her corrections on the 'final' version of this thesis

... and - most of all - Bettina for her her support to simply everything in all these years.

Chapter 1

Introduction

The development of new pharmaceuticals always requires comprehensive tests and detailed analysis of their behaviour in the patient's body. Under the assumption that the pharmaceutical is labeled with a positron emitting nuclide, positron emission tomography (PET) is a reliable way to acquire accurate knowledge of the spatial distribution of the pharmaceutical as a function of time. However, for accurate quantitative analysis PET data do not provide sufficient information. Quantitative analysis can be performed by pharmacokinetic compartment modeling - a mathematical model which describes the distribution of the pharmaceutical in the body (section 1.2). This model requires the determination of the concentration of the pharmaceutical in the arterial blood as a function of time. The function is called the arterial input function (AIF). Due to the radioactive label this can be done by measuring the arterial activity concentration as a function of time. The goal of this study is therefore to develop a measurement system which records the arterial time activity curve (TAC) during a PET scan.

1.1 The EURIPIDES Project

This study is part of the EURIPIDES[1] project which aims at developing in-vivo imaging biomarkers of multidrug transporter functions as a generic tool for the prediction, diagnosis, monitoring and prognosis of major diseases of the central nerve system (CNS), such as for example epilepsy, schizophrenia and depression. One of the problems for patients suffering from such a disease is their resistance against drugs making them immune to medical treatment. The reason for this immunity is located at the blood brain barrier (BBB). The drugs cannot or not sufficiently pass this barrier and, consequently, do not reach a therapeutic efficient concentration. The major goal of the EURIPIDES project is therefore to develop treatment strategies optimised

---

[1]**EU**ropean **R**esearch initiative to develop **I**maging **P**robes for early **In**-vivo **D**iagnosis and **E**valuation of response to therapeutic **S**ubstances, http://www.euripidesfeurope.com/

for each patient that prevent drug resistance caused by the transporter's over activity. In-vivo imaging of those multidrug transporters with biomarkers is therefore a promising method for increasing the efficiency of treatments. The behaviour of multidrug transporters is described by their pharmacokinetic, which is analysed by compartment modeling that requires the arterial input function.

1.2   Compartment Modeling

In order to optimise the individual dose of a drug that needs to be administered to a patient the pharmacokinetics of this drug has to be known in detail. Pharmacokinetics describe the timing and spatial characteristics of medical drugs in organisms. Compartment models are mathematical models that describe these characteristics by separating the body into several parts. A compartment is such a part in which the drug is distributed homogeneously and shows consistent kinetics. By compartment modeling the concentration of a drug in each compartment and the exchange rate between them can be investigated. In the most simple way the body can be described as one compartment to which a dose D of a drug is administered. This dose causes a homogeneous drug concentration C in the body. The change of this concentration depends on itself and the exchange constant k_e:

$$\frac{dC(t)}{dt} = -k_e C(t). \tag{1.1}$$

Consequently, the drug concentration decreases exponentially as a function of time with an initial value C_0:

$$C(t) = C_0 e^{-k_e t}. \tag{1.2}$$

The concentration is simply the fraction of the administered quantity and the compartment volume V. Because the dose cannot be administered at once it takes a time T until the complete quantity is transfered at an infusion rate R into the compartment (body). Hence, the drug concentration rises as long as the infusion lasts and decreases as soon as the infusion is over due to the exchange constant k_e. This leads to

$$C(t) = \frac{R}{V k_e}(1 - e^{-k_e t}) \qquad \text{for} \qquad t < T \tag{1.3}$$

and

$$C(t) = C_{max} e^{-k_e(t-T)} \qquad \text{for} \qquad t > T. \tag{1.4}$$

As a next step the body is assumed to consist of two compartments - arteries and one tissue (e.g. brain). If $C_B(t)$ and $C_1(t)$ are the drug concentrations in blood and tissue 1 as function of time and assuming an
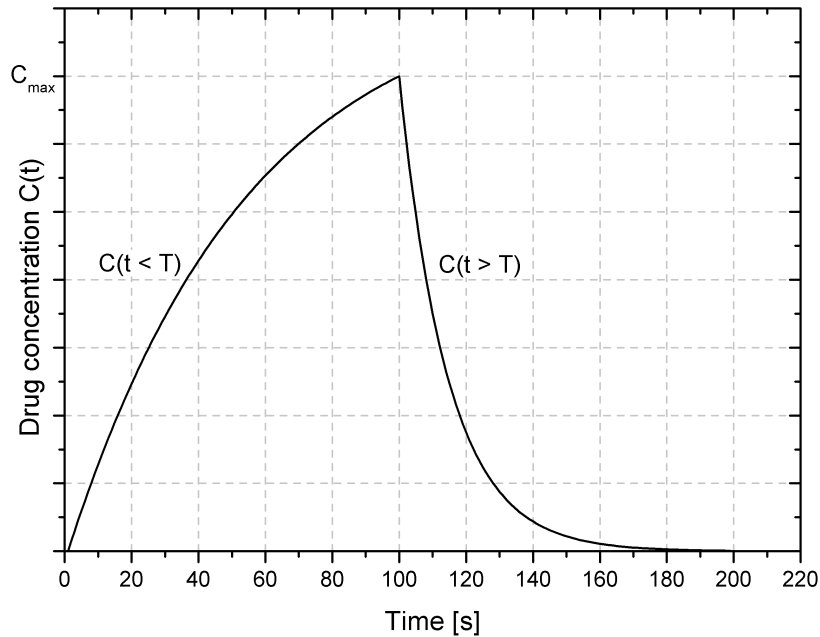
Figure 1.1: Sketch of the drug concentration in a compartment as a function of time. The concentration increases as long as the infusion lasts. Due to metabolism the concentration decreases with an exchange rate k_e [Derendorf et al., 2002]. In figures 5.8 to 5.18 measured concentrations as a function of time are displayed.

irreversible process in which the drug transmits only from the artery into the brain the exchange can be described by

$$\frac{dC_1(t)}{dt} = k_1 C_B(t). \tag{1.5}$$

Because the drugs are labeled with radioactive nuclides (e.g. ^{11}C or ^{18}F) the concentration in arterial blood $C_B(t)$ can be measured directly by determination of the activity concentration as a function of time. $C_1(t)$ is determined via the PET scans.

In reality, however, compartment modeling is of course much more complicated since there are always exchange processes in both directions and between several compartments. Comprehensive information on this topic can be found in the book *Pharmakokinetik* by Derendorf, Gramatte and Schaefer [Derendorf et al., 2002]. A more compact information is provided by the article of Hiroshi Watabe [Watabe et al., 2006].

1.3   Methods and Goals

The arterial input function was acquired so far by drawing manual blood samples during the PET scan. A micro volume tube was placed into the

animal's femoral artery via which the samples were collected in small sample tubes. During the first three minutes after injection of the radioactive tracer small samples of about 20 μl were collected continuously every 2 - 3 seconds. Further samples with larger volumes of about 40 μl were taken every five to ten minutes after injection as long as the measurement lasted. For each sample a time stamp was recorded by pushing a pedal button which triggered a special timing software. The tubes were weighted before and after the samples were collected. The difference together with the density of blood gave the volume of each sample. The activity of each sample was measured in a gamma counter. Both values together with the corresponding time stamps were finally used to calculate the activity concentration as a function of time. Besides the disadvantages of extensive manual laboratory labor and high radioactive dose for those drawing the samples, this method often led to large measurement uncertainties as will be explained in section 5.2.3. It furthermore influenced the metabolism and blood circuit of the animal due to blood losses [Walsh et al., 1980; McGuill and Rowan, 1989]. The recording of the input function using this method required to take out a blood volume of almost 10% of the animals total blood volume.

The goal of this project was therefore to develop an instrument that measures the TAC accurately and online during the PET scan and without any or only minimal blood losses. Moreover, it should be insensitive to interference caused by the activity inside the animal and perform accurate results independent of the tracer and radionuclide. It therefore has to work as flow-through system that measures the activity in the blood outside the animal and returns the blood afterwards. Timing resolution (sampling times) and measurement uncertainties of the TAC should be reduced compared to manual sampling. Moreover, it should be small, mobile as well as easy to be handled and decontaminated.

Pre-clinical studies are carried out using rodents to investigate the pharmacokinetic of new drugs. That leads to one of the major challenges we were faced with during the development of the measurement system. The amount of blood that can be taken out of the animal for measuring its activity concentration is very small compared to that of humans if the animal's metabolism should not be affected.

To measure the TAC outside the animal a shunt between femoral artery and vein is necessary. However, in contrast to manual sampling, this shunt has to consist of a special tubing system that is inserted into the blood vessels as well as mounted in a peristaltic pump and the measurement volume of the detection system. Thereby, no blood will be lost. The peristaltic pump provides a constant blood flow. The whole setup has to be designed to be placed close to the animal in order to keep the amount of external blood as low as possible. However, the small distance (below 50 cm) between animal and detector requires a very effective shielding and rejection system to keep the number of error counts as small as possible. Shortly after

injecting the radioactive tracer into the animal the activity concentration in blood rises quickly but decreases again after a short peak due to the animal's metabolism. Consequently, a few minutes after injection, most of the radioactive substance is inside the animal and only a weak concentration is left in the blood. Therefore, the total activity in the measurement volume is much smaller than that within the animal.

For detailed temporal information the sampling time of the single measurement points of the TAC is important for kinetic modeling and should be shortened compared to manual sampling. Because the blood flow in the tubes has to be chosen to fit best to the animal's blood circuit it cannot be increased infinitely. This causes the limit in timing properties for the flow-through system since the time it takes each element of the blood volume to pass the detector depends on its speed and the measurement volume. Consequently, to provide good timing information a small measurement volume is required. However, the smaller this measurement volume is the lower is the count rate. A lower count rate, on the other hand, leads to larger statistical fluctuations and, consequently, to worse detection capability. Furthermore, the system has to provide a homogeneous and constant blood flow to prevent the blood from clotting and to ensure, that the activity concentration in the blood does not change on its way from the animal to the detector.

Besides this scientific requirements and the surrounding conditions the instrument should offer easy handling, accurate control of the measurement as well as display and store all relevant data. A software especially developed for this application meets those requirements. It furthermore reduces the measurement uncertainty due to statistical fluctuation of the count rate by optimising the integration time.

To sum up, the measurement system has to meet the following requirements:

- No interference by the background activity from the animal

- Measurement should have no influence on the animal's metabolism

- Small external blood volume

- Applicable for all tracers and radionuclides used for investigation

- Small measurement volume for good timing resolution

- Large measurement volume to keep statistical uncertainties low

- Flow-through system

- Constant blood flow

- Low minimum detectable activity (MDA)

- Smoothing of the TAC when the count rate gets low after the peak

- Online system

- Easy handling and control of the measurement

- Input function including the relevant parameters stored in a file

- Instrument has to be mobile

- Instrument has to be decontaminable easily

Right from the beginning it was therefore decided to measure the number of positron disintegrations by detecting both 511 keV photons produced in the annihilation process. Consequently, two detectors (referred to as A and B) built exactly identical and arranged oppositely with the blood volume to be measured in between them are necessary (figure 1.2). The analogue output signals of both detectors are checked for their peak height and if both are produced within the coincident time window. If these conditions are met a digital pulse is produced which increases a time-controlled counter. The instrument was named COBALT, which is an acronym for **C**oincidence **O**nline **B**lood **A**ctivity **L**evel **T**ool.
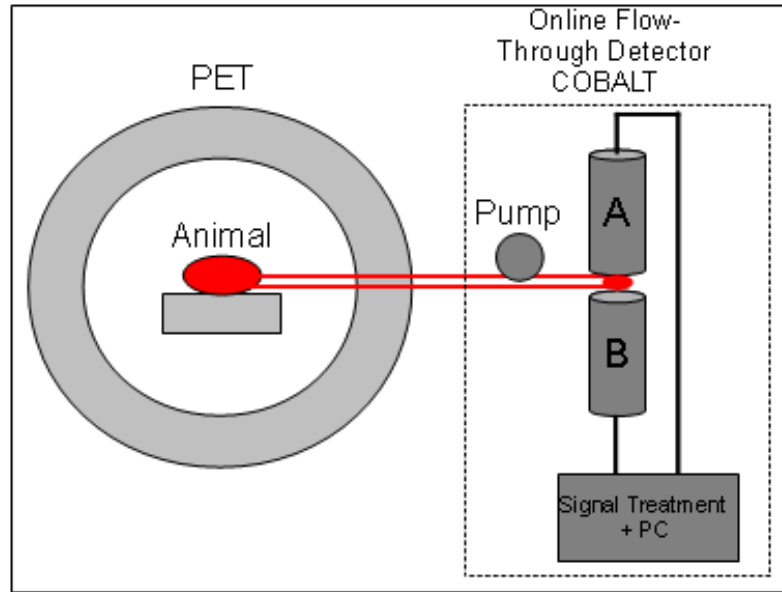
Figure 1.2: Setup for recording the input function during a PET scan by detecting coincident emitted annihilation photons.

1.4 Structure of the Thesis

This thesis describes the development of this online flow-through detection system, its characteristics and the results of its applications. In chapter 2 the design and performance of the detectors are described. The chapter furthermore includes a description of the crystal's characteristics. Chapter 3 includes information on the assembly of the complete measurement system as well as on the function of the software. It also explains the setup of the tube system. The characteristics of the complete measurement system such as interference, background, detection limit and other important features are described in chapter 4. The results of several in-vitro tests as well as the final evaluation of this system by comparing the results of in-vivo measurements with those recorded by manual sampling is provided in chapter 5. Chapter 6 provides information on alternative detector systems that were tested within the scope of this study. Finally, chapter 7 recapitulates the characteristics of this instrument and summarises the results of the in-vitro and in-vivo measurements.

In order to keep this thesis compact and clearly arranged only information concerning the application is provided. For accurate understanding of the explanations in this thesis, basic knowledge in atomic physics, radioactivity, radiation and its interaction with matter [Knoll, 2010; Webb, 1988] as well as in electronic signal processing [Leo, 1994] is required. Furthermore, some basic understanding in statistical data analysis is recommended [Sachs and

Hedderich, 2009].

1.5 Other Works related to this Topic

Kim and Ferl [Kim et al., 2006; Ferl et al., 2007] introduced a method that calculates the input function based on analysis of PET scans whereas [Eberl et al., 1997] used population curves. Both methods get along without any additional measurement instrument. On the other hand [Litton and Eriksson, 1990] introduced a method for trans cutaneous detection of positrons using ^{11}C as radionuclide. These three methods have in common that no invasive surgery is necessary. However, their main disadvantage is, that their reliability for new tracers is not guaranteed. Each time a new tracer is to be investigated these systems have to be validated by manual blood sampling. Also intra-blood-vessel probes have already been tested [Maramraju et al., 2006]. Due to the direct contact with the radioactive substance it is strongly dependent on the positron's kinetic energy and, additionally, it is very sensitive to background radiation as it cannot be shielded. The coincidence method is independent of the positron energy in contrast to other systems that detect the positrons directly [Hutchins et al., 1986; Kanno et al., 1987]. It furthermore offers low sensitivity to interference radiation since the probability of detecting two 511 keV photons within the coincidence time window is much smaller than for single photon detection. This is another advantage compared to direct positron detection. Other flow-through systems work only one way [Yamamoto et al., 2010; Breuer et al., 2010; Kudomi et al., 2003; Convert et al., 2007] causing blood losses that influences the results of the investigation [Walsh et al., 1980; McGuill and Rowan, 1989]. Similar flow-through systems using an arterio-venous shunt were developed by Ingvar and Weber but only tested for [^{18}F]FDG[Ingvar et al., 1991; Weber et al., 2002]. Ranicar and Eriksson introduced a method using BGO-detectors in human PET studies[Ranicar et al., 1991; Eriksson et al., 1988, 1995].

Chapter 2

Design and Characteristics of the LYSO Detector

The main part of the measurement system consists of two identical detectors using LYSO-crystals ($(\text{Lu-Y})_2\text{SiO}_5 : \text{Ce}$) as scintillator material. This chapter will provide substantial and accurate information about how the detectors are designed and what materials are used. Pictures and sketches including dimensions and distances will be displayed in order to give detailed insights on how the detectors are constructed.

2.1 The LYSO Crystal

2.1.1 Performance Relation of Various Crystals

The decision for LYSO as scintillator material was well considered and is based on its short decay time in combination with good stopping power, high light yield and other characteristics which will be explained. BGO ($\text{Bi}_4\text{Ge}_3\text{O}_{12}$) for example would offer better stopping power, however, due to its long decay it is not practical for timing applications. It furthermore reduces the capability of the instrument to process high count rates. NaI and LaBr ($\text{LaBr}_3\text{:Ce}$) have a better energy resolution but are hygroscopic which would have caused difficulties since both detectors were deconstructed and rebuilt again several times. Moreover, the stopping power of LaBr and LaCl ($\text{LaCl}_3\text{:Ce}$) are too small. Although LYSO shows an intrinsic radioactivity due to the isotope [176]Lu [Melcher and Schweitzer, 1992] its performance suits best for selecting 511 keV photons by energy and time. The intrinsic radioactivity can be handled as will be explained in section 2.1.2. Table 2.1 gives an overview about the performance characteristics of all scintillation crystals taken into account for this application.

The stopping power of a scintillation material is one of its major characteristics and displayed graphically in figures 2.1 and 2.3. The total attenua-

Performance	LYSO $(Lu\text{-}Y)_2SiO_5:Ce$	LSO $(Lu)_2SiO_5:Ce$	LuAP $LuAlO_3:Ce$	LaBr$_3$:Ce	LaCl$_3$:Ce	BGO $Bi_4Ge_3O_{12}$
Z_{eff}	60	66	65	47	59.5	75
density ρ [g/cm^3]	7.1	7.4	8.3	5.3	3.9	7.1
light yield [Ph/MeV]	32,000	27,000	11,000	61,000	50,000	9,000
energy resolution [%]	8	10	7.1	3	3	12
wave length [nm]	420	420	365	358	350	480
1/e decay time [ns]	41	40	17	35	20	300
Tot.attenuation coeff. wo. coh. scatt., $T\left(\frac{\mu}{\rho}\right)$ [cm^2/g] @ 511keV	0.109	0.111	0.108	0.0847	0.0889	0.127
Photo absorption co-eff., $P\left(\frac{\mu}{\rho}\right)$ [cm^2/g] @ 511keV	0.0357	0.0379	0.0347	0.0116	0.0136	0.05567
Photo fraction (peak-to-total ratio) [%] @ 511 keV	32.75	34.14	32.13	13.70	15.30	43.78

Table 2.1: Various performance indicators for different scintillation materials. LYSO-crystals offer the best performance - large photo fraction, light yield and density combined with short decay time and an ideal distribution of wave length fitting to the quantum efficiency of various PMTs [Knoll, 2010; Saint-Gobain Ceramics and Plastics Inc.].

tion represents the probability for interaction processes between photon and crystal in which the photon's energy or at least a part of it is deposited. All photons passing the crystals surface are detected, except of those, that cross the detector without any interaction or those that are scattered elastically. Consequently, the probability for getting an electric signal from the detector is the same. This probability of course changes with different photon energies and different crystal thickness. The total attenuation is a function of the corresponding coefficient (T), the density ρ the as well as the thickness x of the scintillation material and calculated by

$$Total\ attenuation = 1 - e^{-T \cdot \rho \cdot x}. \tag{2.1}$$

The corresponding values and units are given in table 2.1. The results are displayed graphically for various crystal thicknesses and scintillation materials in figure 2.1.
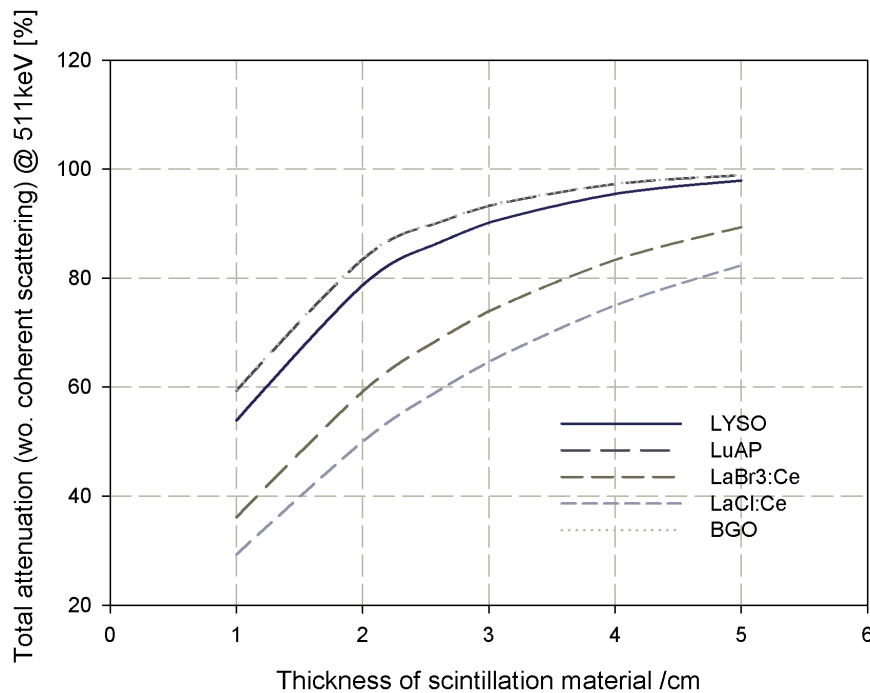
Figure 2.1: The graph displays the total attenuation without coherent scattering of various scintillation materials depending on their thickness. The total attenuation without coherent scattering represents the probability for a photon-crystal interaction in which either the total energy of the photon or a part of it is deposited within the crystal. Consequently, this corresponds to the probability to get a signal from the detector. (The diagrams are calculated using the data of table 2.1.)
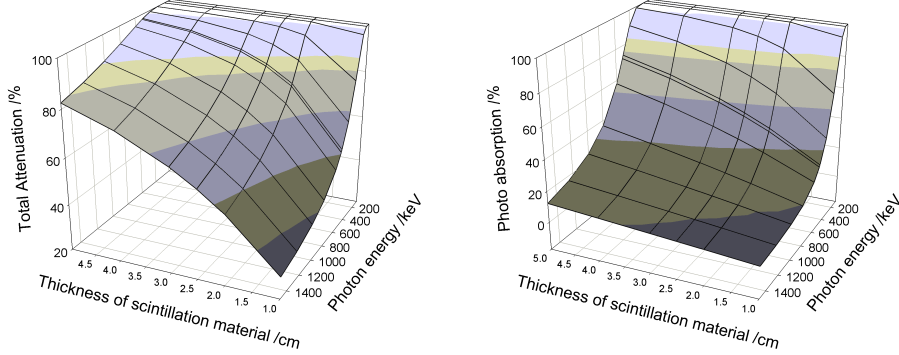
Figure 2.2: Total attenuation (without coherent scattering) and absorption for LYSO-crystals depending on their thickness and the photon's energy. For attenuation all interaction processes are taken into account that cause a change in the photon's energy while for total absorption only those processes which transfer the photon's full energy are regarded. (The diagrams are calculated using the data of table 2.1.)

Based on the fact that photons only within a small energy range (511 keV +/- ΔE) should be detected the photo absorption is even more important than the total attenuation. The photo absorption coefficient depends on the effective atomic number (Z) by Z^n, where n ranges between 4 and 5 [Knoll, 2010]. It is usually expessed as μ/ρ given in cm^2/g (table 2.1) and represents the probability for detecting the photon's full energy contributing to the full energy peak in a gamma spectrum. Only the signals from those full energy interactions of 511 keV photons will be identified as a coincident event if two of these signals are detected within a certain time window. Figure 2.3 compares the photo absorption probabilities for various scintillation materials and thicknesses. The values were calculated by

$$Photo\ absorption = 1 - e^{-P \cdot \rho \cdot x} \qquad (2.2)$$

which is similar to equation 2.1.1. In this case, instead of the total attenuation coefficient T the photo absorption coefficient P needs to be used. Clearly BGO would offer the best performance. However, due to its slow decay time it would be difficult to use in timing applications as mentioned before. Although LuAP would also offer better stopping power than LYSO, its lower light yield would lead to smaller signals making it more difficult to be analysed.

The LYSO crystal chosen for this instrument is of cylindric shape, 2.54 cm in diameter and 2.54 cm thick (Figure 2.6). The energy spectrum of the scintillation photons emitted by the crystal is within the visible range of the electromagnetic spectrum with an maximum at 420 nm. Moreover, the sensitivity of entrance window and photo cathode corresponds to these wave
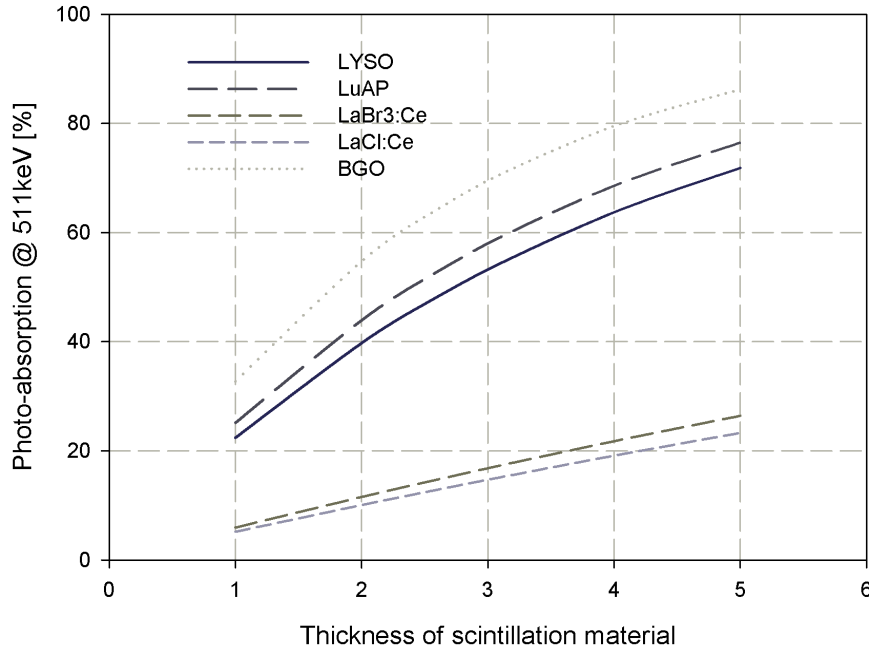
Figure 2.3: The probability for photo absorption of various scintillation materials. The graphs represent the probability for photon-crystal interaction processes in which the total photon's energy is deposited within the crystal. (The diagrams are calculated using the data of table 2.1.)

lengths. It is therefore very important to construct the detector in such a way, that no light from outside reaches the photo cathode. As will be explained in section 2.2 different arrangements have been implemented to guarantee light tightness.

2.1.2 Influence of the Intrinsic Radioactivity

The accurate expression for LYSO is $Lu_{1.8}Y_{0.2}SiO_5$:Ce. Natural occurring lutetium contains 2.6% of its radioactive isotope [176]Lu which decays to [176]Hf via β^- emission with a half-life of $3.8 \cdot 10^{10}$ years. The maximum emission energy of the electron is 593.2 keV leaving the daughter nucleus at an unstable excited state of 597 keV above ground level. This excited state degenerates to the ground state by the emission of photons at three different energies (88.3, 201.8 and 306.8 keV) [Melcher and Schweitzer, 1992]. [176]Hf is a stable isotope. Figure 2.4 displays the decay scheme. Due to their interaction probability the electron and the 88 keV photon will always be detected, however, some of the photons at higher energies might escape. This leads to an energy spectrum to which the various electron energies as well as some of
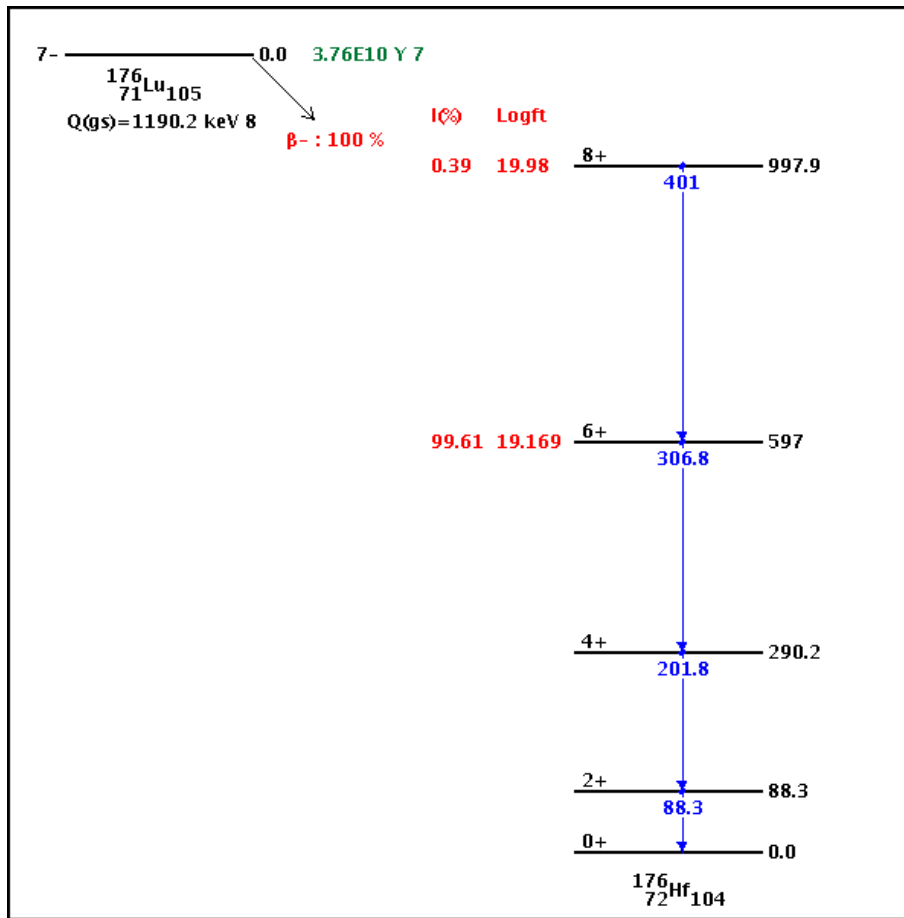
Figure 2.4: Decay scheme of ^{176}Lu with a half life of $3.8 \cdot 10^{10}$ years. The β^- particle will always be detected while some of the photons might escape [National Nuclear Data Center, 2011].

the photons energies contribute. Figure 2.5 shows the energy spectrum of a LYSO-crystal. Although none of the photon's energy as well as most energies of the electrons are in the range around 511 keV the sum of electron and one or more photon energies might be within this range. Consequently, the intrinsic radioactivity of the scintillation material leads to signals that would be interpreted by the electronic instruments as 511 keV events. The activity of a LYSO crystal is declared by the manufacturer with 39 counts per second and gram [Saint-Gobain Ceramics and Plastics Inc.]. Since the crystal used for this thesis is of cylindric shape and has one inch in diameter and length its total weight is 91.38 g and, therefore, its intrinsic radioactivity can be calculated to 3564 decays per second. As will be described in section 3.3 the thresholds for upper and lower level discrimination are set to 415 keV and 680 keV. This causes a natural background of about 1400 counts per second
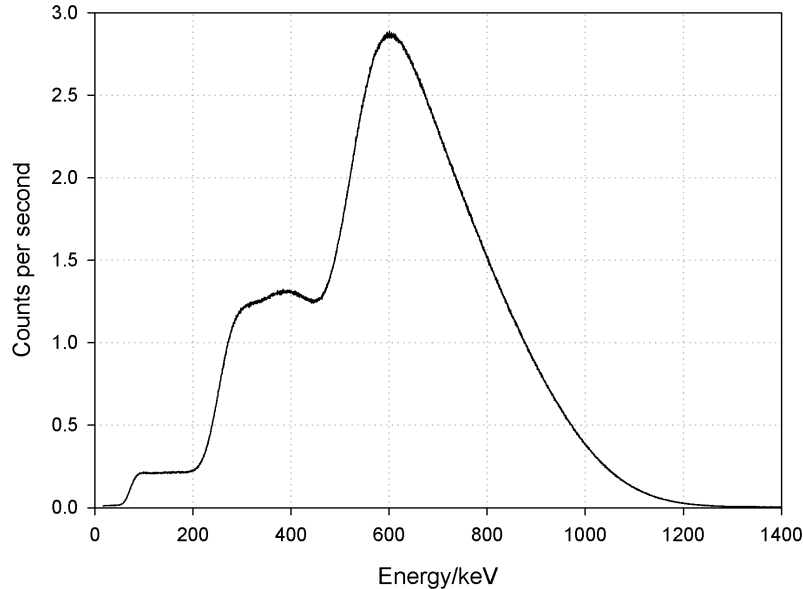
Figure 2.5: The energy spectrum of the radioactive isotope ^{176}Lu in the LYSO crystal. It consists of the gamma lines (88.3 keV, 88.3 + 201.8 keV, 88.3 + 306.8 keV and 88.3 + 201.8 + 306.8 keV) which are superimposed by the energy distribution of the β^- particles [Saint-Gobain Ceramics and Plastics Inc.].

for each detector. However, as the coincidence window is set to 12 ns, the probability for detecting two decays (each in one detector) within this time range is almost zero. Measurements have shown that the random coincidence count rate decreases to 0.1 +/- 0.3 cps if an 8 mm layer of lead was placed between both detectors.

Consequently, the coincidence count rate caused by the intrinsic activity of 1.3 +/- 1.1 cps is caused almost exclusively by detecting one single decay. The β^- particle is detected within the detector where the decay happened while the three gamma photons are registered within the other detector. As the time range in which a decay and the following gamma emissions happen are in the order of pico-seconds, the system cannot filter these random coincident counts. The number of those false coincident counts therefore depends on the distance between both detectors (section 4.2).

2.2 Detector Assembly

In order to improve the light collection the crystal is covered at its bottom and wall with a thin reflection foil and two layers of Teflon. The Teflon acts furthermore as protection for reflection foil and crystal against friction and mechanical stress caused by imperfections of the surrounding lead ring.

Crystal and Teflon are inside a ring of lead which is used on the one hand as shield against background radiation and, on the other hand, to keep all components in their correct position. Its outer side is reduced 1 mm to provide a slot for fixing the μ-metal. Its top is reduced 3 mm in the centre to provide space for the optical interface pad as well as to fix the PMT. A felt stripe is glued at the inner side of this upper reduction. It is necessary for three reasons: First, it should keep the PMT in the detector centre and, thus, exactly in the middle above the crystal. Secondly, it functions as light sealing if not all photons are absorbed by case and foam. And, finally, it is used as additional isolation since the photo cathode is at high voltage (figure 2.6). On the entrance window of the PMT an optical interface pad is attached in order to level out imperfections in the construction of the metal case since this would cause the axis of the PMT to be not in parallel with the axis of the crystal. Another improvement of the optical contact is the optical grease between interface pad and crystal avoiding total reflections. Since the crystal is slightly taller than its surrounding Teflon and lead the contact pressure (brought onto the PMT by the outer metal case) between entrance window and crystal squeezes the pad and the grease leading to an optimal optical coupling (figure 2.7).

Figure 2.6: The LYSO crystal separately and surrounded by Teflon and the lead ring (the reflection foil cannot be seen in this picture). The felt stripe is glued onto the inner part of the lead ring to centre the PMT and to absorb the last light photons that might pass the outer light isolation. It furthermore provides additional electrical isolation which is necessary since the photo cathode is on high voltage.

The μ-metal is plugged into the outer reduction of the lead ring. Between μ-metal and lead ring a stripe of insulating tape provides again for electrical and optical isolation. On top of the μ-metal a foam stripe is mounted to prevent most of the light photons passing the outer metal case from reaching the photo cathode. Several stripes of insulating tape and black strong fixing tape make sure that the four components, lead ring (including the crystal), μ-metal, PMT (including its base) and foam, are fixed together. As case of the whole detector a varnished steel pipe is used counting for mechanical stability and shielding magnetic fields. It furthermore serves as additional

absorber for 511 keV photons making the detector less sensitive for interference counts due to external sources (like the animal would be for example). Taking into account, as a first crude approximation, only 511 keV photons and assuming that the external source would be at the level of the centre of the detector system, the lead and steel would absorb approximately 94% and 64% respectively. Hence, in this case both materials together block nearly 98% of all 511 keV photons.
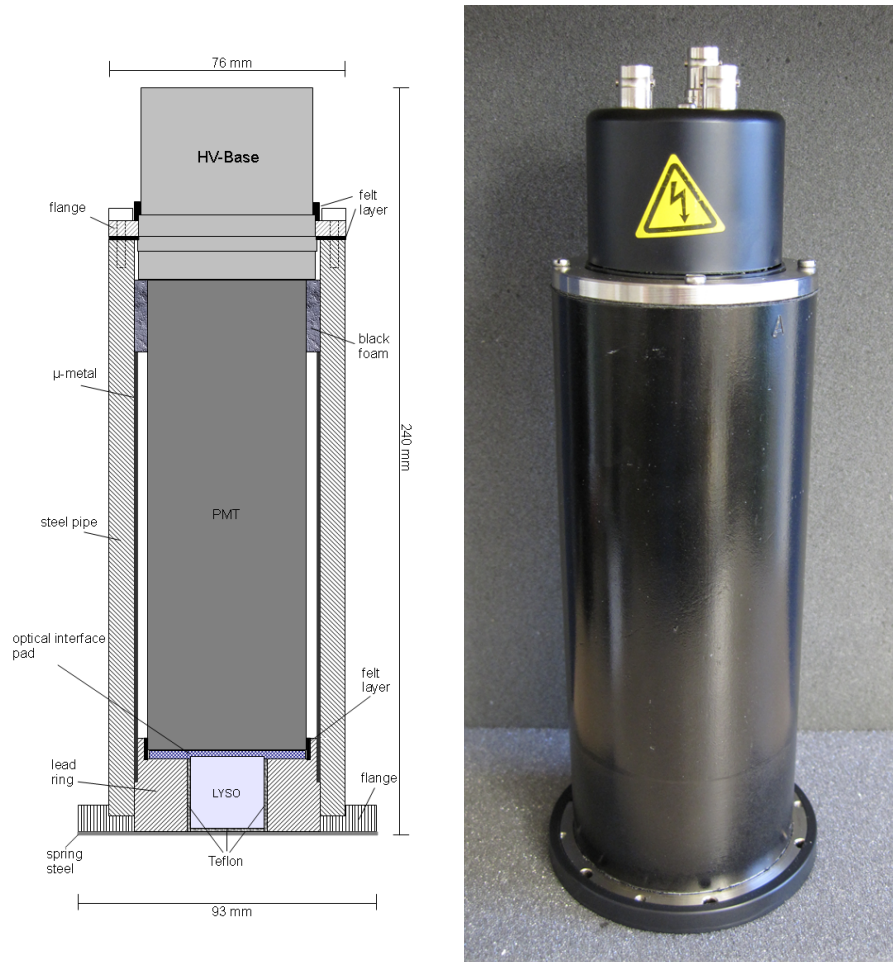
Figure 2.7: Cross section of the detector with all major details (left) and a photograph of one detector (right).

At the upper end of the steel pipe another flange is attached. It centres the base of the PMT and therefore the complete inner part of the detector. Between flange and pipe as well as between flange and base two more felt stripes function as light sealing. The detector is closed at its bottom by 0.2 mm spring steel which is glued onto the lower flange using a black two-component epoxy resin glue. This glue makes sure that the spring steel is

fixed onto the flange strongly and, since it is black, no light from outside can reach the crystal. Several layers of black glue strips around the flange and the spring steel improve the detectors light tightness. Figure 2.7 shows a picture and the corresponding cross section of one detector while figure 2.8 shows all components both detectors are made of.

Figure 2.8: The picture shows all components included in both detectors. μ-metal, lead ring with two layers of Teflon and the crystal in its centre, steel pipe with two flanges on top and bottom and the isolated PMT with the base mounted on its top (from outside to inside).

2.3   Characteristics and Performance

2.3.1   Shape and Characteristics of the Output Signal

Both detectors show linear dependency for different gamma energies in the range from 100 to 1000 keV and a strong potential dependency for different voltages in the range from 800 to 1500 V applied to the PMT. For the measurements with different gamma energies the isotopes ^{241}Am, ^{68}Ge and ^{22}Na were used. Although both detectors are built exactly the same way the output pulse of detector B is larger than that of detector A even if the same gamma energy is measured and the PMT is supplied by the same voltage[1].

---

[1] The difference of the output pulses are caused by different gains of the PMTs. For the detectors the two out of three available PMTs were selected which offer less differences of

In order to get two similar pulses the voltage of detector A is set to 1165 V while that of detector B is set to 985 V. Both pulses then show the following characteristics:

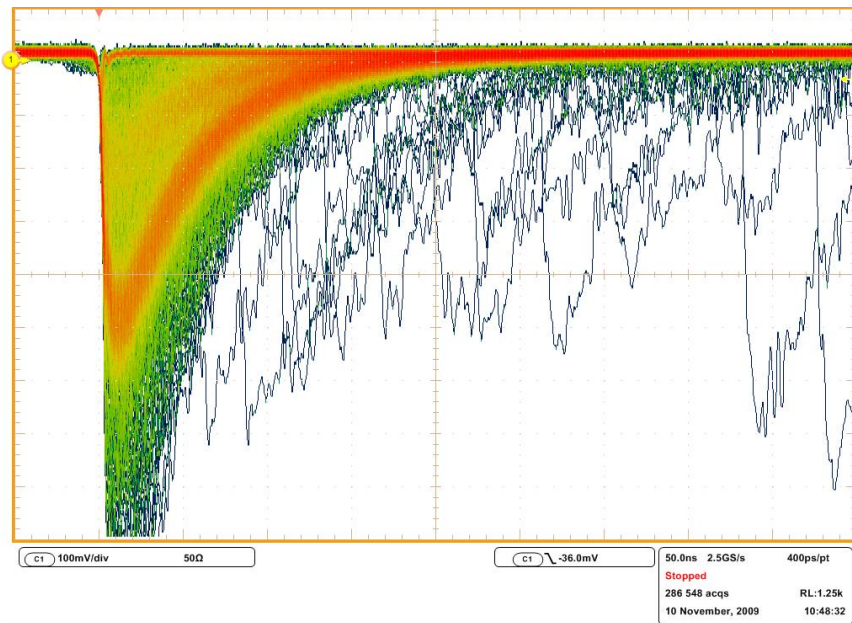|	
Rise time (10/90):	6 ns
Peak voltage for 511 keV (into 50Ω):	-50 mV
1/e decay time:	60 ns

Figure 2.9: The (10 x) amplified pulses from the anode plug as it is displayed on an oscilloscope. The peak belonging to 511 keV full energy events can be seen clearly as it is the most likely event (red-yellow line). The weaker line with a peak voltage of approximately -200 mV represents the Compton edge together with the backscatter peak of the lead shielding.

Figure 2.11 shows the linear dependency of the peak height of the output pulse on the detected gamma energy while figure 2.10 shows the strong potential dependency on the voltage applied to the PMT. Both measurements were interpolated by fit functions which are used later on for further calculation such as light collection and anode current. The output pulse needs to be amplified by a preamplifier because -50 mV as peak voltage of the analogue input pulse would only be slightly above the lower input limit of the CFD. Because the gain of both PMTs turned out to be unstable above 1200 V an increase of the voltage supply leads to a drift of the count rates (section 4.8). Furthermore, a larger (not amplified) output pulse reduces

---

their gain.
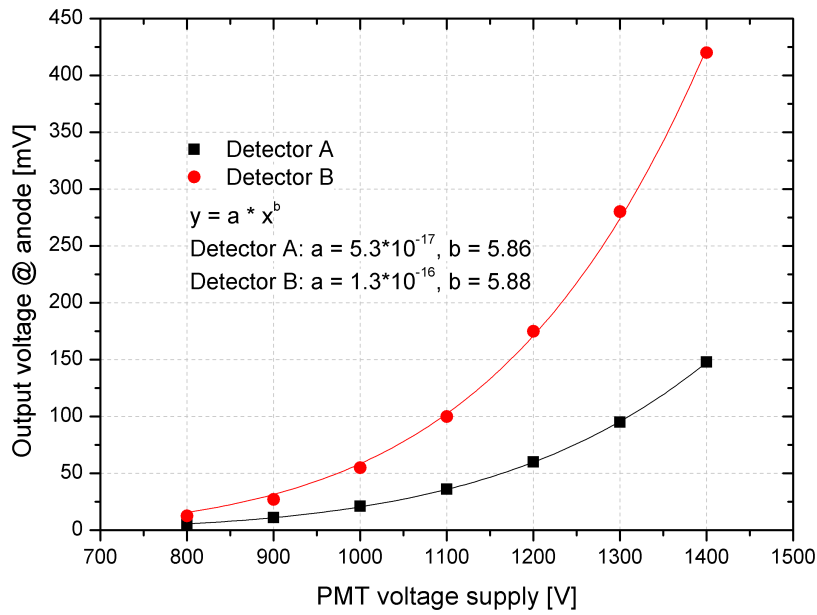
Figure 2.10: Peak height of the output pulse of a 511 keV full energy event depending on the voltage supplied to the PMT. Although both detectors are identical the output voltage of detector A is approximately one third of that of detector B if the PMT voltage is the same.
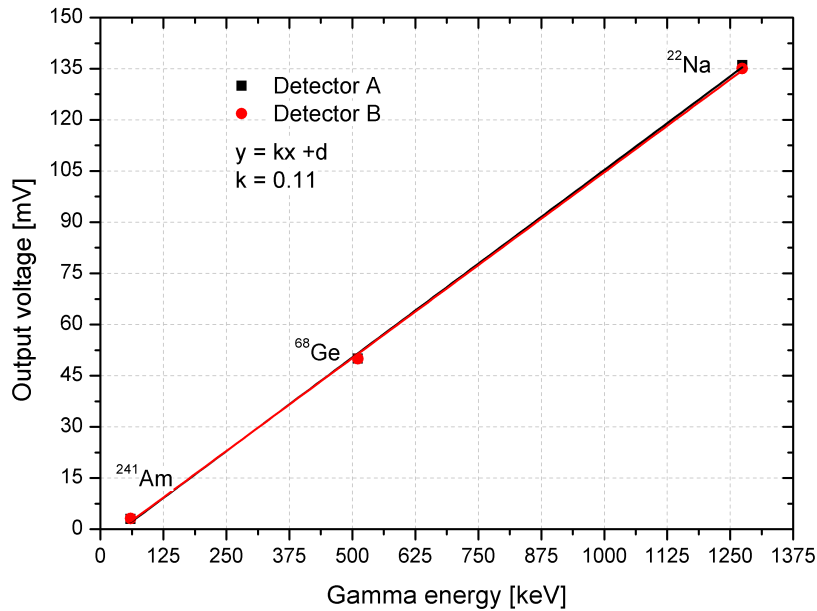
Figure 2.11: Peak height of the output signal for different gamma energies 60 keV (^{241}Am), 511 keV (^{68}Ge) and 1274 keV (^{22}Na). The voltages applied to the PMTs are 1165 V for detector A and 985 V for detector B.

the maximum count rate in order not to exceed the maximum average anode current (section 2.3.3). Figure 2.9 shows a screen shot of the amplified output pulses recorded with an oscilloscope.

2.3.2 Estimation of the Effective Light collection

The light yield for LYSO crystals is idealy 32 photons per keV of the absorbed gamma radiation. However, since reflection and optical coupling are never perfect the effective number of photons striking the photocathode is smaller. Consequently the number of detected scintillation photons at the photocathode and, furthermore, the number of charge carriers at the anode of the PMT counts as an indicator for reflection and optical coupling between crystal and PMT. The electric charge per output pulse is given by

$$Q_{pulse} = \frac{U \cdot t}{2R},\qquad(2.3)$$

if the pulse is assumed to be a triangle and U in mV and t in ns are peak voltage and duration. R is the input resistivity of 50 Ω. The charge is then calculated in pC. Taking 50 mV for the peak voltage and 150 ns for the pulse duration (figure 2.9) the measured output charge is 75 pC per pulse. If F_{HV} is the gain of the PMT for the applied voltage, η_{420nm} the quantum efficiency of the photo cathode for scintillation photons (420 nm) and q the elementary charge, the number of photons striking the cathode N_{PC} is calculated by

$$N_{PC} = \frac{Q_{pulse}}{F_{HV} \cdot \eta_{420nm} \cdot q}.\qquad(2.4)$$

Because the gain of the PMT for the applied voltage is $2 \cdot 10^5$, the quantum efficiency of the photo cathode is 25% and the elementary charge is $1.6 \cdot 10^{-19}$ C the number of photons per pulse striking the cathode caclulates to approximately 7,500. The crystal produces $32 \cdot 511 = 16,500$ photons per absorbed annihilation photon. Consequently, this estimation leads to a light collection of 46%.

2.3.3 Maximum Count Rate

The dynodes of the PMT are sensitive to thermal stress. If the temperature of a dynode got too high its coating might evaporate leading to a change in the characteristics of the PMT. In order to avoid this effect the average anode current should not exceed 0.2 mA. The current depends on the voltage applied by the HV supply, the photon energy absorbed by the scintillator and the effective activity of the source the detector is exposed to. While the first two factors influence the height of each pulse the latter one causes the number of pulses. Besides a minority number of high energy events (e.g. muons) most of the absorbed energies are related to 511 keV annihilation

photons. The peak height is therefore mainly determined by the voltage supply of the PMT. Because the PMTs are unstable above 1200 V (section 4.8) a lower voltage is used for each detector leading to a smaller output pulse. This increases the count rate at which the maximum average anode current is reached. The calculation for estimating this maximum count rate is carried out regarding the output pulse as a triangle and by the following equation:

$$\text{count rate} = \frac{2R}{U \cdot t} \cdot I_{max-count}, \tag{2.5}$$

where $I_{max-count}$ is the maximum tolerable average anode current given in mA, U the peak voltage in mV and t time in ns of the signal due to a 511 keV full energy event. $(U \cdot t)/2$ is the estimated charge flowing over the anode due to such a full energy event. For the PMT voltages used in the final settings the corresponding values are 50 mV and 150 ns for a 511 keV full energy event causing a maximum count rate of approximately 2.5 million cps (figure 2.12). As will be described later on, this corresponds to an activity concentration of 300 kBq/μl. Since this level would never be reached in measurements this instrument is made for, there is no risk for the dynodes to be damaged.
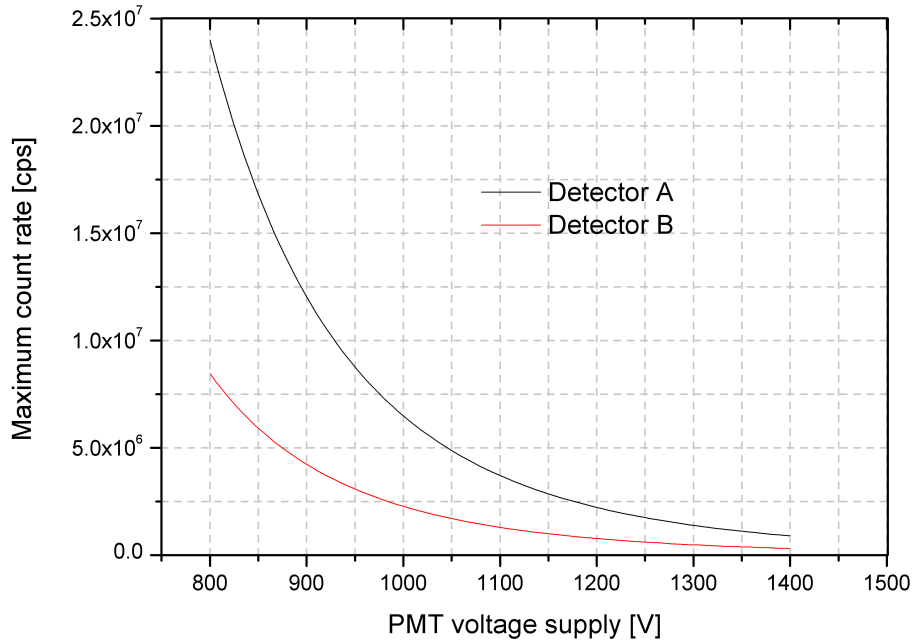

Figure 2.12: Maximum counts per second for 511 keV photons (full energy events only) in order not to exceed an average anode current of 0.2 mA depending on the voltage applied to the PMT.

2.3.4 Single Efficiency for Point-Like Sources

In order to investigate the spatial sensitivity of both detectors depending on the position of the radioactive source, a point-like source was moved perpendicular to the detector's central axis. This measurement was carried out when both detectors were already assembled in the final measurement geometry. The source was placed between the detectors 4.5 mm away from both front surfaces and moved from the center of the detector system towards its margin. The count rates corresponding to each position of the source were recorded separately for both detectors. As figure 2.13 shows the efficiency at the center of the detector system is 16.2% for detector A and 16.4% for detector B while it decreases to 10.6% and 10.8% as the source was exactly between the margins of the LYSO crystals at 12.7 mm. The coincident efficiency for point like sources and for various measurement geometries are explained in detail in section 3.1.
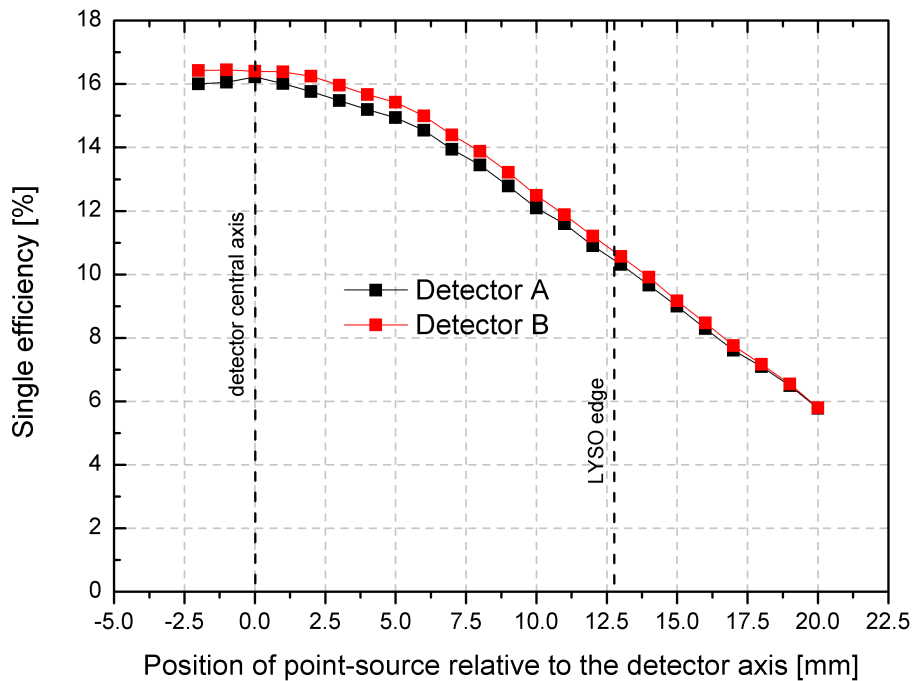

Figure 2.13: Single efficiency for both detectors and point-like sources depending on the source position relative to the detector's central axis.

Chapter 3

Function and Design of the Measurement System

This system was planned originally to be split into a fixed crate containing electronics and PC for signal treatment and counting as well as a movable part consisting of two detectors which are mounted onto a vertical stator with wheels. These two parts should be connected via a few meters of BNC-cables (RG-58). However, because the regulations of the laboratory, where the micro-PET team works, changed, it became necessary to meet all requirements for clean rooms. For example all parts of the system had to be covered by plane, resistant and easy to be cleaned surfaces. It furthermore turned out that the room the micro-PET was placed offers not enough space for any fixed part of the system. Hence, the decision was made to mount all parts into and onto one trolley in which all electronic instruments for signal treatment and the PC for measurement control are included. Together with the peristaltic pump and an additional lead shield the detector system is mounted to a vertical steel pipe that is screwed onto the top plate of the trolley. Figure 3.1 gives a detailed overview how the system is assembled. The trolley's side panels are made of stainless steel while bottom und top plate are made of Decoral (aluminium). A front door allows easy access to the PC and the electric installation. NIM-bin and fan are covered with acryl glass. The trolley can therefore be cleaned easily. All fans at the side panels include filters that can be cleaned or exchanged. Since the system should always be aligned such that the lead shield is between detector system and the animal the steel pipe can be turned in steps of 90 degrees if the measurement during a PET scan requires a new setup. A red emergency push-button next to the green on-off rotary switch interrupts the electric circuit immediately when pressed. Except of the pre-amplifiers all electronic instruments involved in signal treatment are based on the NIM-standard and mounted in a 19 inch NIM-bin. A detailed explanation of all instruments and their functionalities are given in section 3.3.
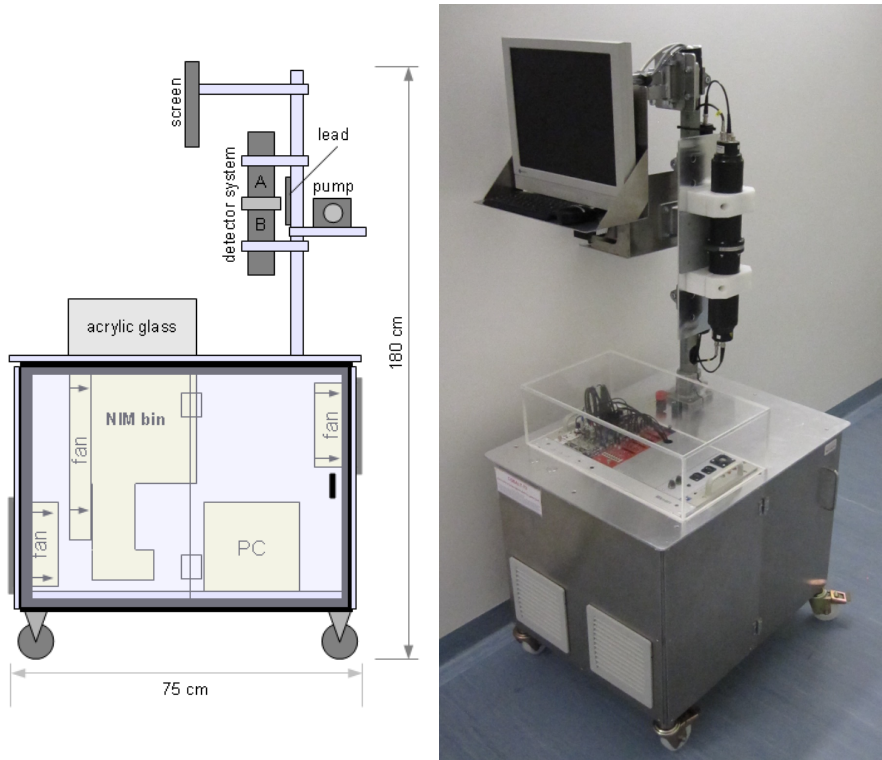
Figure 3.1: Schematic sketch and picture of the measurement system COBALT.

To keep the blood flow at a constant level for the duration of a measurement a peristaltic pump is used. It requires a special pump tube which is connected at both ends to Teflon tubes using hollow needles as connectors. One Teflon tube is connected to the arterial catheter and the other one to the venous catheter. In other words the activity concentration in the animal's blood is measured at a femoral bypass. Settings, performance and characteristics of pump, tubes and how they are fixed in the detector center are described in detail in sections 3.1 and 3.2.

3.1 Measurement Geometry

Coincident photons are emitted at an angle of 180° with a small divergence of $\pm 0.6°$ due to remaining momentum of the positronium (e^+e^- pair). Therefore, it is necessary to place two detectors in opposite position. Consequently, the radioactive substance to be measured has to be exactly in the middle between the two detectors. For an accurate calibration and for correct comparisons of different measurements the geometry has to be stable and reproducible.

In order to meet all those requirements a ring shaped steel panel is fixed

with screws between both detectors. The inner diameter of this ring is a little larger than the scintillation crystal while its outer diameter matches exactly that of both detectors. The opening in its center allows to insert a tube fixture (section 3.1.1) which places two coils of the tube containing the active blood right in the center between the scintillation crystals of both detectors. This setup offers an efficiency of 6.5% for 511 keV coincident photons (section 3.1.2). Since tube fixture as well as the tube itself cannot be placed in different ways, this geometry enables a reliable and reproducible geometry for each measurement.
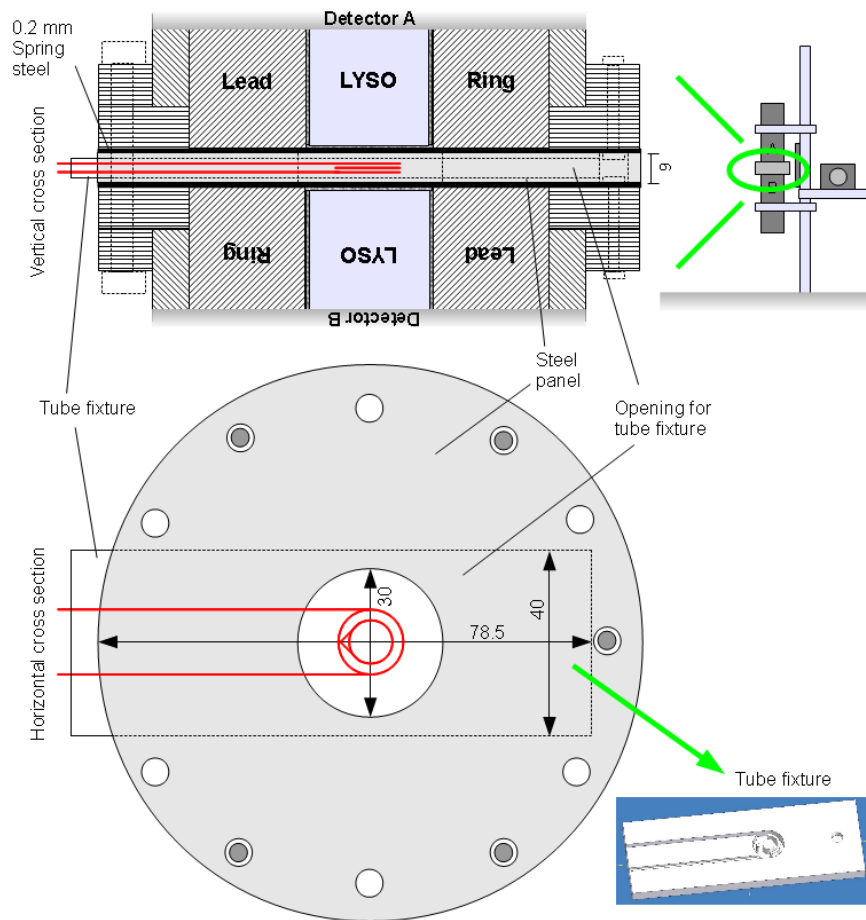
Figure 3.2: Sketch of the center of the detector system. Between the two detectors a ring shaped steel panel is mounted. Its position is fixed by screws that also fix the detectors together. The inner diameter of the steel ring is a little larger than the diameter of the scintillation crystal. The tube fixtures are designed to fit exactly into the rectangular opening of the steel panel. The red lines represent the tubes filled with blood.

3.1.1   Tube and Tube Fixtures

During the development of this system various measurement geometries and different ways of how to place the tube in the center of the detector system had been designed and tested. In order to reduce the background count rate due to the intrinsic activity of the LYSO crystals the first tube fixtures were made of lead. As the relative statistical uncertainty is inverse proportional to the counts recorded for each measurement point, the measurement geometry was designed to exhibit the blood volume within the detector as large as possible. The tubes leading to and from the detector were therefore connected to a Teflon tube with an inner diameter of 4 mm and an outer diameter of 5 mm. To guarantee a reliable and stable geometry a tube fixture made of lead and consisting of two halves each one with a half-pipe cutout was developed (TubeFix 2). The diameter of the cutouts fits the outer diameter of 5 mm of the Teflon tube. In both halves of the fixture two conic holes are milled in their centre such that no lead is between the active blood and the scintillation crystal (figure 3.3, top).

   Although this measurement geometry together with the lead fixture offers the best signal to noise ratio it finally turned out to have two main disadvantages. Since the diameter of the tube inside the detector is much larger than that of the tubes leading to and from the detector (4 mm compared to 0.5 mm) the blood drops into the larger tube until this is filled up and the blood is pressed into the tube leading back to the animal. Even though the animals are heparinised the blood might clot and therefore plug the flow in the tubing system. The second disadvantage is the time it takes to fill the whole measurement volume. As will be described in chapter 5 the TAC should exhibit a high and sharp peak shortly after injection of the active tracer. However, if the time to fill the measurement volume is large compared to the time the maximum of the activity concentration in the blood lasts this peak would never be sharp[1]. Consequently, a tube fixture in which the inner diameter of the tubes remains constant and the measurement volume is filled within a few seconds had to be developed.

   The next setup was therefore to use a tube fixture made of lead (TubeFix 4) in which a loop of a standard pump tube (outer diameter = 2.4 mm, inner diameter = 0.5 mm) was placed. This setup simplified the tube system as only two tube connections were necessary (arterial catheter tube - pump tube and venous catheter tube - pump tube). However, due to the small measurement volume the count rate was too low for accurate measurements. To increase the measurement volume TubeFix 5 was developed. It consists of a PVC block in which two channels and a ring are milled to fix the standard pump tube. The tube has to be pressed into the deeper channel and spirally coiled four times in two layers and finally pressed into the lower channel.

---

[1] The performance of the pump cannot be increased because this would have a negative influence on the animal's circuit.
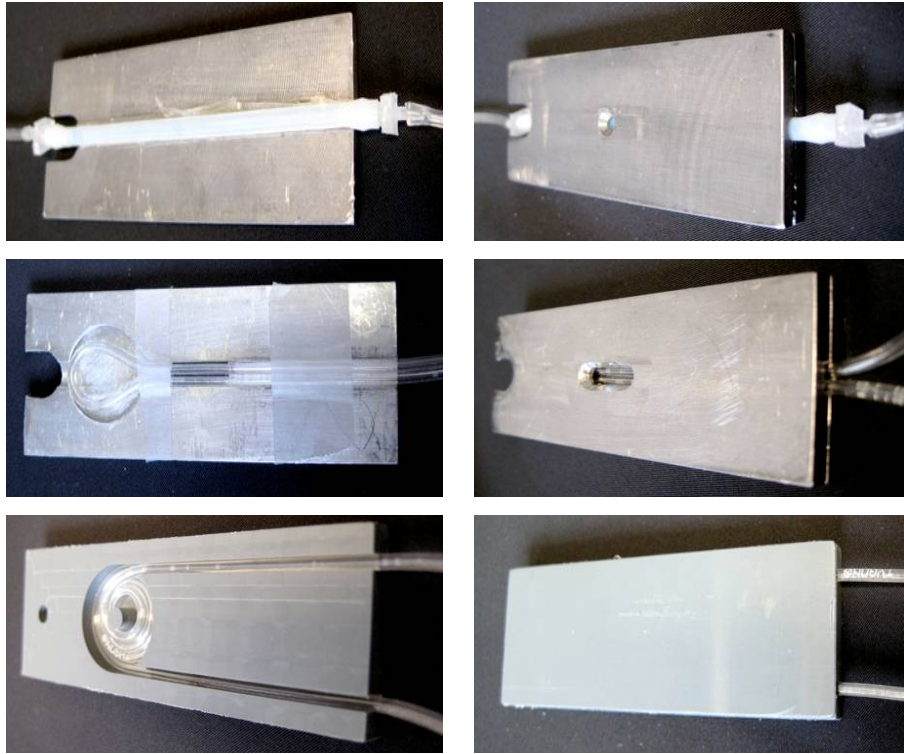
Figure 3.3: Pictures of the tube fixtures that were designed and tested during the development of the measurement system. Although some considerations and features of these methods to place the tube in the detector system lead to promising results, it finally turned out for each of them that they have major disadvantages. This figure shows TubeFix 2, 4 and 5 from top to bottom and opened (left) and closed (right). TubeFix 6 is similar to number 5, however instead of four only three coils each consisting of two layers are spooled in this geometry.

In-vitro tests using $[^{18}F]$FDG in a NaCl solution have pointed out that the time it takes to fill the measurement volume is too large and the efficiency is too small (table 3.1) for an accurate determination of the time activity curve. In order to improve efficiency and to decrease the time to fill the measurement volume TubeFix 6 was developed. Its construction is similar to TubeFix 5, however, in this case the outmost coil is skipped (three coils, two layers) leading to a smaller and more central measurement volume.

Although both geometries offer a constant inner tube diameter and a short time of a few seconds to fill the measurement volume (table 3.1) it had to be redesigned since another problem occurred. Because the used ^{11}C tracers are lipophilic most of the radioactive substance adheres to the walls of the pump tubes. It became therefore impossible to separate the signals caused by the radioactivity in the blood from the signals caused by the radioactivity at the inner tube walls. Additionally, the activity concentration at the inside of the tube wall increases constantly as long as the active solution or blood

flows through the tube. Even priming the tube with the inactive substance before each measurement did not solve the problem. Moreover, this might influence the pharmacokinetic of the active tracer in the animal during a measurement. Also the usage of pump tubes offering ultra smooth inner walls (*Tygon Silicone Pt3350*) did not solve the adhesion problems (section 5.1).

As final solution to all problems a combination of pump and Teflon tubes turned out to work best (section 3.2). Consequently, it became necessary to fix a Teflon tube instead of the pump tube in a reliable and reproducible geometry in the center of the detector system. TubeFix 3 is designed similar to TubeFix 6, however, in this case the tube is spiraled in two coils each consisting of three layers (figure 3.4). Furthermore, the wall thickness of a Teflon tube (0.5 mm) is smaller than that of a pump tube (0.9 mm). Both facts account for better efficiency on the one hand and a smaller measurement volume on the other hand. Since a Teflon tube is rather inflexible, it has to be fixed by channels milled into the PVC block.
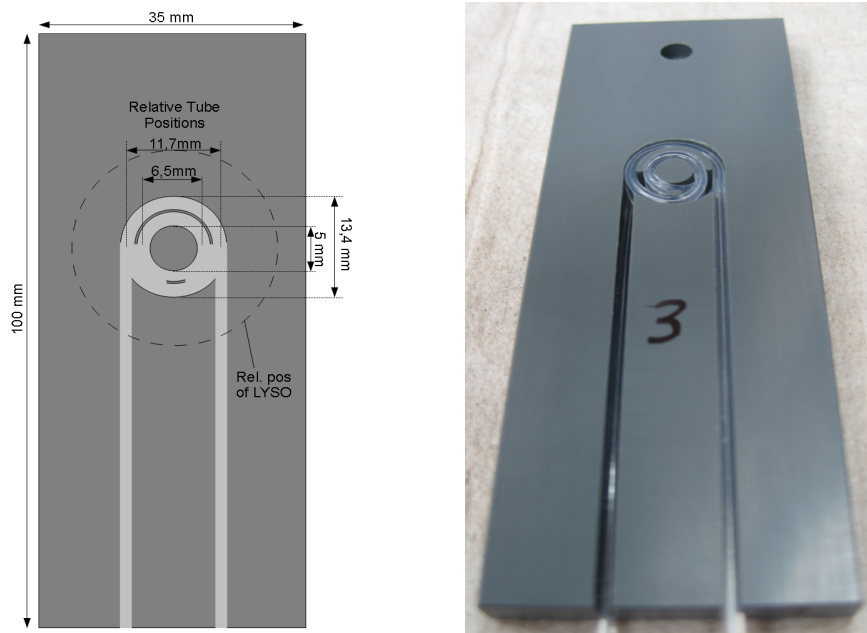
Figure 3.4: Sketch and picture of TubeFix 3. The Teflon tube is spiraled in two coils in the center of the detector system.

Although Teflon hardly shows any adhesive properties it is necessary to prime each tube with the inactive substance (chemical identically but not radioactive) to ensure that no ^{11}C tracer is glued to the tubes wall. Because this inactive tracer would be flushed from the tube into the animal as the measurement starts after priming, it would have a strong influence on the behaviour of the active tracer. However, since this behaviour is the focus

of investigation this effect has to be avoided by flushing the tube before the measurement starts. This flushing removes most of the inactive tracer and leaves just a thin layer of it glued at the wall. All measurements carried out during the tests (section 5.1) showed that such a primed tube combination (Teflon and short pump tube) does not cause considerable adhesive effects no matter what tracer is used.

The adhesive problems do not occur for the used ^{18}F tracers even if only pump tubes are used for the transport of the blood. In section 5.1 the results of several in-vitro measurements in which ^{18}F as well as ^{11}C tracers with different tubes and within 0.9% NaCl solution or blood are displayed.

3.1.2   Coincident Efficiency

The efficiency for measuring both annihilation photons in this measurement geometry was first analysed by measurements with a point-like source (section 2.3.4). The best efficiency is obtained if the source is placed right in the center of the detection system between the two scintillation crystals. Since this is a flow-through system it is difficult to define the measurement volume exactly. As figure 3.5 shows the coincidence count rate as a function of the position of a point-like source is approaching the zero-level slowly when the source is moved away from the central detector position.

Hence, the decision was made to consider only the volume within the coils as measurement volume. However, since active blood from the tubes leading from and to the coils also contributes to the total coincident count rate the efficiency appears to be larger than it would be for the coils alone. The radius of the inner coil is 3.25 mm while that of the outer coil is 5.85 mm (figure 3.4). According to figure 3.6 the corresponding efficiencies would be 6.5% and 5.0%. As the measurement volume is divided into 35.7% for the inner coil and 64.3% for the outer one the assessed efficiency for the whole measurement volume is 5.5%.

The radioactivity from the tubes outside this measurement volume increases the coincident counts so that the efficiency was estimated to be 6% to 6.5% as a first appoximation. To determine the exact value for the efficiency for all tube fixtures several calibration measurements were performed. For these calibration measurements [^{18}F]FDG tracers mixed in an 0.9% NaCl-solution were used. The activity concentration AC was first determined by measuring the total activity in a gamma counter. The volume was given by the scale of the syringe which was used to prepare the solution. The efficiency ϵ was then calculated by recording the count rate Z with COBALT using the setting described in section 3.3 and the following equation:

$$\epsilon = \frac{Z}{f \cdot MV \cdot AC} \cdot 100. \tag{3.1}$$

The activity concentration is given in Bq/μl, the count rate in counts per
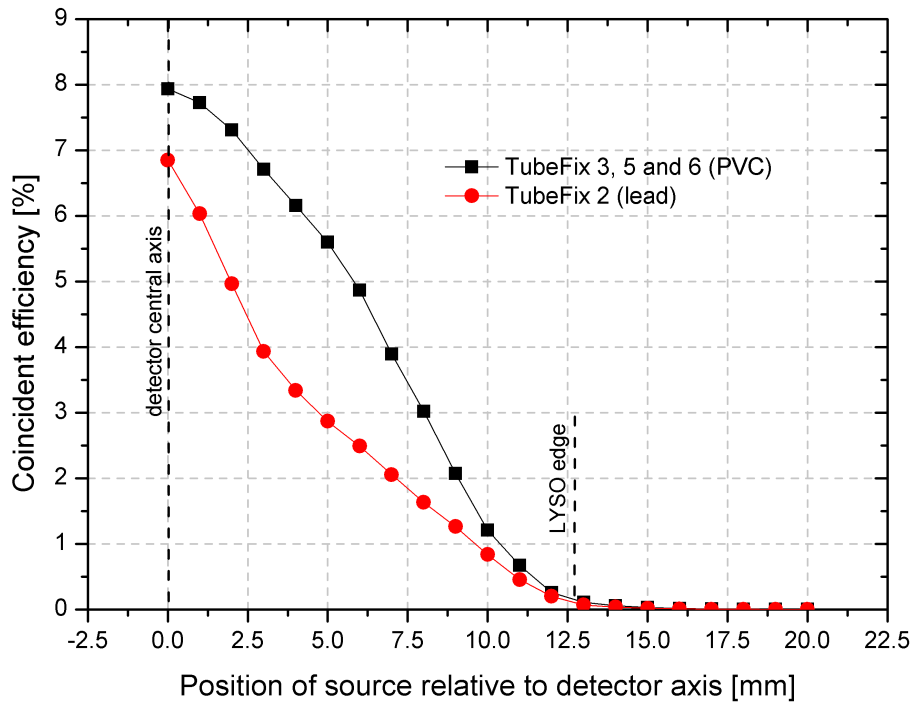
Figure 3.5: Efficiencies for tube fixtures made of PVC and lead depending on the source position relative to the central axis of the detector. The graph shows clearly why it is important to place the tubes containing the activity mostly in the center of the detector system. The larger the distance to the central axis the smaller the efficiency becomes. Due to the larger absorption probability of lead the efficiency for TubeFix 2 is smaller than for those made of PVC.

second, the measurement volume MV in μl and the efficiency in percent. f is the emission probability of positrons for ^{18}F. The results showed that 6.5 $\pm$ 0.1% is the correct value for the efficiency. As various in-vitro tests have confirmed later this value also accounts for ^{11}C tracers in blood.

Comparing the coincident efficiency curve of figure 3.6 with that for single photon detection displayed in figure 2.13 shows clearly why it is important to place the blood containing the radioactive tracer as close to centre of the detection system as possible. While the number of single counts changes slowly as the source is moved out of the centre the number of coincident counts decreases rapidly due to the emission angle of 180° for annihilation photons. The difference between single and coincident efficiency in the centre (16.1% and 7.9%) is caused by the absorption probability of the LYSO crystal which is almost 50% for 511 keV and 25 mm thickness.

This measurement geometry requires 285 mm of the Teflon tube to be mounted in TubeFix 3 where 110 mm are in the channel leading to and from the edge to the outer coil and 175 mm are used to form the coils. This
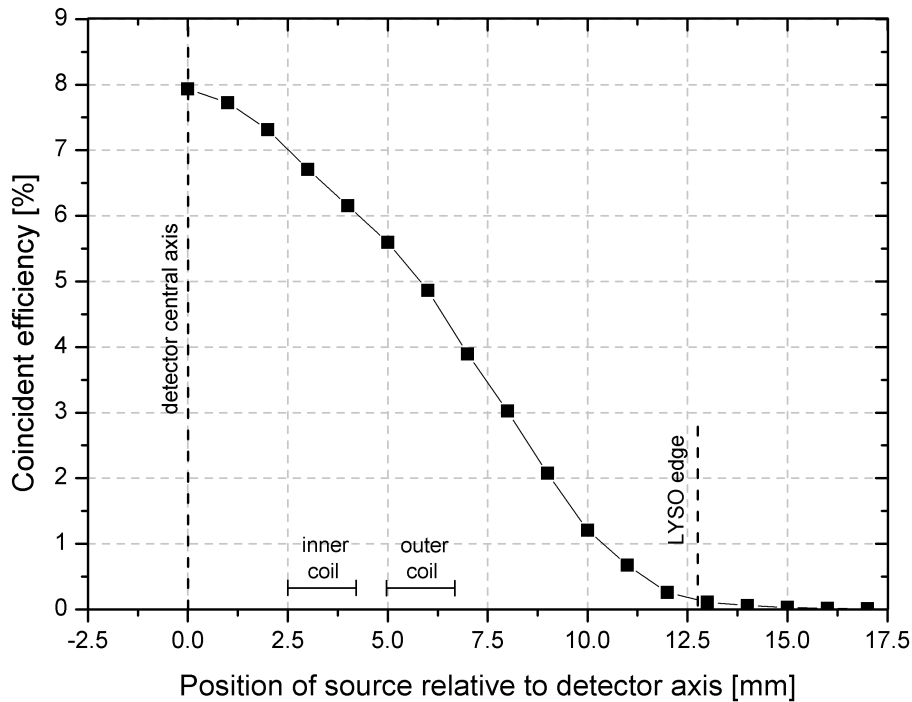
Figure 3.6: The efficiency for TubeFix 3 as a function of the source position relative to the central axis of the detector system. The more the source is moved from the center to the edges of the scintillation crystals the less coincident events are detected. However, even if the source is outside the margins of the crystals still some coincident events are detected.

corresponds to 55.8 μl in the tube fixture as well as 22.4 μl and 33.4 μl in the channels and coils, respectively. The volume within the coils is 12 μl for the inner one and 21.4 μl for the outer one. In table 3.1 these values are listed together with the corresponding results of the other tube fixtures. Comparing these values also explains why TubeFix 3 is the best solution.

TubeFix	2	3	5	6
Material	lead	PVC	PVC	PVC
Appropriate tube (ID[mm])	T (4)	T (0.5)	S (0.51)	S (0.51)
Total volume in TubeFix [μl]	1181	56	94	68
Meas. volume [μl]	163	33	72	46
Time to pass TubeFix [s]	84.4	4.0	6.7	4.9
Time to pass meas. volume [s]	11.6	2.4	5.1	3.3
Coincident efficiency [%]	2.6	6.5	3.4	3.9

Table 3.1: List of the main characteristics of various measurement geometries (T = Teflon, S = Silicone).

3.2 Pump and Tube Connections

The further analyses of the tracer by compartment modeling require a time activity curve (TAC) of the arterial blood that is based on constant blood flow. A peristaltic pump placed between animal and detector provides such conditions. The blood withdrawal depends on the inner diameter of the pump tube and the speed settings at the pump. Several tests with female Sprague-Dawley rats showed that a blood withdrawal of $14\,\mu\mathrm{ls}^{-1}$ matches well the animal's circuit.

All tube systems tested during the development of this system had to be connected to the two medical micro-volume tubes made of Tygon with an inner diameter of 0.508 mm. Both tubes are used as catheter, placed in the femoral artery and in the femoral vein of the animal.

As already mentioned in section 3.1.1 the combination of a short pump tube with Teflon tubes turned out to work best. The tubes are connected using a prepared hollow needle with an inner diameter of 0.50 mm and an outer diameter of 0.55 mm. To ensure no air can get into the tubes and for mechanical stability the needle is covered with liquid glue before it is inserted into the tubes. As a precaution the connections are fixed by a silicon tube and two cable ties (figure 3.7). The pump tube should be as short as possible to keep adhesive effects small. For the pump used in this system a length of approximately 10 cm is required. Because it offers one of the longest service lives and very small gas-permeability the tube *PharMed BPT* by *Saint Gobain* is used.
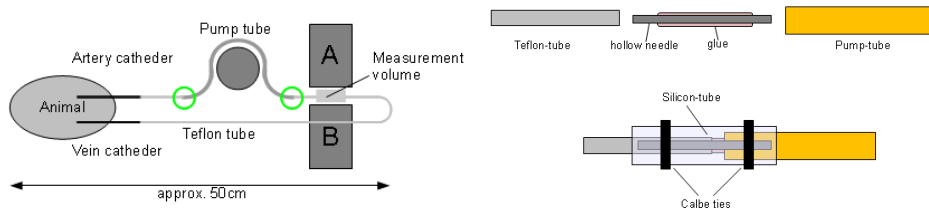
Figure 3.7: Overview on the tubes used in this measurement system, their function and how they are connected. The left sketch shows the tube-arrangement: Two tygon tubes are used as catheter in the femoral artery and vein of the animal. Both are connected via hollow needles (without any further glue or fixture) to Teflon tubes. The connections between Teflon and pump tube within the green circles are displayed in detail in the right figure. For the connection between Teflon and pump tube the hollow needle is covered with a liquid glue before it is inserted into the tubes. This accounts for mechanical stability and ensures, that no air can be aspirated.

3.3   Signal Processing

Since this measurement system aims at detecting positrons by detecting both 511 keV annihilation photons it is necessary to filter the signals produced by the detectors with regard to their energy as well as their time difference. Before the signal is analyzed it needs to be amplified, because the original output voltage at each detector offers a maximum level of only -55 mV. This is exactly the minimum input voltage required by the constant fraction discriminator (CFD). However, because all signals belonging to a 511 keV event are within a range of several mV it would be impossible to handle the original detector output.

The signal at the output of the pre-amplifier of one detector has a maximum voltage of about -450 mV into 50 Ω and a duration of approximately 250 ns (see figure 2.9). This duration is, however, not the time which is important for the following signal treatment but only the time it takes for the signal to decline to ground level. For further signal processing it is more important to watch the signal at the input level of the following instrument. Since this is the input threshold of the CFD, which is set to -180 mV, the analogue pulse duration would be, from the technical point of view, approximately 70 ns. This is the time the signal is above the threshold level and, consequently, the CFD is occupied.

The CFD is used for two purposes. It first filters the analogue signals with regard to their height of the voltage peak. Only those with a voltage peak between the lower level discriminator (LLD) at -350 mV and the upper level discriminator (ULD) at -630 mV are assessed to be produced by a full energy 511 keV event. These voltages correspond to a gamma energy of 415 keV and 680 keV leading to an energy range of 265 keV around 511 keV. As figure 3.8 shows it is necessary to set the LLD right at low-energy end of the 511 keV coincident peak in order to avoid too many false counts. In contrast, the ULD can be set generously to a higher level since above the peak hardly any coincident counts are recorded.

After this energy filter the signal is converted to a digital pulse using a constant fraction technology. This technology reduces the "walk" of the digital output pulse due to different rises[2] of the analogue input pulses within the selected energy range. The height of the analogue pulses produced by the PMT varies due to statistical fluctuations in both, the number of scintillation photons and the number of electrons emitted at the photo cathode. The CFD compensates these fluctuations. At first, the input signal at the CFD is duplicated. While one is delayed the other one is inverted and attenuated. The time the first signal is delayed is determined by the length of the cable between output and input of the delay loop. Finally, both signals are added leading to zero-crossing independent of the original signals rise time. This

---

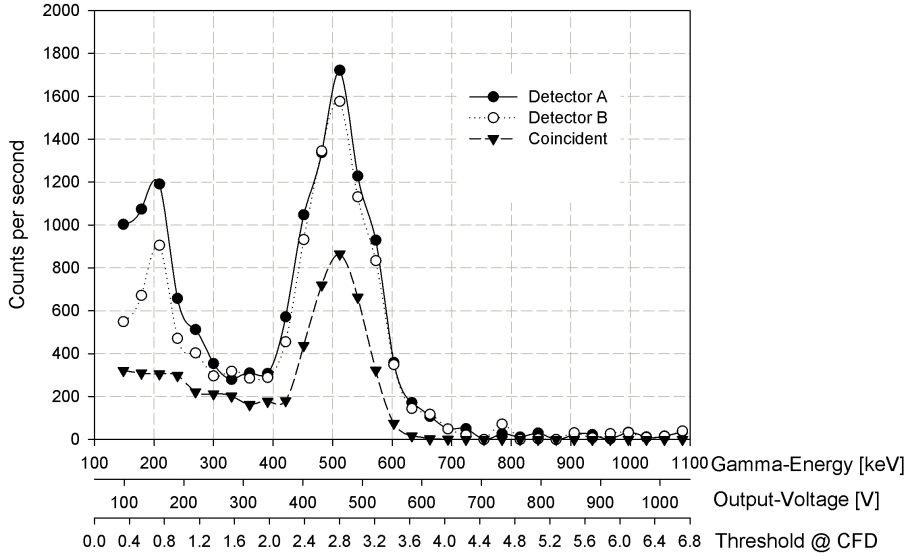[2]Different pulse height but same rise time

Figure 3.8: Single and coincidence spectrum of a ^{68}Ge source. For further signal treatment only pulses corresponding to an energy between 415 keV and 680 keV are accepted. The energy resolutions of both detectors are 23% (section 4.7)

zero-crossing is used as start point for the digital output pulse [Bedwell and Paulus, 1979; Gedcke and McDonald, 1968]. The function is also explained graphically within figure 3.11. If the digital pulse would be generated just as the analogue pulse exceeds a trigger level the time of this generation would depend on the rise of the analogue pulse.

The digital pulses produced by both CFDs are transmitted to a majority logic unit where the pulse of channel A is stretched to a digital pulse of 8 ns. The pulse of channel B is delayed by 2 ns between CFD and logic unit. The cable of channel B is 40 cm longer than that of channel A which corresponds to a transmission time 2 ns longer than that of channel A. The pulse of channel B is then converted to a 4 ns digital pulse. Both pulses are furthermore transmitted to another channel of the logic unit which is configured as logic AND. It only produces an output pulse if the input signals of both input channels (A and B) exceed the input thresholds (-500 mV, 750 ps). This output pulse is finally regarded as a reliable signal for detecting two coincident 511 keV gamma quanta in each of the two detectors. Because these gamma quanta are regarded to be produced in an annihilation process between a positron and an electron, this final digital pulse accounts for the measurement of a positron emitted by the tracer within the blood. Conse-
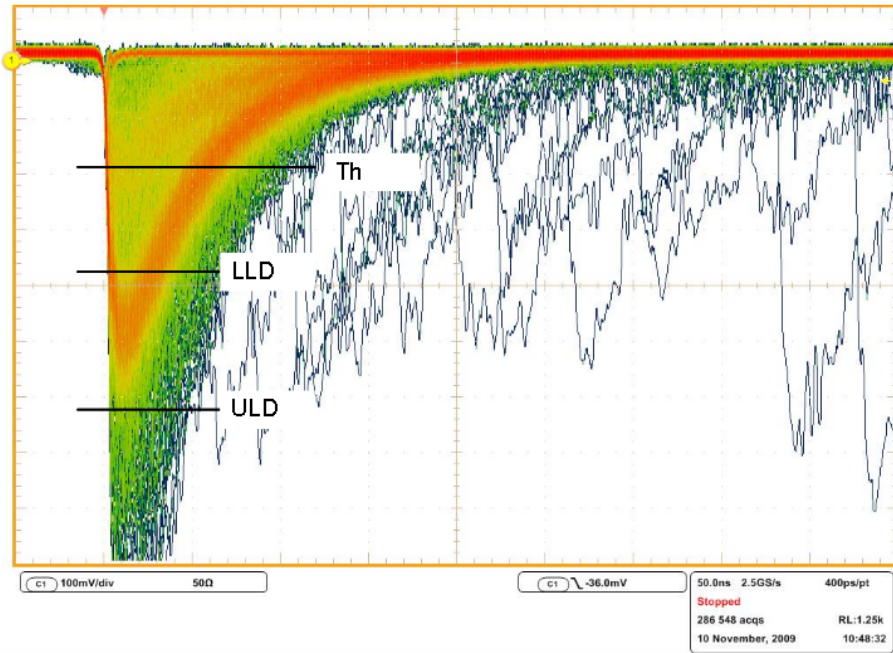
Figure 3.9: Analogue output signal of one detector. The signal is processed if its peak is higher than the threshold level (Th). An digital output pulse is produced if the peak height is between the lower (LLD) and upper level discriminator (ULD).

quently, the coincidence time window is 12 ns (width of pulse from channel A + width of pulse from channel B). Finally, the pulse is sent to the input channel of the PCI card installed in the PC where the counter is increased. All further steps of the measurement are then controlled and executed by the software.

Figure 3.10: Instrumental block diagram showing the signal treatment to process two coincident pulses corresponding to 511 keV events.

Figure 3.11: Functional block diagram showing the signal treatment to process two coincident pulses corresponding to 511 keV events.
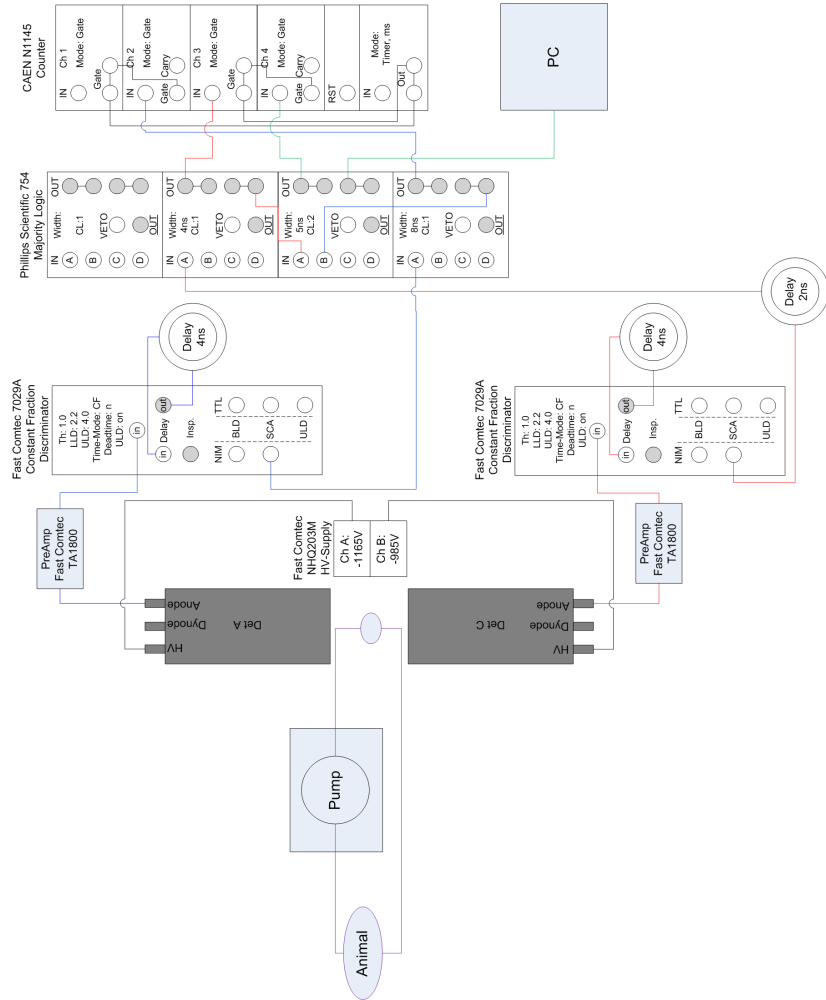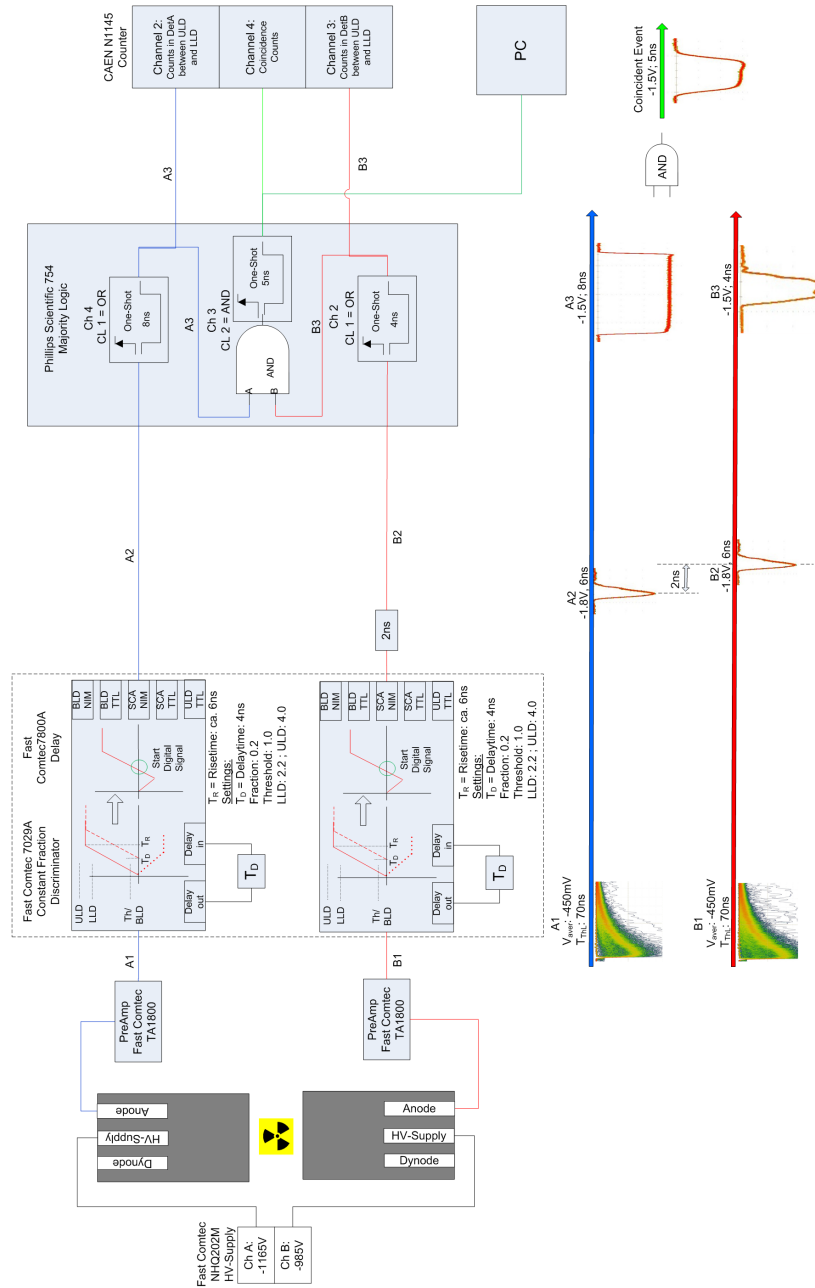
3.4   Software

The software was created especially for this application. It is written in Visual Basic and communicates with the PCI card via the DLL that was provided by the manufacturer. This DLL in turn acts as a communication terminal to a server-program that finally controls the PCI card. At startup, the software calls up several *.ini files. One contains settings and instructions for the server program controlling the PCI card [3]. The other ones contain the values of background counts per second for each tube fixture, length of the tube within each tube fixture, efficiency values and the current file number for the log file to save the data. All data recorded during a measurement (including the selections in the parameter field) are stored in this log-file immediately as soon as they are available. A detailed description about how this software really works can be found in the appendix where a flow-diagram and the main parts of the source code can be found. This section should only give an overview from the user's point of view.

3.4.1   Measurement Control and Display

The software offers a graphical user interface (GUI) via which the user can control the measurement. The GUI is divided into four main parts: command field, parameter field, display field and output field (see figure 3.12).

Command Field   Because the timing of each measurement is a very important point the software offers the possibility to control the measurement and set time stamps by simple mouse clicks.

- **Check** This button is for safety reasons only. Before the measurement starts the user has to click on this button. The program then checks if all parameters are entered in the parameter field and if they are within their correct ranges. If everything is correct, the blue status sign `Stand-by` turns into a green `Ready` and if not an appropriate error message is displayed. Because the actual measurement starts as the tracer is injected (click on `Start Inj`) this procedure prevents failure in timing properties. If one or more parameters are not correct the system would deliver an error message before the tracer is injected. Without this safety control the system would not start the measurement due to an error although the tracer is already about to be injected. After pushing the `Check` button the current count rate is displayed at the display field as well as in the output field. However, no further calculation (such as activity concentration, half-life correction and so on) is performed. This feature is just for a rough check, if the whole setup (settings of electronics, tube fixture installed

---

[3]See attachment for details

properly) works fine. Because no activity is present in this status of the measurement only background counts should be displayed. If the counts per dwell time do not correspond to the settings chosen for this measurement the user should check the adjustments for electronics and measurement geometry.

- **Start Inj**: As soon as the status sign is green the measurement can be started by clicking on `Start Inj` simultaneously to the beginning of the injection of the tracer. From now on all features of the software work as they are described in section 3.4.2.

- **Stop Inj**: This button has to be pushed when the injection is stopped. This only sets a time stamp in the data file.

- **Start Flush** and **Stop Flush**: The same procedure has to be performed when the injection cannula is flushed. Again, these buttons have no direct influence on the measurement but only set time stamps in the data file.

- **Stop**: This command ends the measurement after confirmation.

- **Reset**: All measurement points and data in the display field and in the output field are deleted and the system is prepared for the next investigation. Consequently the user should first save the latest measurement before the system is reseted. Only the user settings in the parameter field remain.

- **Save**: All data referring to the current measurement are saved in a file. Name and extension have to be chosen by the user.

- **Write into file**: In case the user wishes to store additional information on the current measurement, the text written in the entry field above this button is written into a separate comment file including a stamp of the time at which the button is pushed.

Parameter Field In the parameter field the user can select and enter the parameters that are necessary to calculate the activity concentration in Bq/μl based on the counts per dwell time. The dwell time is the time the system uses to accumulate the counts for one single measurement value. Furthermore, the isotope for appropriate half-life correction and the tube fixture for correct efficiency, measurement volume and background count rate can be chosen. Since usually TubeFix 3 will be used for all investigations this is the default value. However, if for any reason the user wishes to use any of the other measurement geometries, it just requires a mouse click on the appropriate tube fixture to change the implemented values for efficiency, background and measurement volume. If none of the displayed tube fixtures correspond

to the setup used for a special measurement the user can select TubeFix 0 for an undefined measurement geometry. In this case the values for measurement volume and efficiency have to be entered manually. Furthermore no automatic correction for background counts would be performed. For correct results and easier handling the software offers four different methods to correct the measurement data:

- **Delay**: The distance between animal and detector is usually approximately 40 cm. However, this distance might change if a different setup is required. Furthermore, the demands on the pump speed of the blood flow might vary for different animals. Both reasons account for a difference in time it takes the tracer in the blood to reach the detector. Because all further analyses require the time activity curve of the blood within the animal, the data have to be corrected for this time delay. In other words, the measurement values should be the same as if the detector would be placed right at the animal's femoral artery and not several cm away from it. To determine this delay the time between the click on the `Start Inj` button and the arrival of the activity is measured. This arrival is detected by the software that checks whether the count rate rises quickly enough to be taken into account.

- **Half-life Correction**: As it is not the tracer itself that has to be investigated but its behaviour inside the animal, all values need to be corrected for the half-life of the isotope.

- **Variable Integration Time**: As soon as the tracer is injected the metabolism of the animal starts to absorb it. Because the injection is usually faster than the animal can absorb the tracer the activity concentration rises quickly. Consequently, after the injection is finished the activity concentration decreases due to the animal's metabolism. The screen shot in figure 3.12 shows a typical measurement curve. Since lower count rates always lead to larger statistical uncertainties an algorithm evens the measurement curve as the activity concentration gets low. This allows for more precise results.

- **Background**: Finally, from all values the background corresponding to the dwell-time and measurement geometry is subtracted.

In order to use this instrument for any kind of different measurements of positron emitting sources, all these corrections can be deactivated.

Display Field The current number of counts per dwell time is first corrected based on the selections in the parameter field. Afterwards these values are displayed as vertical offset of small black circles relative to the base line of the display field. Since it is not obvious which values need to be displayed

the default maximum value at the beginning of each measurement is very low and corresponds to 30 Bq/μl. As the count rate rises the display field changes its vertical resolution optimised to the new value that is larger than the original maximum value. In contrast to the vertical arrangement the software does not offer any automatic change of the horizontal display resolution. The default value is 60 minutes. If the user wishes to display a longer or shorter time range of the measurement curve the appropriate value has to be entered in the text field below the right margin of the display field. The software then changes the horizontal resolution of the display field so that the desired period of time of the measurement curve is displayed.

Output Field This part is for detailed control of the current measurement. It displays various values that are useful to be watched since not all of them can be seen in the display field.

- **Channel Number**: Shows the number of the channel in which the current counts per dwell time are recorded.

- **Counts**: Number of counts per dwell time without any corrections or calculations.

- **Started @**: Displays the time at which the `Start Inj` button is pushed.

- **RunTime**: Time elapsed since the `Start Inj` button was pushed.

- **MeasTime**: Measurement time - time since the arrival of the tracer at the detector was recognised by the software.

- **MeasValue**: Measurement value - counts per dwell time corrected due to the settings in the parameter field.

- **Bq /μl**: Calculated activity concentration based on the measurement value.

- **HLC**: Indicates whether the data are corrected for the half-life of the selected isotope.

- **VIT**: Indicates whether the time activity curve is smoothed by a larger integration time.

- **Delay**: Displays the time in seconds how long it took the tracer from the beginning of the injection to reach the detector.

- **File-No**: Displays the number of the log file in which the current measurement data are stored.

Since the log-file contains all data that are available during a measurement it is difficult to be used for further analyses. The user might therefore save each measurement in a separate file that is created by pushing the `Save` button. In this case only the part of data that are relevant for compartment modeling are stored. Besides a header in which time stamps, measurement geometry and isotope are stored, it includes four columns in which runtime, measurement time, activity concentration and its relative uncertainty are listed.
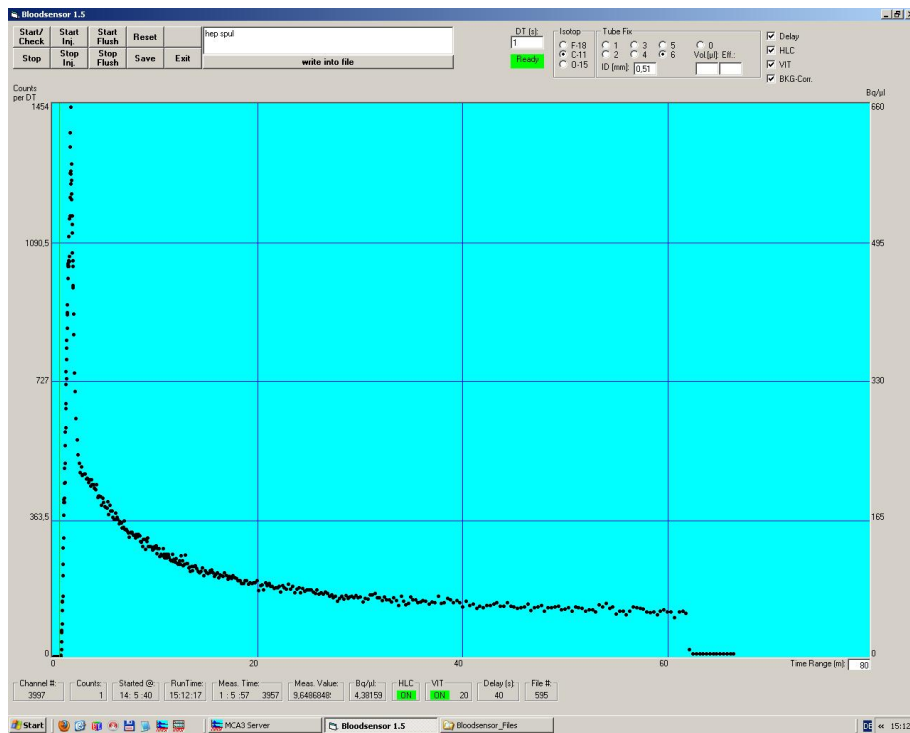

Figure 3.12: Screen shot of the graphical user interface (GUI). It shows the time activity curve of mephobarbital - a ^{11}C tracer - that was observed for more than one hour. The GUI is divided into four major parts: The control field (top-left) where the measurement can be controlled by clicking on the buttons, the parameter field (top-right) where some important parameters such as isotope and dwell time can be chosen, the display field in which the measurement values per dwell time are displayed and finally the output field where some important values of the current measurement are displayed (bottom).

```
********** Header **********
Measurement/Injection started at: 12:38:4
Injection stopped at: 0:0:0
Flush started at: 0:0:0
Flush stopped at: 0:0:0
Measurement stopped at: 9:41:52
Dwell-Time [s]: 1
Delay-Time [s]: 0
Tube-Fix: 3
Measurement-Volume [micro-l]: 33,37844
Efficiency [%]: 6,5
Isotope: F-18; Half life [s]: 6583,68
Half-life corrected (0=no, 1=yes): 0
Background reduced (0=no, 1=yes): 1
VIT used (0=no, 1=yes): 0
********** Header **********

Runtime;;Measurement Time;;Activity Concentration;Rel.Uncertainty
 0 ;12:38:4; 0 ;0:0:1; 29169,8222924674 ; 3,97505764946921E-03
 1 ;12:38:5; 1 ;0:0:2; 29125,5744723836 ; 3,97807597420534E-03
 2 ;12:38:6; 2 ;0:0:3; 29180,8842474883 ; 3,97430414116988E-03
 ...
```

3.4.2   Principles of Operation

As already mentioned this software includes some special features to derive the correct input function for further analyses with compartment modeling. Besides the calculation of the activity concentration out of the recorded counts per dwell time, these are in particular delay time, half-life correction, variable integration time and background correction. Control and operation of the software and the measurement in general is explained in section 3.4.1. In this section a detailed description of how some major parts of the software really work is given.

Activity Concentration: The calculation of the activity concentration AC in Bq/μl is given by

$$AC = \frac{Z}{f \cdot DT \cdot MV \cdot \epsilon}.$$

(3.2)

Z is the number of counts per dwell time, f the emission probability of positrons for the corresponding isotope, DT the dwell time in seconds, MV the measurement volume in μl and ϵ the efficiency. This calculation is performed permanently as soon as the count recording for the current measurement point is finished.

Delay Time: The algorithm of the program to check whether the tracer has reached the detector is based on the method of linear regression and least squares estimation. The program uses eight consecutive measurement values to calculate the slope of the linear regression function which is derived by

$$\hat{y} = \hat{k}x + \hat{d} \tag{3.3}$$

with

$$\hat{k} = \frac{\sum_{i=1}^{N} x_i y_i - N\overline{xy}}{\sum_{i=1}^{N} x_i^2 - N\overline{x}^2}. \tag{3.4}$$

If this slope $\hat{k}$ is larger than 0.7 the system assumes that the active blood has reached the detector. The difference between this moment and the mouse-click on `Start Inj` is then considered to be the delay time for all further investigations. This event furthermore triggers the measurement time to start since the system should provide a input function as if the detector is placed at the animal's femoral artery. From now on, all count rates are corrected for the half-life of the isotope if the user has clicked the appropriate check box. Figure 3.13 displays the sequence of the time related functions of the software.

Half-Life Correction: Based on the formula for radioactive decay the values are corrected as if the number of disintegrations does not change at all. The corrected count rate Z is therefore given by

$$Z = Z_{meas} \exp \frac{\ln 2 \cdot t}{t_{1/2}} \tag{3.5}$$

where Z_{meas} is the recorded count rate, t the current run time and $t_{1/2}$ the half-life of the isotope.

Variable Integration Time: To compensate statistical fluctuations as the count rate gets low the measurement curve can be smoothened by averaging. In order not to miss any short term changes of the activity concentration, this procedure should be performed after the peak when the animal's metabolism has absorbed most of the tracer. To make sure that this algorithm does not start too early a control routine checks the behaviour of the activity concentration. It starts as soon as the arrival of the tracer is recognised (equation 3.4) and proceeds similarly. However, in this case the software checks the negative slope of the linear regression function. If the slope is below -0.7 the software now recognises the decrease of the activity concentration which corresponds to the right end of the peak of the time activity curve. As a next step, the VIT function uses the method of linear regression with equations 3.3 and 3.4 to calculate the statistical fluctuations of the measurement values. Because the measurement curve after the peak

resembles more a decreasing exponential function than a linear function, the measurement values used for this calculation first need to be logarithmised. The values for $\hat{y}$ in equation 3.3 and 3.4 are therefore not as they are recorded but their logarithms. The statistical fluctuation is larger the larger the absolute differences of the logarithmised measurement values to the linear function are. The relation between these fluctuations and the linear function derives the relative uncertainty:

$$E = \hat{\sigma}/\overline{\hat{y}} \tag{3.6}$$

with

$$\hat{\sigma}^2 = \frac{\sum_{i=1}^{N}(\hat{y}_i - y_i)^2}{N(N-2)} \tag{3.7}$$

as well as

$$\overline{\hat{y}} = \frac{\sum_{i=1}^{N}\hat{y}_i}{N}. \tag{3.8}$$

Furthermore, the variation coefficient VC for the current measurement value[4] has to be calculated by

$$VC = \frac{\sqrt{Z}}{Z}. \tag{3.9}$$

If this relative uncertainty E is larger than the variation coefficient of the measurement values and the maximum tolerable uncertainty the software does not display the measurement values but the values calculated by the linear regression function. In order to increase the integration time step-by-step the VIT function starts with only four measurement points (xy-pairs) to calculate the linear regression function. Only if the relative uncertainty is larger than the maximum tolerable uncertainty the number of measurement points is increased by two each time the calculation is carried out up to a maximum of 20 values.

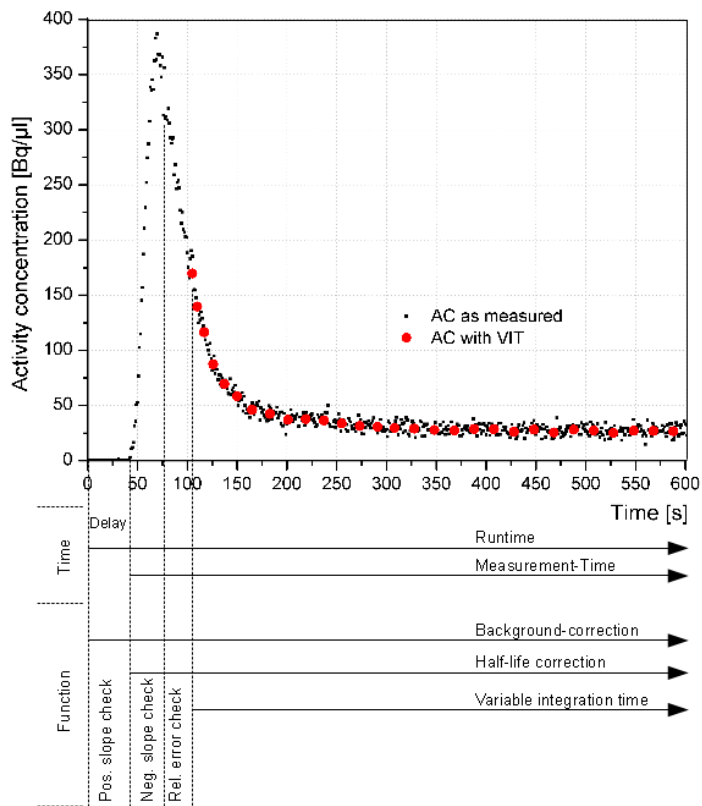[4]The standard deviation of Poisson-distributed data is the square root of its mean.

Figure 3.13: This diagram shows how the time related function of the software works in order to derive the appropriate input function.

Chapter 4

Characteristics and Performance of the Measurement System

4.1 Estimation of the Interference due to External Activities

The whole measurement system needs to be placed next to the PET system where the animal is investigated since the blood volume taken out of the animal should be as small as possible. Furthermore, the animal's metabolism absorbs most of the activity in the blood within the first minutes after injection. Consequently, most of the activity during the measurement is within the animal.

Although most of the photons are absorbed in the steel pipe, the lead ring and the additional lead shield, there is still a small chance of getting coincident error counts for two reasons. One is simply the detection of two 511 keV photons - each in one detector - that penetrated all shielding without loosing any energy. The other possibility is that one such 511 keV photon is detected in one detector while a decay due to self-activity (see section 2.1.2) causes a signal within the coincident time window and within the selected energy range. Both possibilities lead to error counts depending on the injected activity and the distance between animal and detector.

In order to estimate how many error counts the animal would cause a 185 MBq ^{68}Ge source was placed at 10, 20, 30 and 40 cm distance to the centre of the detector axis. The recorded count rate was then reduced by the background count rate caused by self-activity. Figure 4.1 displays the results in detail. The usual experimental setup requires a distance of approximately 40 cm between animal and detector. That would cause an interference count rate of 0.1 cps. This is less than other systems for recording the input function offer (5 cps for 37 MBq at 10 cm [Convert et al., 2007] and

8 cps for 1 GBq at 30 cm [Kudomi et al., 2003]). Based on this investigation and because the count rates of common measurements are much larger, the uncertainty due to the activity within the animal can be neglected.
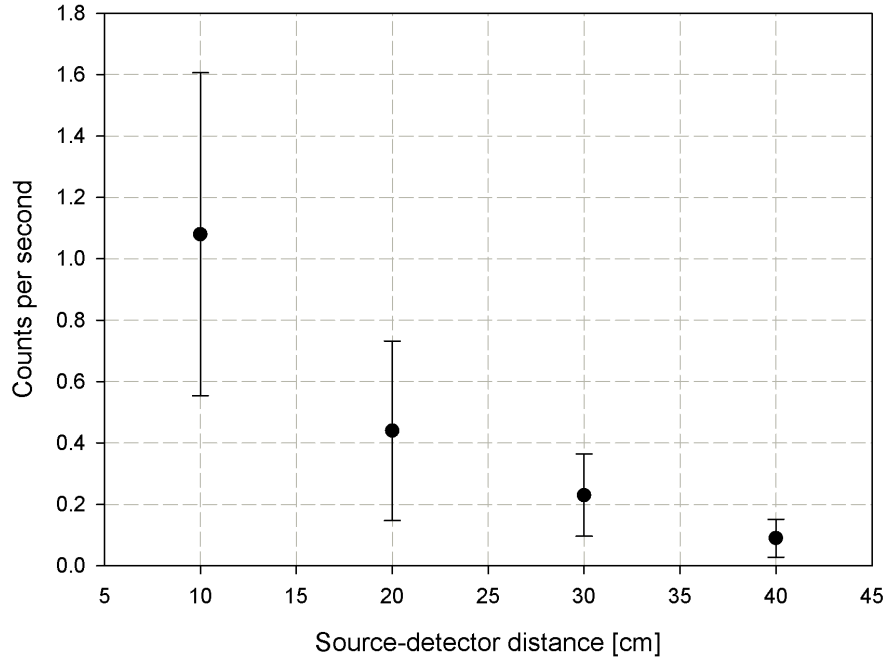

Figure 4.1: Number of error counts due to an external 185 MBq interference source like the animal would be for example. Because the common setup would require a distance of about 40 cm between detector and animal and usually not more than 185 MBq are injected the error count rate due to interference would not exceed 0.1 per second.

4.2   Background

In section 2.1.2 the intrinsic activity of LYSO crystals is explained in detail. Because it is mostly one single decay that causes a false coincident event the number of such events decreases as the detectors are moved apart (figure 4.2). The number increases at shorter distances since the probability for a photon escaping one crystal and being absorbed by the other crystal increases due to the larger solid angle. In order to investigate how many error counts are caused by detecting two decays of ^{176}Lu, each in one detector, the detectors were separated completely. This setup leads to approximately 0.1 counts per second. Since it can be sure that no gamma emission caused by a decay in one detector can be measured by the other detector this number of counts is only caused by detecting two decays - each in one detector - within the coincident time window. This demonstrates, that more than 90% of all background counts based on the intrinsic activity are caused by detecting on

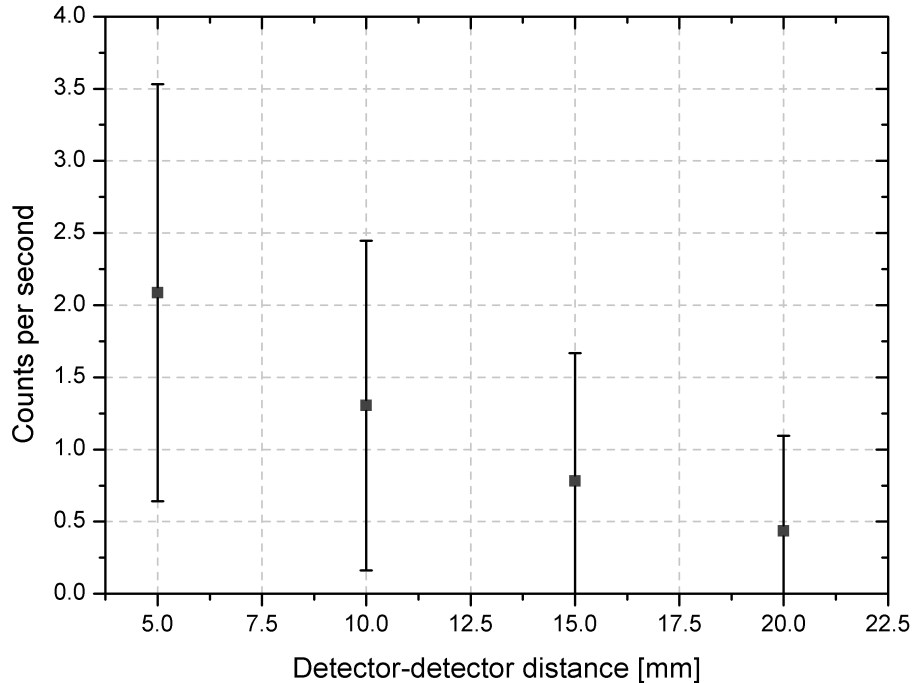single decay in both detectors. Although it might be obvious to place the

Figure 4.2: Most of the random counts due to the intrinsic activity of the LYSO crystals are caused by one single decay. In this case, the electron is detected in one detector while all three gamma photons emitted because of this decay are detected in the other one. Consequently, the number of such error counts decreases as the detectors are moved apart.

detectors at a larger distance to keep the number of background counts small, the coincident system was mounted as close as possible since the efficiency decreases more rapidly if the distance between the detectors gets larger. In the final setup, the distance between both front surfaces is only 9 mm. Because each crystal is protected by two layers of Teflon (each 500 μm) the distance between the crystals is 11 mm. The total background count rate is therefore 1.3 +/- 1.1 cps.

4.3   Detection Limit

In radiation physics it is common to use the *Currie Equation* [Currie, 1968] to calculate the minimum detectable activity. However, Currie assumed a number of background counts much larger than the number of net counts and as well as Gaussian distribution of both values. Because these conditions are not met by the measurement data recorded by COBALT the detection limit has to be derived by taking the probability distribution into account.

The calculation of the detection limit was therefore carried out using the probability distribution of a background measurement and an estimated

probability distribution of a measurement with activity in the measurement volume. Because these distributions depend on the integration time and since this integration time is variable and chosen by the software (section 3.4) the detection limit changes during a measurement. The distributions of the background measurements are Poisson-like for integration times below ten seconds and can be approximated by a Gaussian distribution for larger integration times. To show how the detection limit changes, five different integration times (1, 5, 10, 15 and 20 seconds) are used for its calculation.
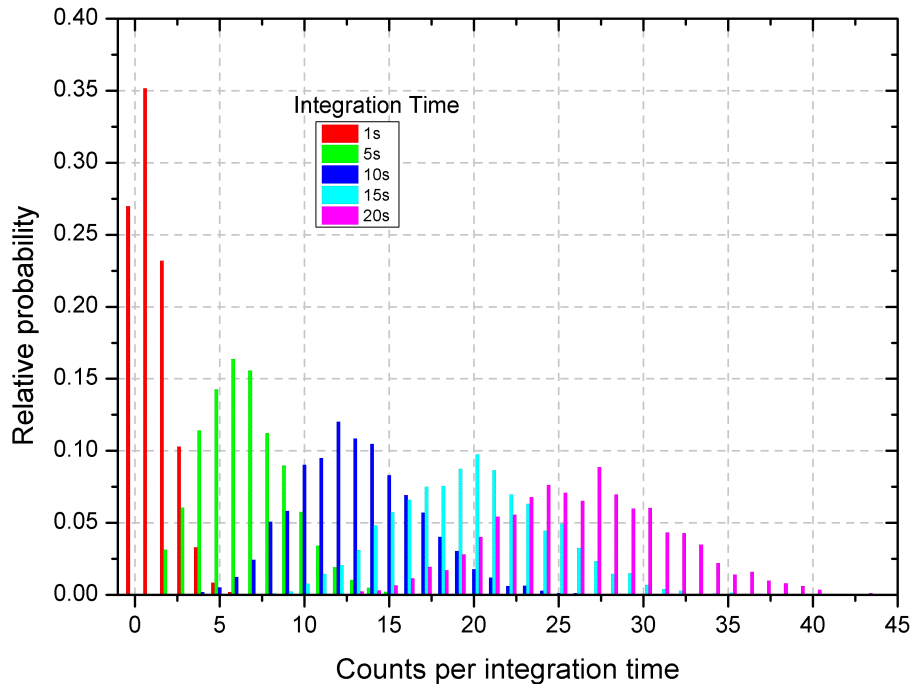

Figure 4.3: The distribution of the relative probability depends on the duration each measurement point is recorded (integration time). Its shape is basically always Poisson-like, however, above an integration time of 10 s the distribution can be approximated by a Gaussian due to its symmetry.

Based on the background probability distribution of each integration time the critical limit L_C is set to a level to ensure that the number of false positive counts (α error) does not exceed 5%. Following the assumption that the probability distribution shows the same shape for each integration time if a weak source [1] is in the measurement volume, an identical probability distribution is calculated such that its 5% quantil matches the L_C of the background probability distribution (see figures 4.5 and 4.6). Therefore, the number of false negative counts (β error) is below 5%. Finally, the mean

---

[1] The source is considered to be weak, if its activity meets the MDA-value (figure 4.4). Counts per integration time is only increased slightly, so that the shape of distribution does not change from Poisson to Gauss.
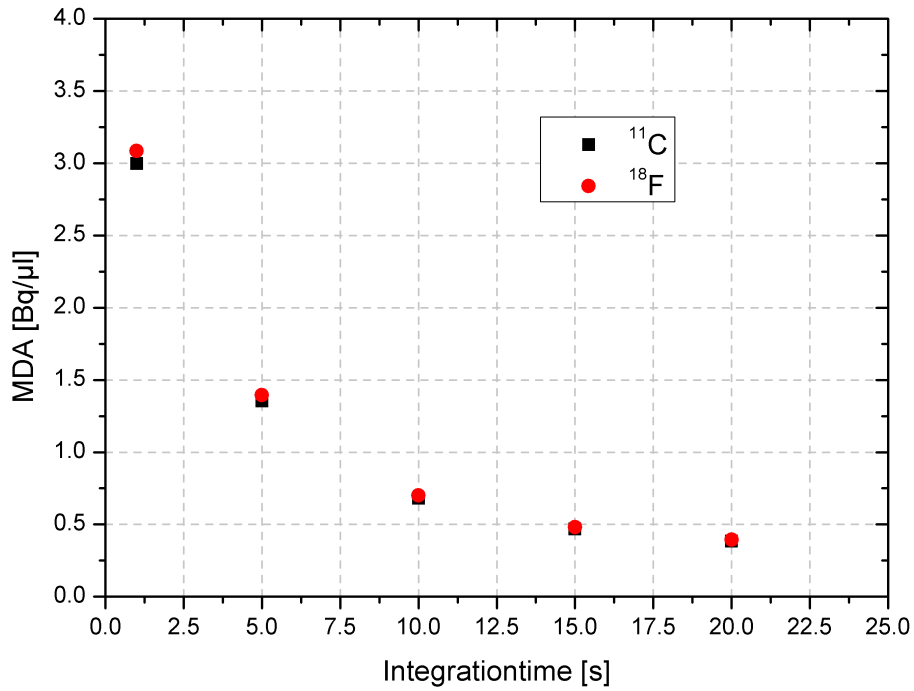
Figure 4.4: The minimum detectable activity (MDA) depends on the time the current activity is measured. The longer this integration time is the smaller is the relative uncertainty. This leads to a smaller detection limit. The difference between ^{11}C and ^{18}F is due to their different positron emission probabilities.

values μ_B and μ_S of background and this calculated distribution are used to derive the minimum detectable activity for each integration time:

$$MDA = \frac{\mu_S - \mu_B}{f \epsilon V T}. \tag{4.1}$$

In this equation V is the measurement volume (33.4 μl), ϵ the efficiency (6.5%), T the integration time and f the emission probability of positrons for the corresponding isotope (99.75% for ^{11}C and 96.86% for ^{18}F). The results of this calculation are displayed in figure 4.4. These results also explain why 20 s is the maximum integration time since the value of MDA would not improve significantly anymore.

Figure 4.5: Poisson-like probability distributions for integration times up to 10 s. The positions of the distributions assuming a detected source were calculated with an α (false positives) and β (false negatives) error smaller than 5%.
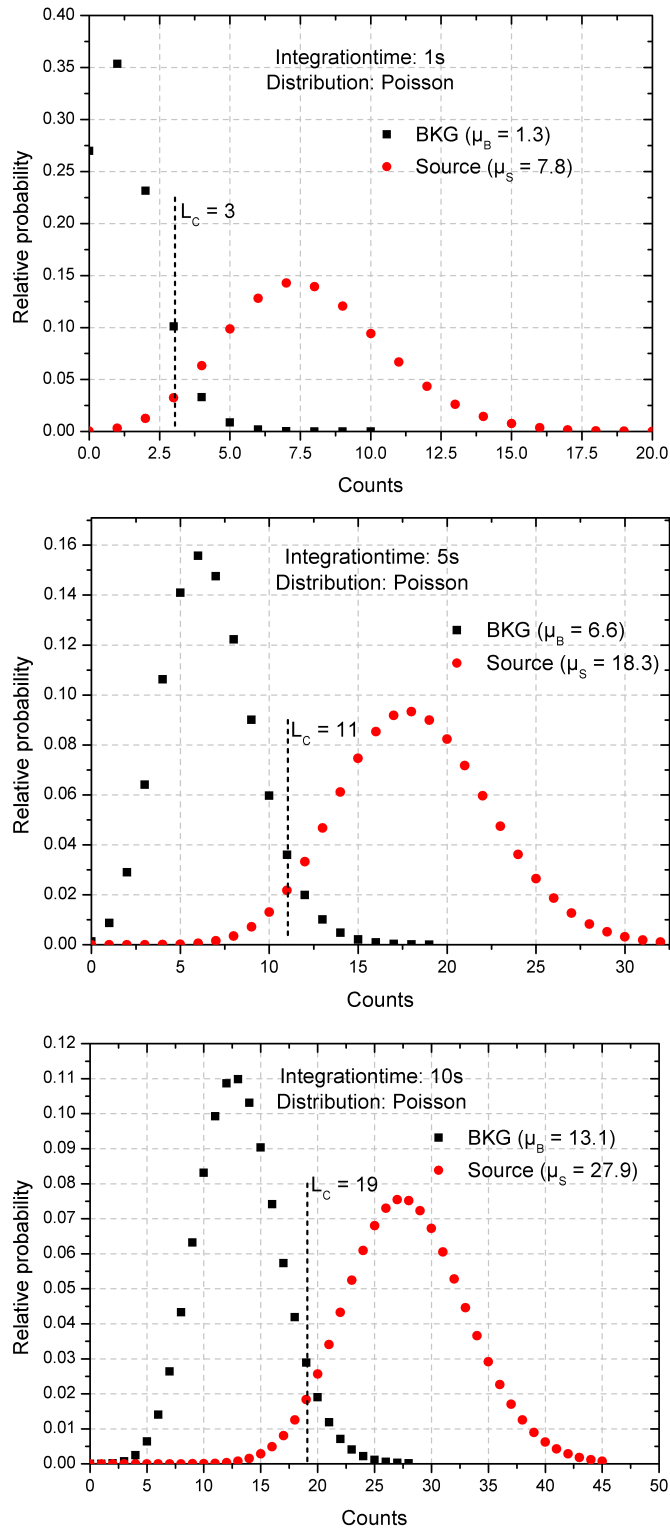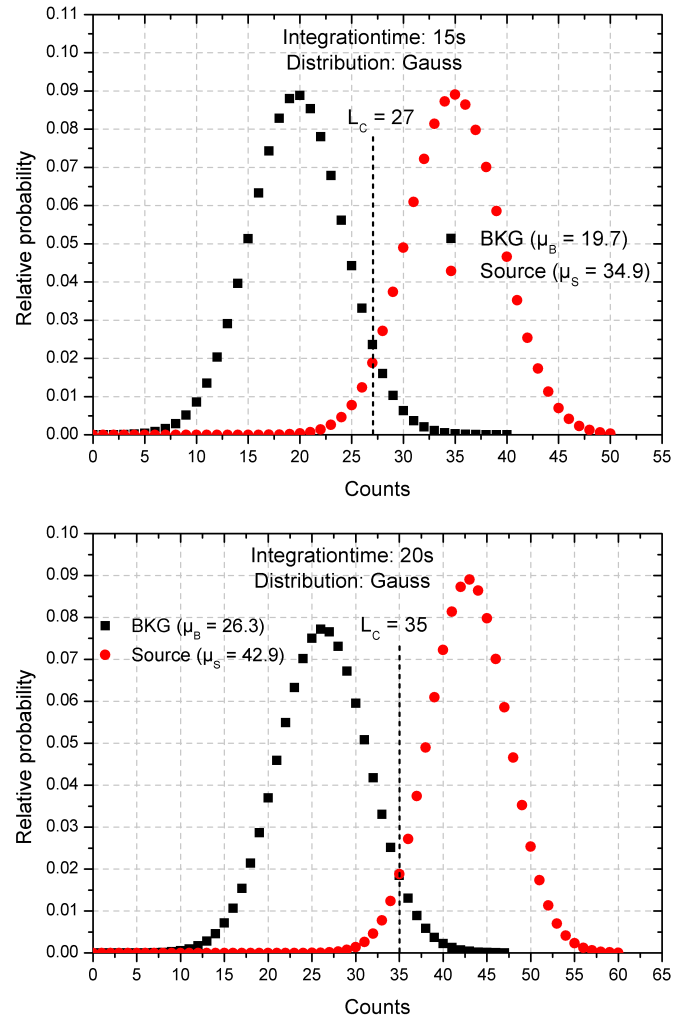
Figure 4.6: Gaussian probability distributions for integration times above 10 s. The positions of the distributions assuming a detected source were calculated with an α (false positives) and β (false negatives) error smaller than 5%.

4.4   Time Resolution

The time spectrum of this coincident measurement system shows a peak at 2 ns with a FWHM value of 550 ps. The position on the time axis of this peak at 2 ns is related to the time the digital pulse of detector B is delayed compared to that of detector A (section 3.3). Besides the fluctuations of the transit time of the PMT two reasons influence the shape of the time spectrum: walk and jitter. The reason for the walk are different raises[2] of the analogue pulse while the jitter is caused by the noise superimposing each analogue pulse. These effects lead to fluctuations in the points of time the analogue pulse exceeds the threshold of a discriminator and, consequently, to the Gaussian peak shape in the time spectrum. The measurement of the time resolution was carried out using the TDC 7072T by FAST Comtec and taking the digital pulse of channel A as start and the pulse of channel B as stop signal. The result is displayed graphically in figure 4.7.
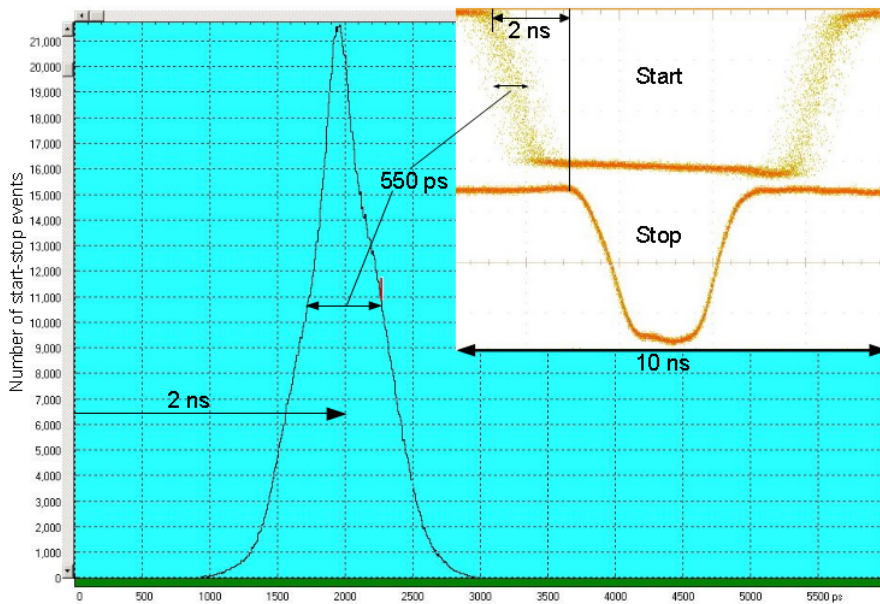
Figure 4.7: Screen shot of the time spectrum (blue background) and the digital pulses with the trigger set on the pulse of channel B. The fluctuations between these two signals limits the time resolution of the coincident system to 550 ps.

One reason for this fluctuation is attenuated by using a constant fraction discriminator (CFD). It reduces the influence of the walk as described in section 3.3. For optimal performance the settings at the CFD should meet the requirement expressed by

$$t_D \geq (1 - f)t_R. \tag{4.2}$$

---

[2]Different pulse height but same rise time.

In this equation f is the CFD fraction and t_R the rise time of the analogue input signal. Since the CFD fraction was set to 0.2 and the rise time of the analogue input pulse is 6 ns [3] the optimal delay time for the best timing resolution t_D would be 4.8 ns. To confirm whether this calculation is correct, the FWHM values were measured for different CFD delays. Figure 4.8 shows the results of this investigation. The shorter the CFD delay is the smaller the jitter becomes. However, if the delay is too short the number of output signals and, furthermore, the number of coincident signals decreases. The optimized total CFD delay was found to be 5 ns. Because the internal delay time of the CFD is approximately 1 ns the external delay has to be 4 ns. This corresponds to a length of the BNC cable of 80 cm, which is mounted between the BNC delay connectors at the CFD.
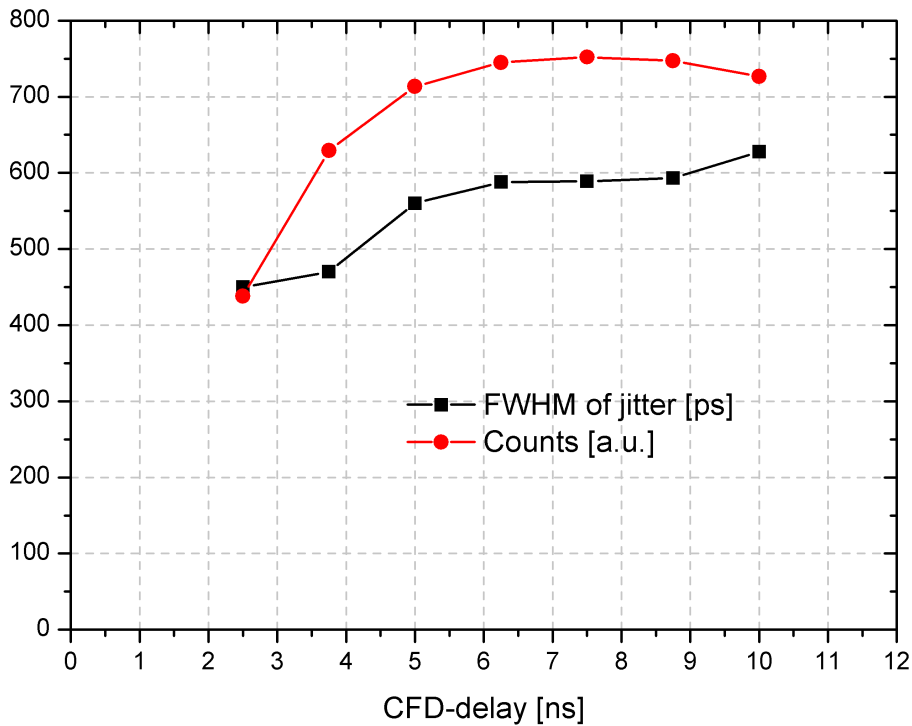
Figure 4.8: The FWHM value of the peak in the time spectrum decreases as the CFD delay is reduced. However, because below 5 ns the number of coincident events decreases rapidly the CFD delay was defined as optimal at this level. Since the internal delay of the CFD is approximately 1 ns the external delay has to be 4 ns, which corresponds to a cable length of 80 cm.

The time properties described so far correspond to the coincident system. Because both detectors and the signal treatment of both channels are identical as well as independent the relation between single and coincident

---

[3]The rise time was determined by measuring the average time it takes the pulse to rise from 10% to 90% of its average maximum height.

fluctuation is given by

$$\sigma_{coinc} = \sqrt{\sigma_A + \sigma_B} = \sqrt{2}\sigma_A = \sqrt{2}\sigma_B \qquad (4.3)$$

Consequently, the fluctuation of each of both detectors is simply the fluctuation of the coincident system divided by the square root of two. Based on the coincident time resolution of 550 ps each single detector has a uncertainty of its timing property of 389 ps.

4.5   High Count Rate Capability

The capability of each radiation detection system using scintillation crystals and PMTs depend on the crystals decay time, the relation between transit time and its fluctuation within the PMT and on the timing characteristics of the electronics used for signal processing. Because no part of the signal chain (from scintillator to logic majority unit) can process two events at the same time the number of output signals increases slower than the number of input signals when the number of events per measurement time gets larger. The time it takes the system to process such an event is called dead time since it is incapable to handle any other events during this period.

For this system the capability to process high count rates was determined using [18F]FDG with an initial activity concentration of 75 GBq/ml. The measurement was followed for more than 10 half-lives. Assuming that all pulses can be processed at low count rates the decay curve was calculated from lower to higher count rates. As initial count rate value the mean over 60 seconds was used in order to avoid wrong results due to statistical fluctuations. The results were the same for all mean values below a count rate of 1000 per second. As figure 4.9 shows, the measurement data matches the calculation pretty well up to a level of about 20,000 coincident counts per second. Beyond this value the system can not process all pulses anymore.

One way of investigating the capability of the system for high count rates is simply to plot the relation between the calculated and measured decay curve (figure 4.9) as as a function of the activity concentration. The result is shown in figure 4.10. Up to an activity concentration of approximately 8 kBq/μl all pulses can be processed. Above this level more and more true coincident events are lost due to the systems dead time. For example at a level of 28 kBq/μl only 90% of all coincident events are counted.
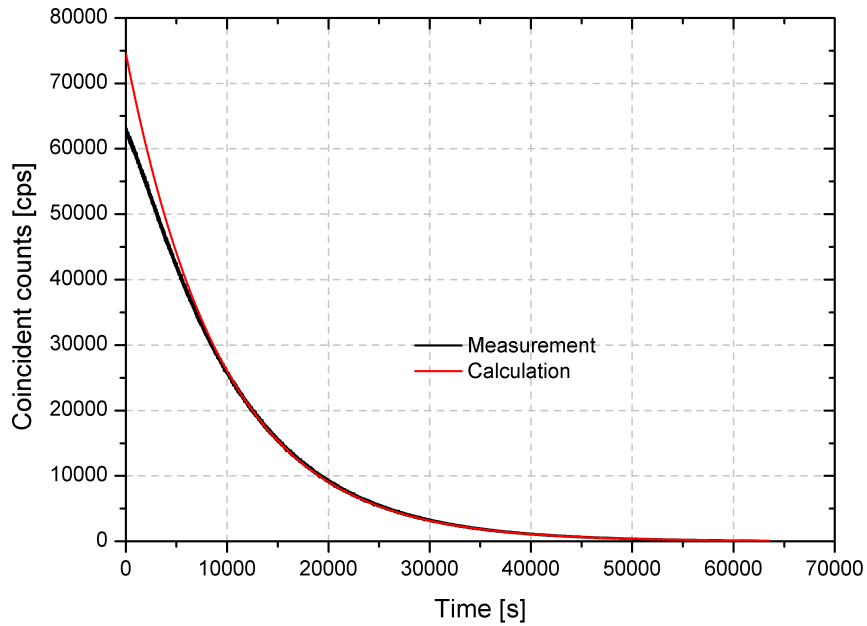
Figure 4.9: Decay curve of a ^{18}F source with an initial activity concentration of 75 MBq/μl. Above a level of approximately 25,000 cps the system can not process all signals anymore. The red curve was calculated by the decay law using the measured count rate at a lower level initial value.

Figure 4.10: Relation between measured and calculated decay curve as a function of the activity concentration. Below an activity concentration of 10 kBq/μl the system can process all coincident events.

4.6   Temperature Dependence

The light output of LYSO crystals is similar to that of LSO (table 2.1), which is known to depend on the temperature. It decreases with increasing temperature. This leads to a smaller number o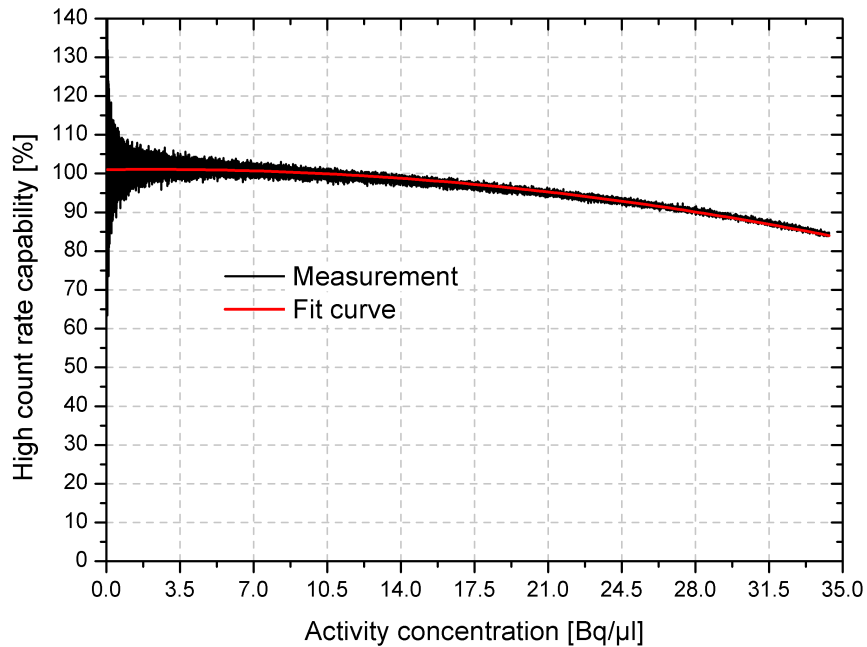f photoelectrons at the cathode and, finally, to a lower peak height of the output signal at the anode. Consequently, although caused by a 511 keV full energy event more signals will be below the LLD level. The number of digital output signals of the CFD will therefore be lower. Various measurements with increasing and decreasing temperature have shown, that the actual relation is given by

$$\Delta CR = \frac{-0.5\%}{\Delta T} \tag{4.4}$$

with ΔCR as the relative change of count rate and ΔT as the temperature difference.

4.7   Energy Resolution

The energy resolution of LYSO crystals is known to be 8% for 511 keV. However, since this system is optimized for fast timing applications the actual energy resolution is only 23% for this energy level (figure 3.8).

4.8   Stability

The stability of this instrument was determined by measuring the activity of a 99 kBq ^{68}Ge source over a period of 9 h. The count rate for this measurement is 7831 ± 11 cps with a drift of 0.02%/h. The same investigation was performed without a source showing that the background count rate of 1.3 ± 1.1 cps has a drift of 0.2%/h.

4.9   Estimation of Measurement Uncertainty

Assuming constant environmental conditions the total measurement uncertainty includes the uncertainty of the net and background count rate due to statistical fluctuations of each single measurement value, as well as interference and system dead time. However, due to the very small contribution by interference of only 0.1 cps at the common experimental setup (about 40 cm between animal and detector, see section 5.2.2), this contribution can be neglected compared to that by the background. Furthermore, the contribution of the system's dead time including the multiplicative effect due to the crystal's intrinsic activity can be neglected, because it only becomes important above an activity concentration of 10 kBq/μl. This level is usually never reached. For this estimation only the statistical fluctuations of the count

rates of background and the radioactive source are taken into account. The number of counts N_S caused by the sample only is therefore given by

$$N_S = N_T - N_B \tag{4.5}$$

where N_T is the total number of counts and N_B is the number of background counts. These numbers are always with respect to the dwell time. Using the square root of the mean values to calculate the standard deviations the overall uncertainty is given by

$$\sigma_{N_S} = \sqrt{\overline{N_T} + \overline{N_B}} \tag{4.6}$$

The relative uncertainty is therefore calculated by

$$E_{rel} = \frac{\sigma_{N_S}}{N_S} = \frac{\sqrt{\overline{N_T} + \overline{N_B}}}{N_T - N_B} \tag{4.7}$$

However, if the variable integration time is active, the relative uncertainty does not depend on a single measurement value but on the fluctuation of all measurement values covered within the current integration time. It is calculated by

$$E = \sigma / \overline{\hat{y}} \tag{4.8}$$

where σ is the standard deviation of the measurement values with respect to the linear regression function and $\overline{\hat{y}}$ the mean value of this regression function. Both terms refer to the current integration time. See section 3.4.2 for details. In figure 4.11 the relative uncertainties with and without variable integration time for two different measurements are displayed. All curves show a kind of inverse peak that results from the large numbers for N_T in equation 4.7. As the count rate decreases after the peak the relative uncertainty increases constantly if no variable integration time is active. In contrast, if the VIT function is active the relative uncertainty only increases slightly because the integration time is stretched as soon as the relative uncertainty gets larger. The corresponding measurement curves are displayed in figure 5.14 and 5.18.
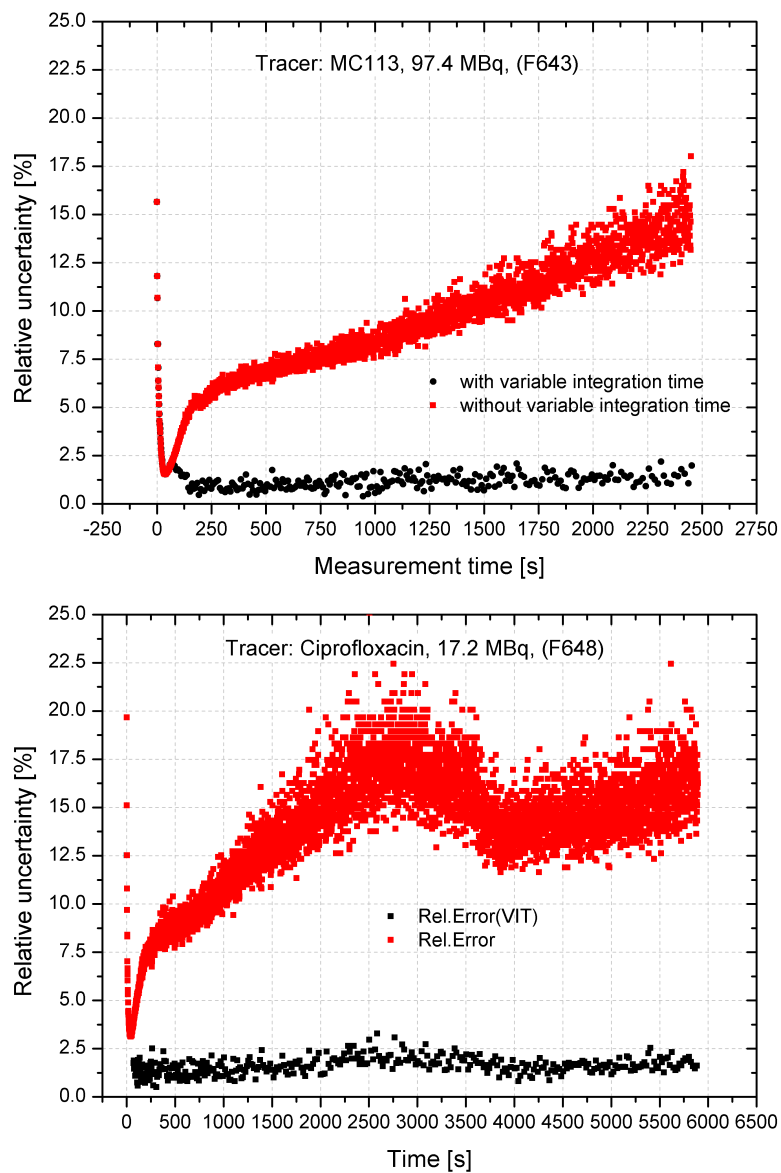
Figure 4.11: Differences between relative uncertainties depending on whether the variable integration time is active or not.

Chapter 5

Applications and Results

5.1   In-Vitro Measurements

After all hard and software components were ready for the first tests, several
in-vitro measurements were carried out before the instrument was used with
animals. For these measurements the radioactive tracers were either mixed
in NaCl or in blood. The setup was similar to that for in-vivo tests and
for the real application during PET scans. However, instead of an animal,
a 10 ml glass vial containing the active solution was used. These in-vitro
tests showed serious problems with lipophilic tracers in pump tubes due to
their adhesive behaviour at the inner tube walls (figures 5.2 and 5.3). As is
explained in detail in section 3.1.1 a combination of Teflon and pump tubes
which are primed with the corresponding inactive substance and flushed
thoroughly prior to each measurement solves the adhesive problems.

Even before these adhesive problems were detected, it turned out, that
the original measurement geometry TubeFix 2 cannot be used. The large
inner diameter of the Teflon tube (4 mm) would cause the clotting of the
blood because it takes quite a long time until it is filled during which the
blood would not move. For the same reason the timing information of the
time activity curve is reduced considerably. Apart from that, the handling
turned out to be complicated as the tube leading from the detector back
to the animal has to be thread through the detector before it is connected
to the venous catheter. Furthermore, efficiency and measurement volume of
the other tube fixtures (TubeFix 4, 5 and 6) had to be improved, since on
the one hand a high count rate is preferable to reduce statistical errors and,
on the other hand, a small measurement volume is required to offer exact
timing information in the activity concentration. All these points together
finally lead to the combination using a Teflon tube and a short piece of pump
tube inside the pump as well as to TubeFix 3, that is optimised for Teflon
tubes.

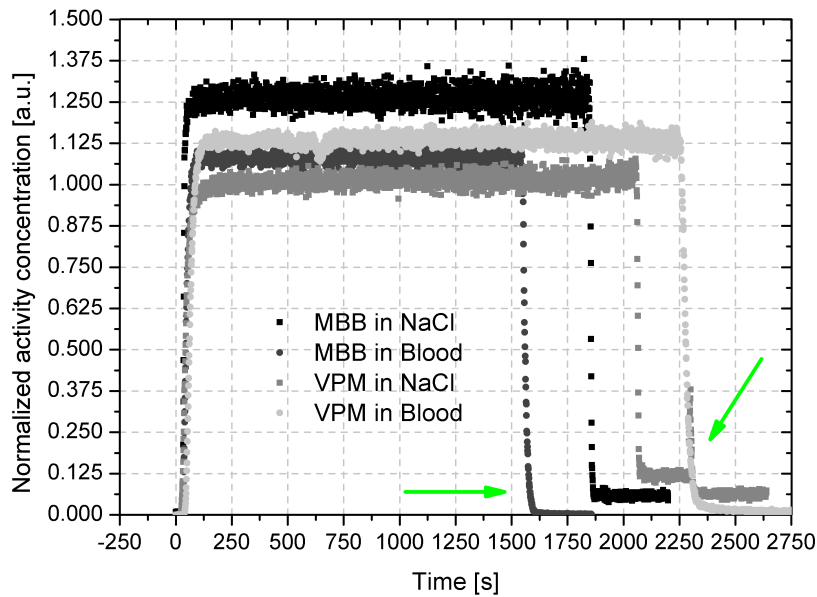Besides the conclusions for improving tubing and measurement geometry

Figure 5.1: Difference whether the tracer is transported within blood or in a NaCl solution. Even if the Teflon tube was primed before the measurement a small amount of active tracer remains at its walls if the transport medium was a NaCl solution. This problem vanishes if the transport medium is blood.

a small difference in adhesive matters between blood and NaCl solution was discovered. If the tracer is mixed in NaCl a small amount of active tracer remains at the inner walls although the tube is primed and flushed as described above. Only if the tracer is mixed in blood no adhesive effects can be observed. This can be seen in figure 5.1 where the TAC returns to 0 when using blood whereas it remains above 0 for NaCl.

After numerous and time intensive in-vitro tests the overall conclusion was a setup for each measurement, that has to meet the following requirements:

- The tubes have to be a combination of mostly Teflon and a small piece of pump tube.

- The measurement geometry (TubeFix) has to offer small measurement volume, optimized efficiency and easy handling.

- The tubes have to be primed with the respective inactive substance and to be flushed prior to each measurement.

- The transport medium in which the tracer is mixed should be blood.

Figure 5.2: In-vitro measurements using different kind of tubes and tracers in a 0.9% NaCl solution. For all measurements the tubes were primed with the respective inactive substance and flushed thoroughly. It is obvious that pump tubes cannot be used with lipophilic tracers such as $[^{11}C]$verapamil due to their adhesive property. In contrast, hydrophil tracers like $[^{18}F]$FDG hardly cause any adhesive effects.
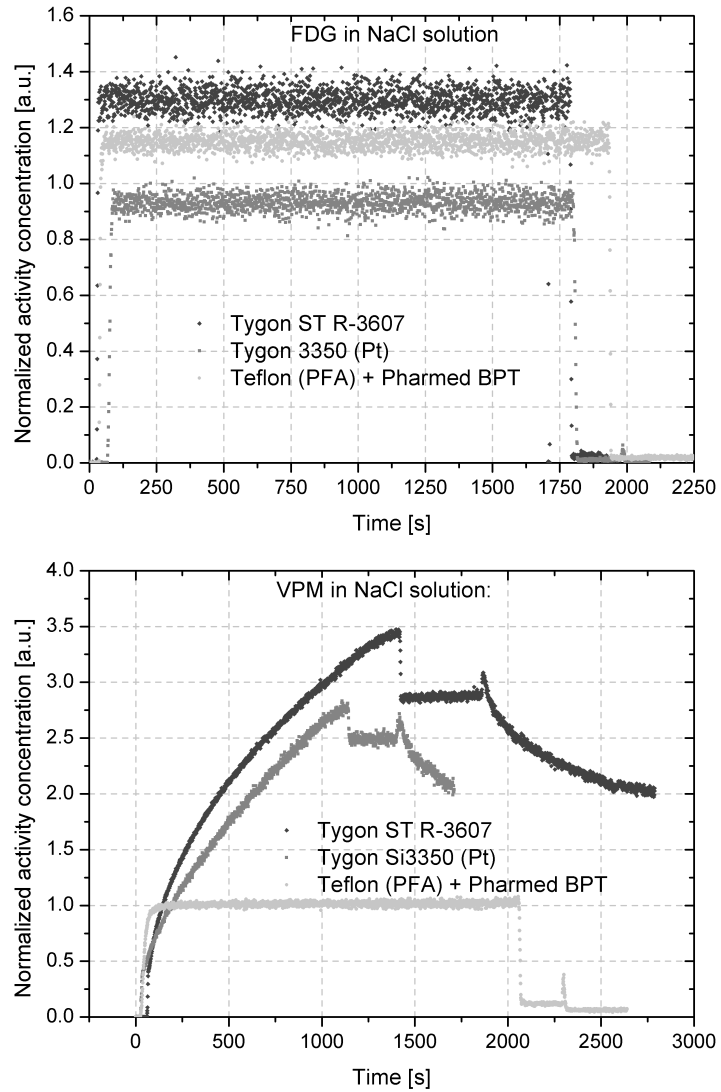
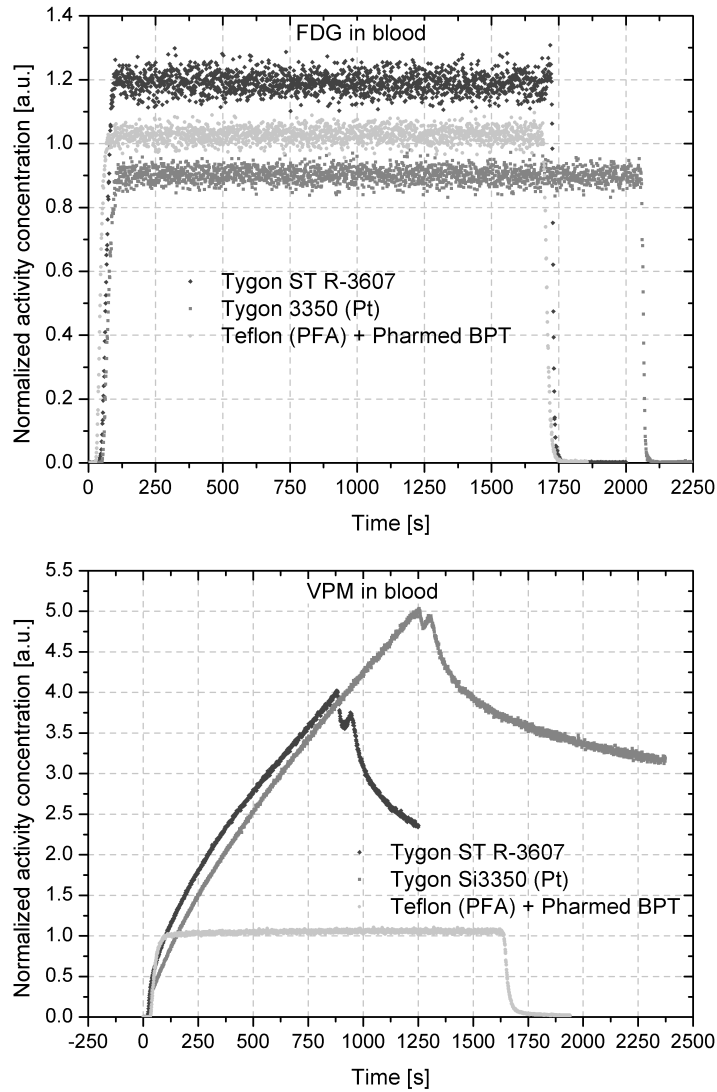Figure 5.3: In-vitro measurements using different kind of tubes and tracers in blood. For all measurements the tubes were primed with the corresponding inactive substance and flushed thoroughly. Even though [11C]verapamil has strong protein binding properties it is obvious that pump tubes cannot be used due to their adhesive behaviour. In contrast, hydrophil tracers like [18F]FDG do not cause any adhesive effects.

5.2 In-Vivo Measurements and Evaluation

After finally all in-vitro tests were performed successfully, the instrument was used to measure arterial input functions (AIF). For these studies within the *EURIPIDES* project adult female Spague-Dawley rats were used. The animals were kept under controlled environmental conditions ($22\pm1°$C, $40-70$ % humidity, 12h light-dark cycle) with free access to standard laboratory animal diet and water. This study was approved by the local Animal Welfare Commitee (LF1-TVG-34/048-2008). All procedures were performed in accordance with the Austrian Animal Experiments act.

Within this section first a detailed description of the experimental setup and investigation procedure of the in-vivo tests will be given. Subsequently, the setup and procedure of the investigation during PET scans will be explained. Finally, all in-vivo measurements were used for the evaluation of COBALT by comparing the results of this instrument with those recorded by manual sampling. Due to the similar setup and procedure of the measurements for the in-vivo tests and for the final PET scans the measurements are independent whether they are recorded during a test or during an actual PET scan. The results are therefore summarised in one section (5.2.3).

5.2.1 Experimental Setup and Measurement Procedure

Before a measurement starts the animal is placed in a chamber that is flooded with oxygen containing 2% isoflurane. After the animal has lost its consciousness it is taken out of the chamber and connected to a mask to be kept under anaesthesia by a humidified gas mixture with 0.6 to 1.8% isoflurane (depending on the depth of anaesthesia). The catheter tubes (S-54-HL made of tygon, inner diameter = 0.508 mm and outer diameter = 1.524 mm) are inserted into the animal's femoral vein and artery leaving the ends open for now. In order to prevent the blood from clotting in the catheters, the animals are administered with 0.9% aquaous saline solution containing 20 IE/ml sodium heparin. The detector tubing system is mounted at the pump and within the detector as shown in figure 5.4. However, is is not yet connected to the catheder tubes but to a vial containing the 0.9% aquaous saline solution which is pumped in circles. Shortly before detector tubes and catheder tubes are connected the pump is stopped and the Teflon tube between pump and animal is connected to the arterial catheder tube. The pump is then started again immediately and the saline solution is collected in a vial until blood reaches this open end. The pump is then stopped a second time for only a few seconds and the Teflon tube between detector and animal is connected to the veneous catheder tube. After the pump is turned on again, a arterio-venous shunt with a continuous blood flow-through the detector is established. For the connection between Teflon and catheder tubes the same hollow needles are used as for the connection between Teflon and pump tubes. However, in

this case no glue or additional fixing is used because this connection has to be disconnected for manual blood sampling.
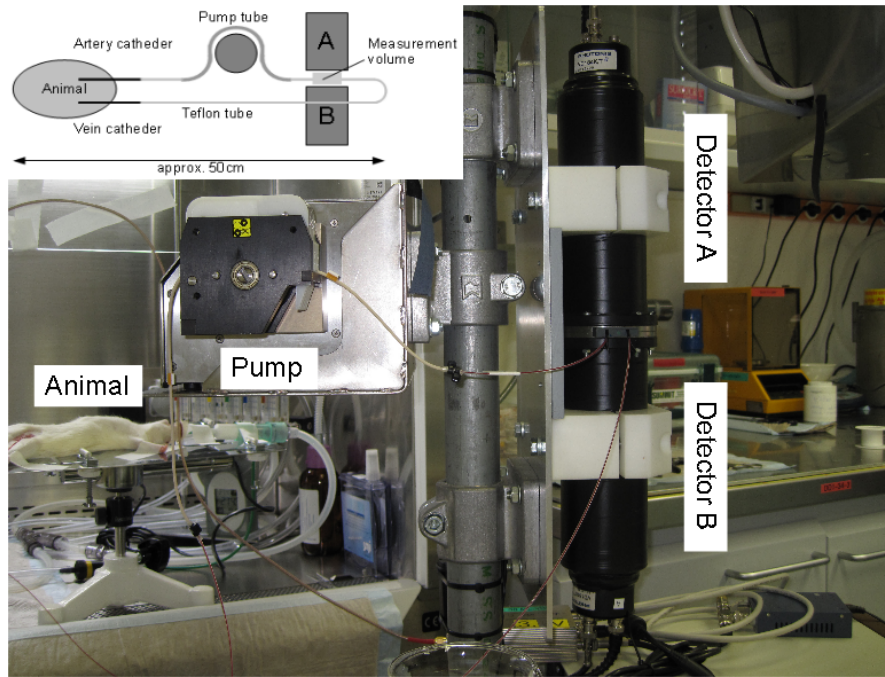

Figure 5.4: Experimental setup of the in-vivo tests. At the left top a schematic sketch of this setup is displayed.

To inject the radioactive tracer the shunt is disconnected at the venous side. The radiotracer is then injected into the animal via the venous catheter tube within approximately 50 seconds. Subsequently, the injection channel is flushed with a NaCl solution in order to administer as much tracer as possible. Finally, Teflon and catheter tube are connected again. The syringe is measured for its activity before and after the injection. The difference is the amount of tracer administered to the animal. The beginning of the injection is also the moment the user should push the `Start Inj` button of the measurement system (see section 3.4.1). To evaluate and calibrate the system the Teflon tube was disconnected from the arterial side of the catheter tube and manual blood samples were taken. For the first three minutes after injection every $2-3$ seconds samples consisting of around 20 μl were collected within sample tubes. After 5, 10, 20, 30, 40, 50 and 60 minutes further samples were taken each consisting of around 40 μl. The sample tubes were weighted before and afterwards. The blood volume of each sample is then simply given by the difference and the density of blood. The radioactivity within each sample tube is measured in a Wallac gamma counter which was cross calibrated with the PET scanner. For each sample a time stamp is taken using a pedal button which triggers a special software recording time

and duration of the sample collections. The values recorded by the gamma counter are corrected for the half-life of the isotope with respect to the time stamps. The half-life corrected activity concentrations together with their time stamps finally yields the manual AIF.

5.2.2 Experimental Setup and Procedure for PET Scans

After all in-vitro and in-vivo tests were performed successfully COBALT was used for recording the AIF during a PET scan as initially planned. The instrument was placed as close as possible to the scanner to keep the blood volume outside the animal small (figure 5.5). In order to confirm the results of the in-vivo tests and to make sure that setup and procedure works well during a PET scan the measurement was controlled again by manual sampling.
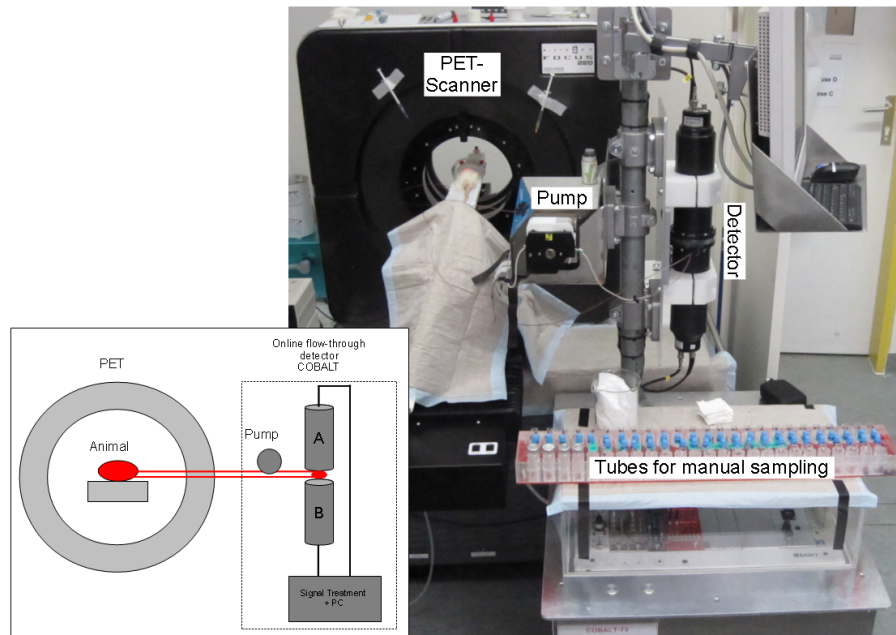
Figure 5.5: Experimental setup for recording the AIF during a PET scan.

5.2.3 Results

Within this section the results of the in-vivo tests and measurements during PET scans are collected and displayed in the diagrams 5.8 to 5.18. The input functions of both measurements (online flow-through detector COBALT and manual sampling) show good correlation for all tracers and most of the measurement time. However, as some figures show, the AIF recorded by manual sampling sometimes contains incorrect measurement values during

the peak shortly after injection. These uncertainties are mostly due to the small blood samples collected in the sample tubes leading to low count rates and small differences in weight of the sample tubes. The calculated activity concentration therefore contains larger statistical uncertainties.

The results also show differences in the behaviour of the tracer in the animal's body. For example, [^{11}C]mephobarbital and [^{18}F]FDG are less absorbed by the animal's organs and therefore remains more in the blood than [^{11}C]verapamil or [^{11}C]tariquidar do. To check again if the problems concerning adhesive behaviour of the tracer at the inner wall of the tubes are solved, the Teflon and catheter tubes were disconnected after the measurement was finished and the system was flushed with heparin solution. Because the measurement values fall off to background level immediately, obviously no tracer is left at the tube walls.

Each diagram contains a zoomed part in which the first minutes of the measurement is displayed in detail. This offers a much more detailed information about the TAC. It also shows how useful the variable integration time can be. Due to the small amount of radioactive tracer administered to the animal the software had some difficulties in analyzing the data (figure 5.15 and 5.16). The variable integration time was therefore activated later by the control function than usual (after 100 and 250 seconds, respectively) which caused a larger statistical fluctuation of the values up to these points. For the measurement displayed in diagram 5.17 the settings in the software were too less sensitive by that time to recognize the decrease of the activity concentration. The smoothing function was not started therefore. The software was corrected later on by changing the subroutine that controls the decrease of the measurement values after the peak.

Another advantage of COBALT is its better sensitivity as can be observed in figures 5.11 and 5.18. Both measurements show a slight increase of their TAC (at 170 s in the first and at 3,500 s in the second measurement) which cannot be observed by manual sampling.

In addition to each TAC the relative uncertainties for each measurement point are displayed separately. The values for these uncertainties related to TACs recorded by COBALT are calculated using equation 4.8 if the VIT is active or 4.7 if the values are not smoothed. The uncertainties of the results acquired by manual sampling are calculated always by equation 4.7.

Besides optical comparison of the TACs recorded by manual sampling and the flow-through system the values for the AUC and for the peak activity concentration can be used for more detailed analyses. The first value corresponds to the numeric integral over the measurement period while the second value is the maximum of the TAC. Table 5.1 summarises the values of the AUC and peak height for all in-vivo measurements. Furthermore, the relative differences between both methods are listed for those values. The mean of the relative differences of the AUC values is $-7.9 \pm 8.0\%$ and that of the peak values is $0.9 \pm 7.1\%$, respectively. In figures 5.6 and 5.7 the

Tracer	Nuclide	Act.	Act.	Inj. Time	AUC manual	AUC COBALT	AUC Diff.	Peak manual	Peak COBALT	Peak Diff.
		μCi	MBq	s	kBq/μl·h	kBq/μl·h	%	Bq/μl	Bq/μl	%
VPM	^{11}C	1566	57.9	25	188.3	170.6	-9.4	814.6	901.7	10.7
VPM	^{11}C	867	32.1	57	145.9	117.5	-19.4	649.2	618.4	-4.7
TQD	^{11}C	1124	41.6	23	137.6	142.2	3.3	1125.4	1005.0	-10.7
TQD	^{11}C	1073	39.7	46	148.9	121.4	-18.5	752.3	753.5	0.2
MBB	^{11}C	1490	55.1	28	655.1	636.7	-2.8	1810.5	1668.3	-7.9
MBB	^{11}C	1557	57.6	40	606.4	531.3	-12.4	1046.2	1048.1	0.2
MC113	^{11}C	2631	97.3	55	381.5	365.7	-4.1	1852.5	2056.4	11.0
FDG	^{18}F	187	6.9	61	159.8	147.9	-7.4	242.3	248.4	2.5
CFX	^{18}F	314	11.6	55	134.1	132.7	-1.0	267.4	286.7	7.2
CFX	^{18}F	149	5.5	80	42.7	35.7	-16.4	113.7	117.3	3.2
CFX	^{18}F	466	17.2	37	219.8	223.8	1.8	488.0	477.2	-2.2

Table 5.1: Summary of the results of all in-vivo measurements. The table compares the AUC and the peak heights of the TAC recorded by manual sampling and the online flow-through system COBALT for different tracers and injected activity.
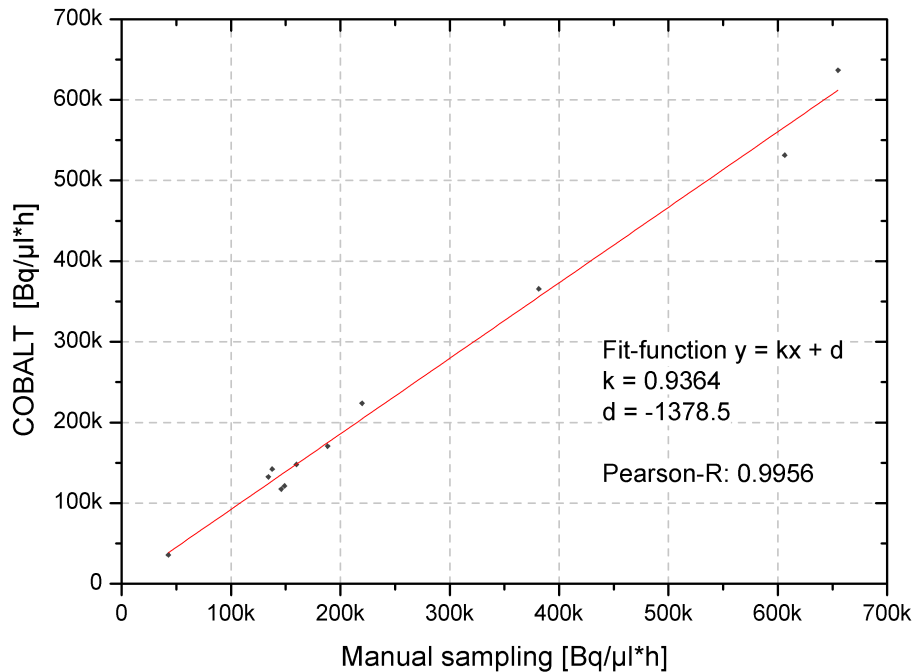
Figure 5.6: Correlation of the AUC values for all in-vivo measurements performed by the online flow-through system COBALT and by manual sampling.
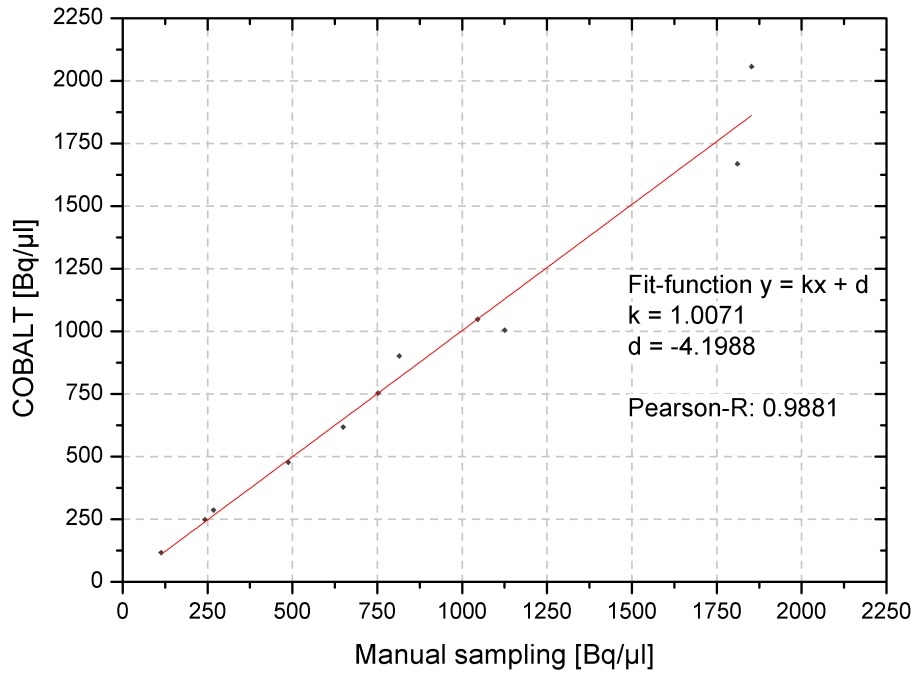
Figure 5.7: Correlation of the peak heights of the TACs for all in-vivo measurements performed by the online flow-through system COBALT and by manual sampling.

AUC and peak values of both methods are compared for each in-vivo measurement. The slope of the linear regression function as well as the Pearson coefficient R[1] are both close to 1. This proves a good correlation between the different methods for recording the arterial input function.

---

[1] The Pearson coefficient is a dimensionless number, which describes the linear correlation between two variables
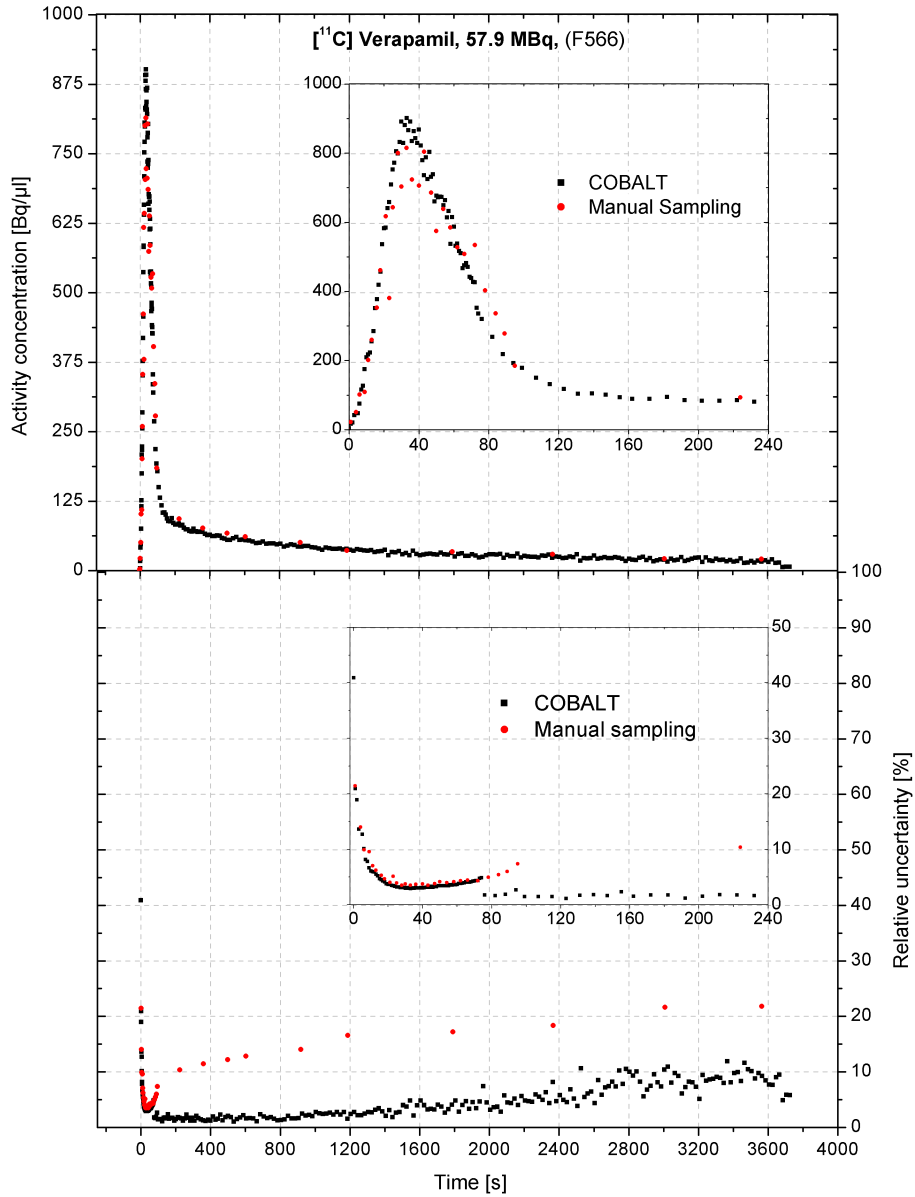
Figure 5.8: Arterial input function of the radiotracer [11C]verapamil.

Figure 5.9: Arterial input function of the radiotracer [^{11}C]verapamil.

Figure 5.10: Arterial input function of the radiotracer [^{11}C]tariquidar.

Figure 5.11: Arterial input function of the radiotracer [^{11}C]tariquidar.

Figure 5.12: Arterial input function of the radiotracer [^{11}C]mephobarbital.

Figure 5.13: Arterial input function of the radiotracer [^{11}C]mephobarbital.

Figure 5.14: Arterial input function of the radiotracer [^{11}C]MC113.

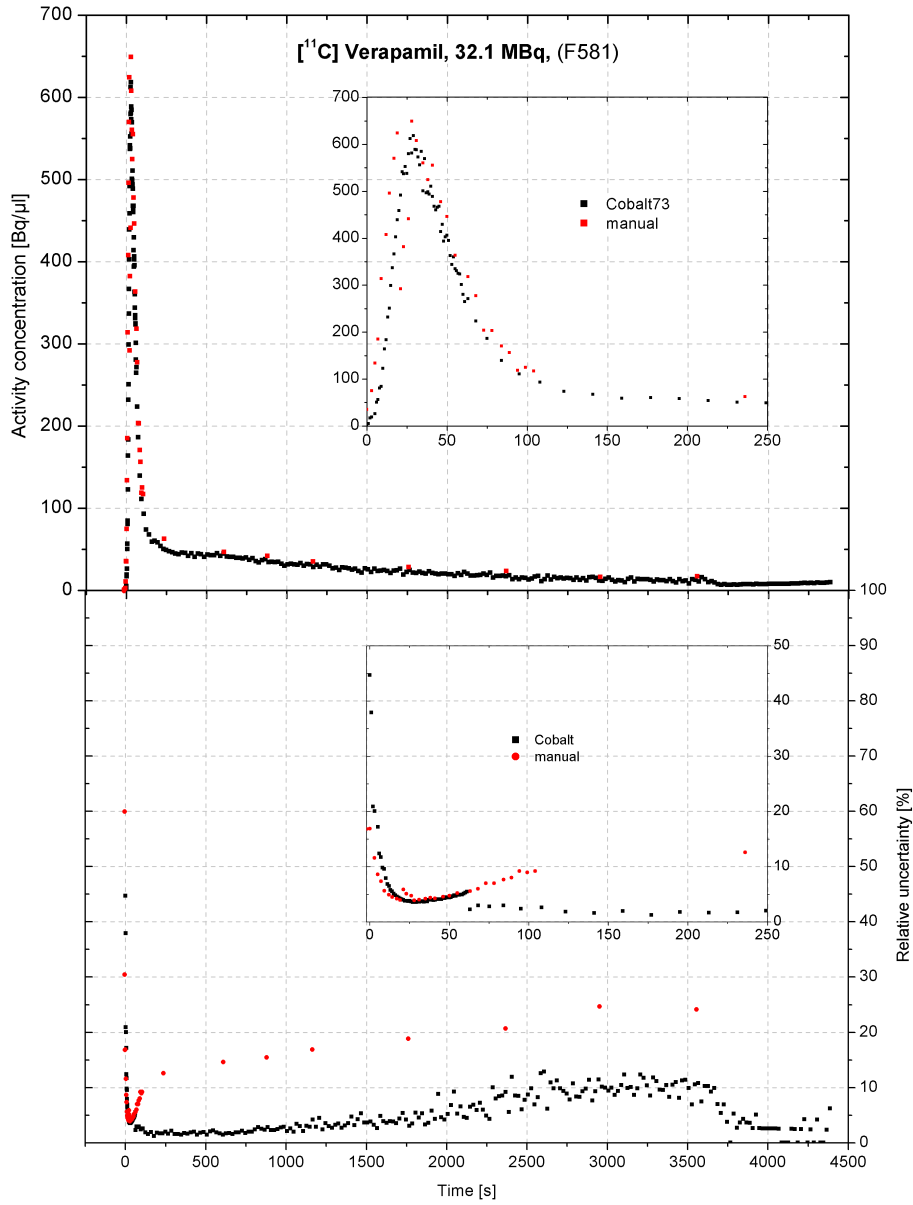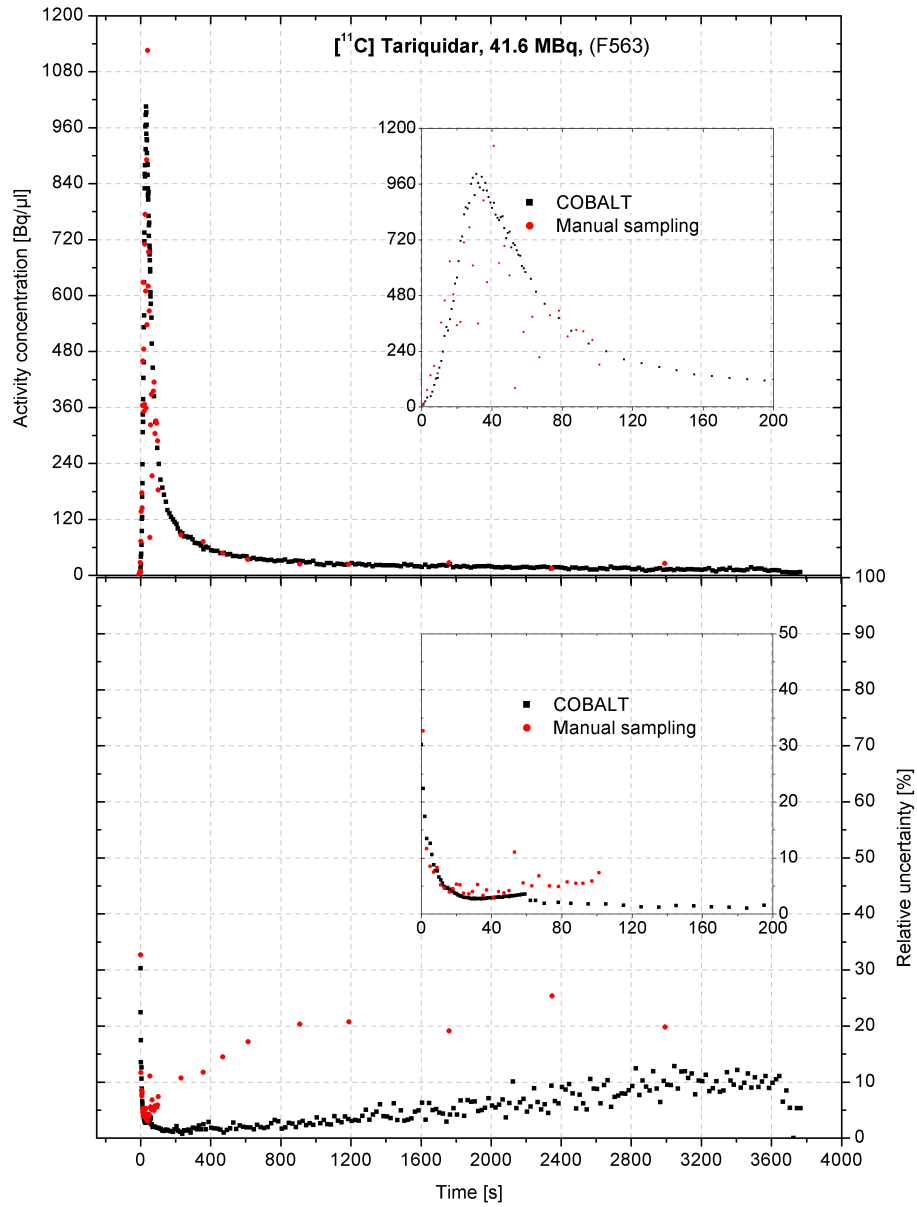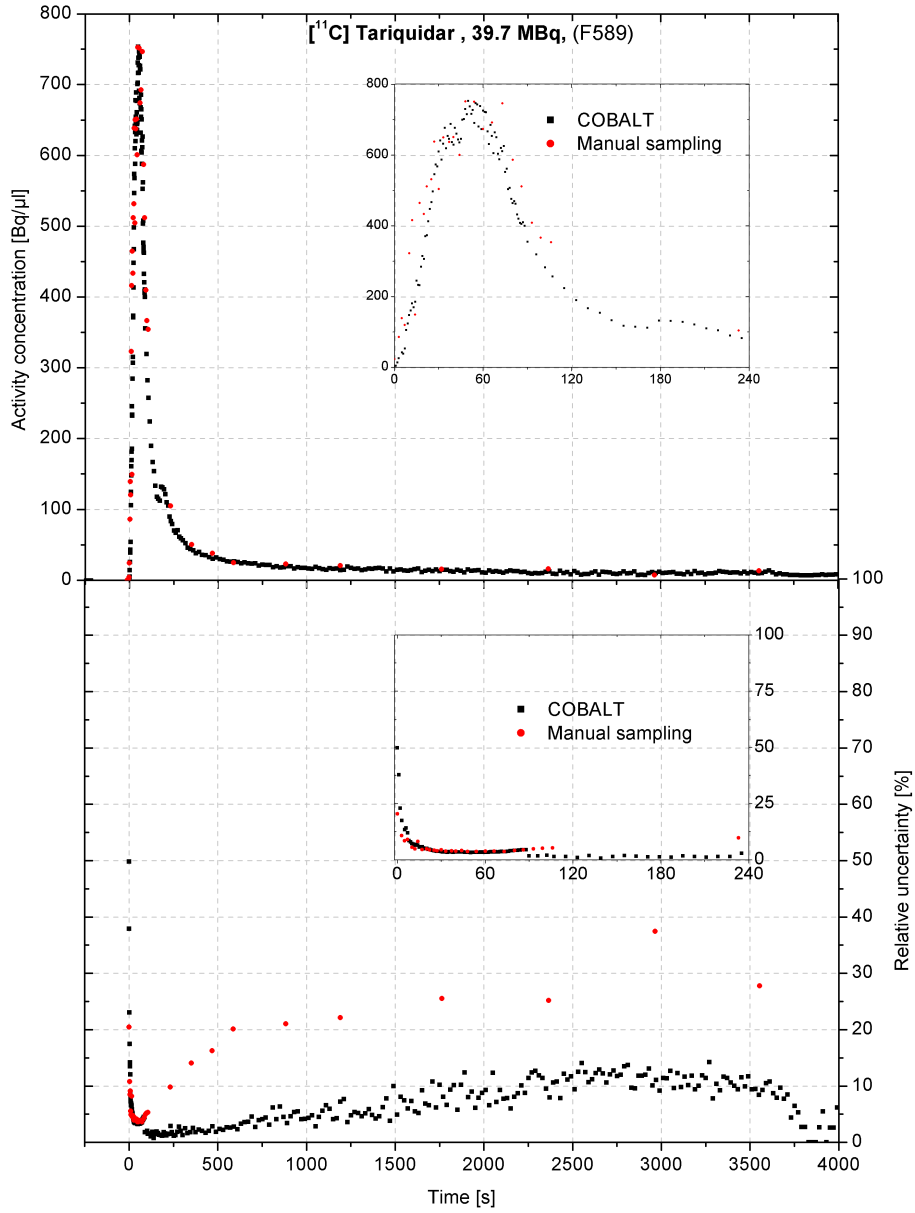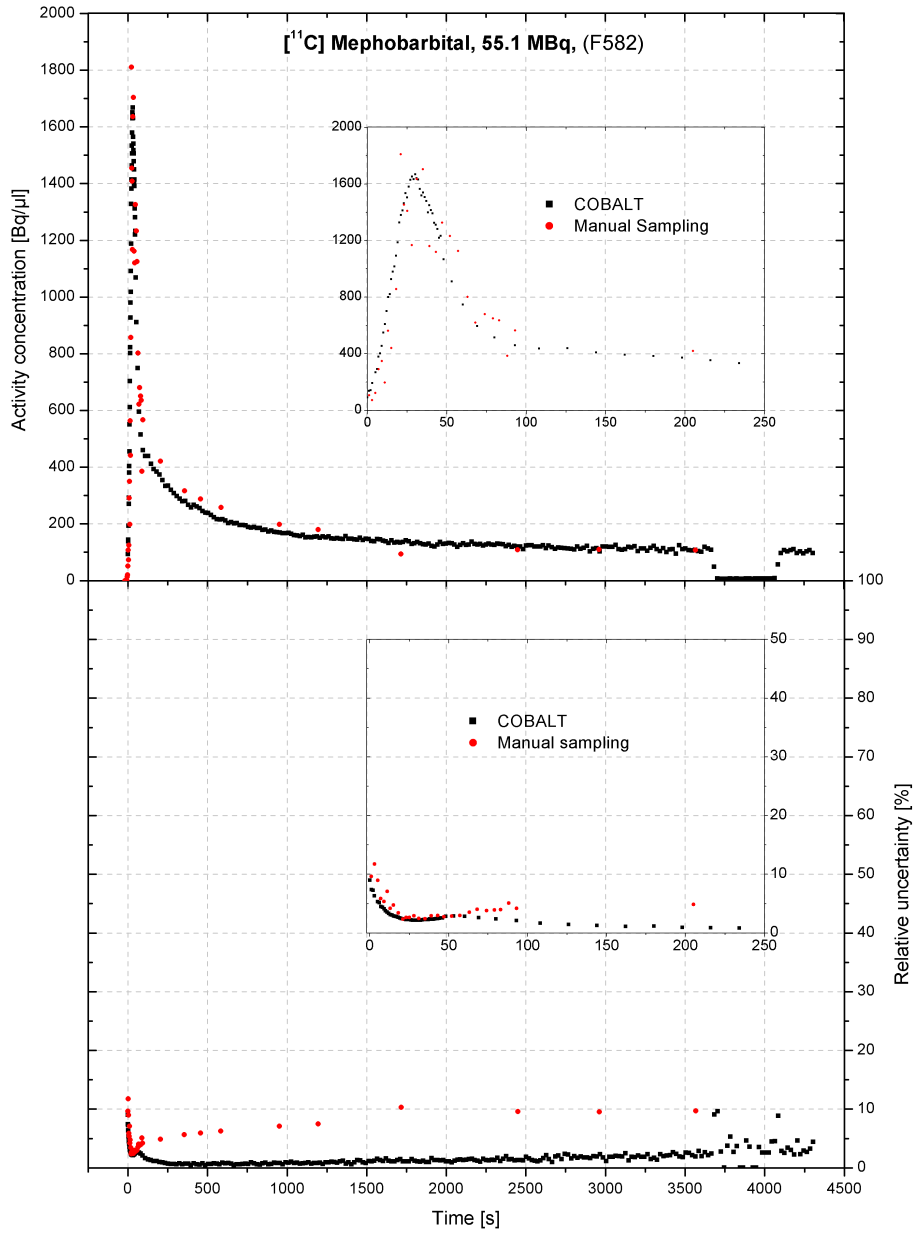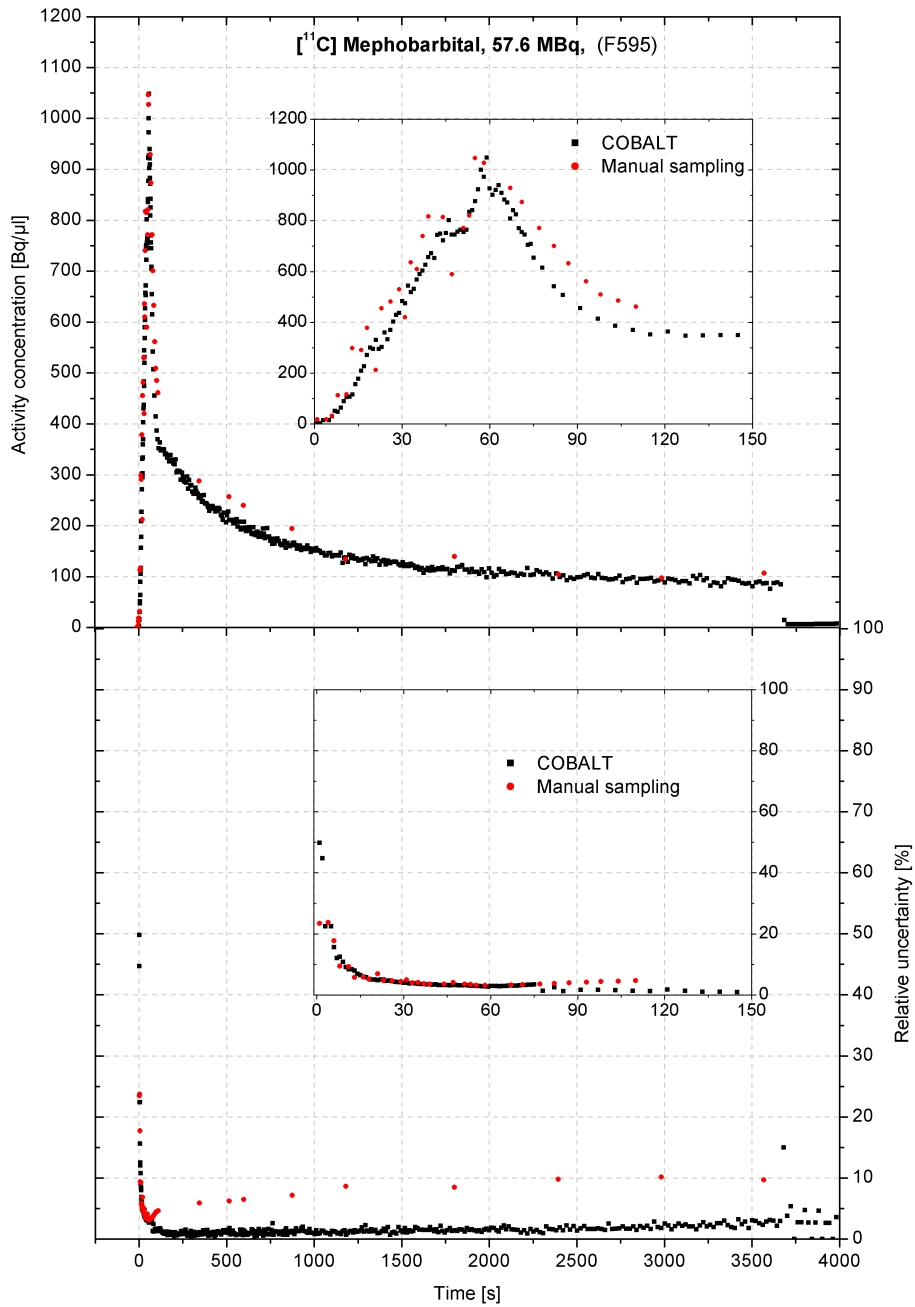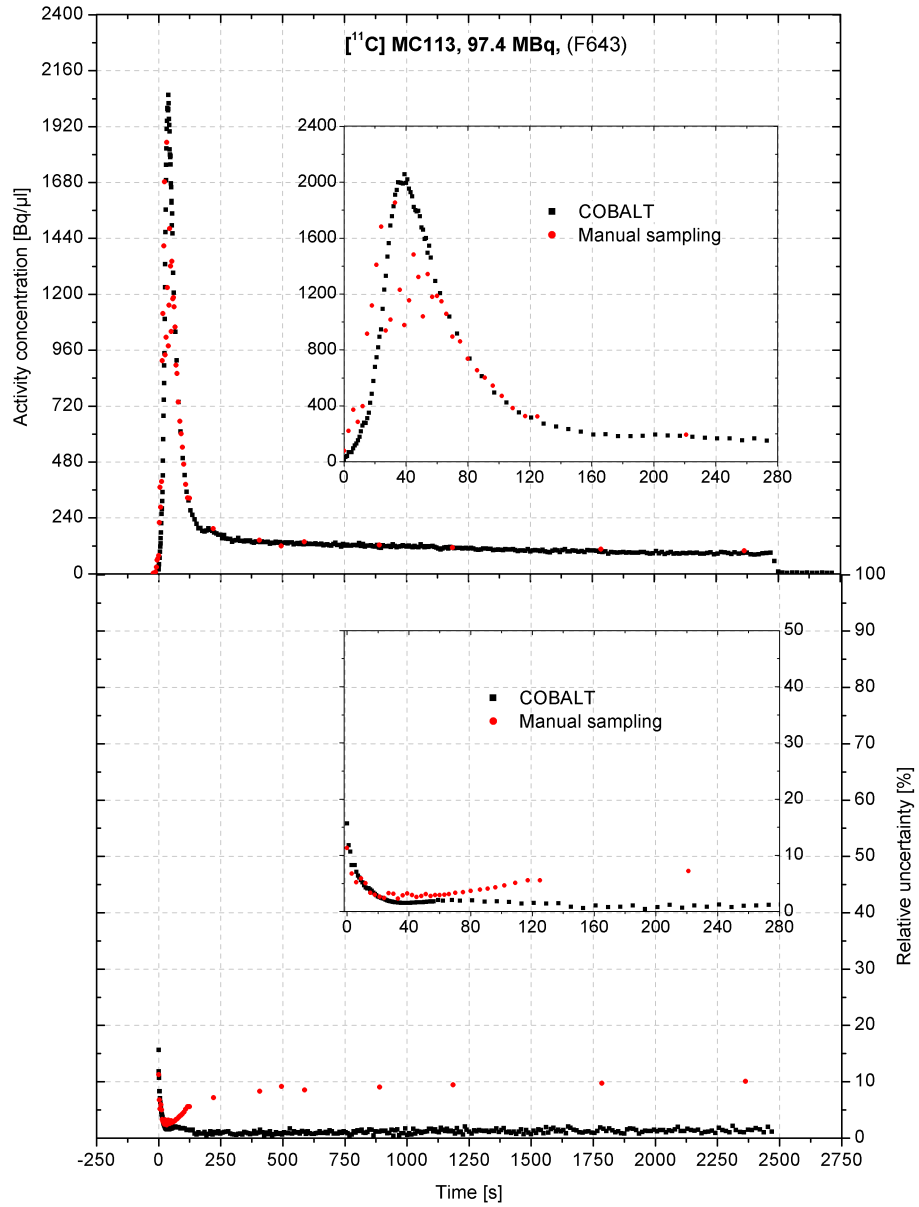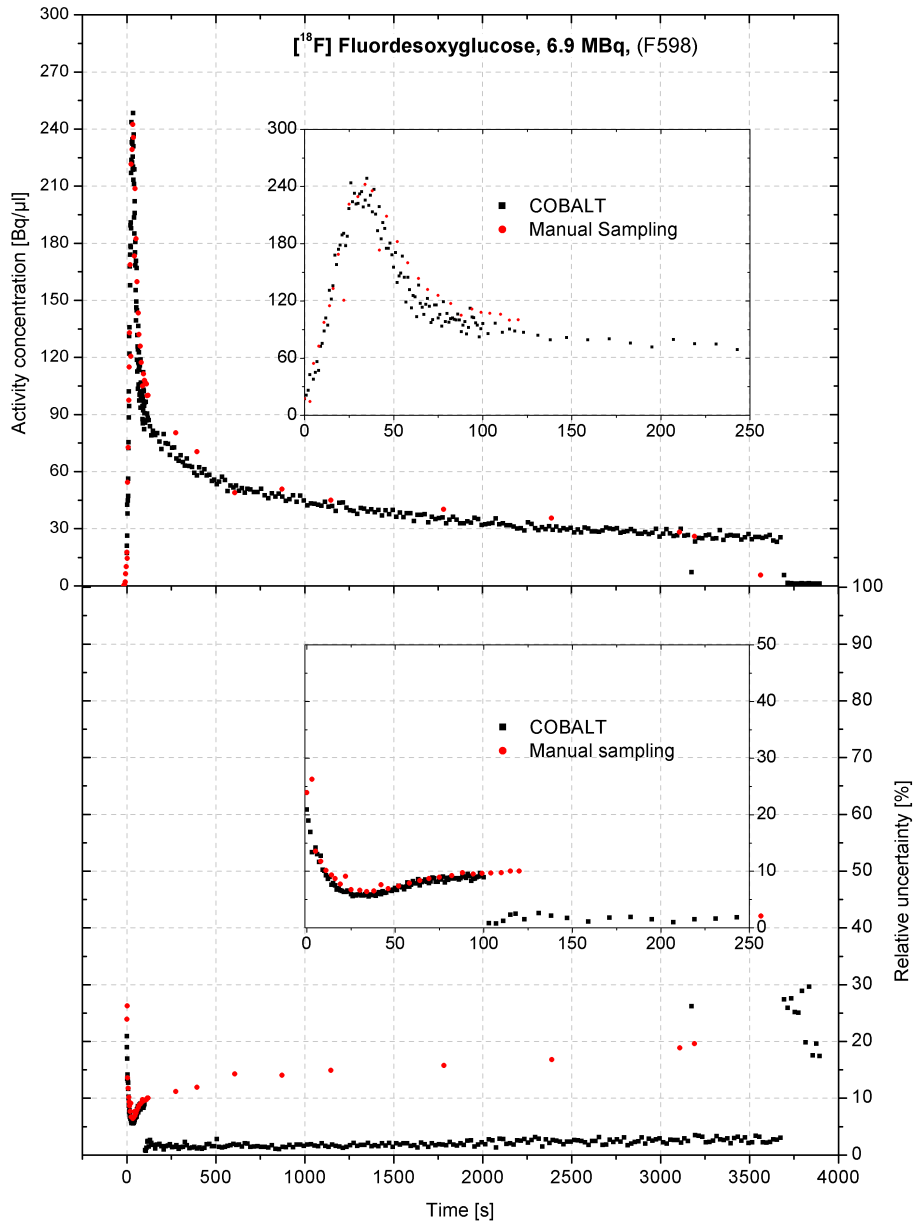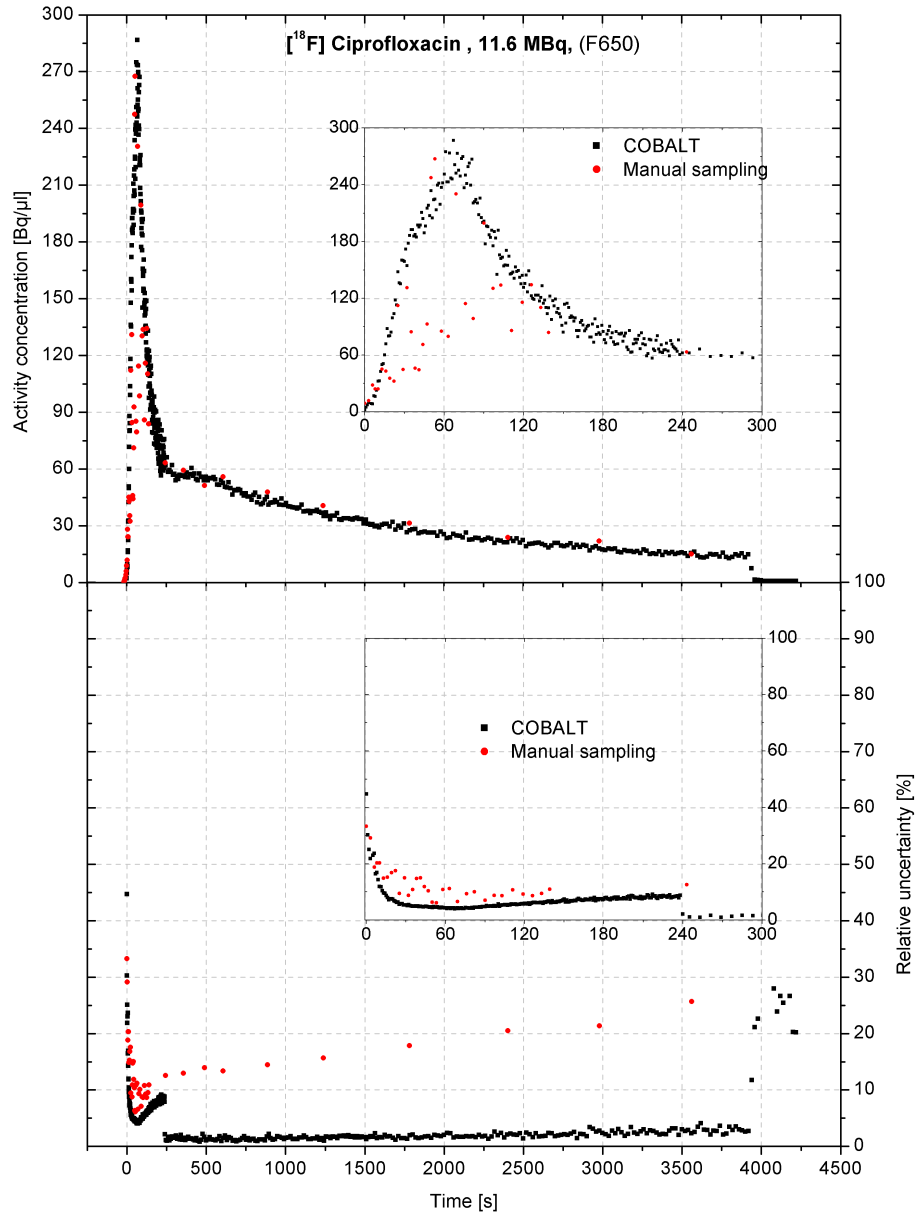Figure 5.15: Arterial input function of the radiotracer [^{18}F]fluordesoxyglucose.

Figure 5.16: Arterial input function of the radiotracer [^{18}F]ciprofloxacin.
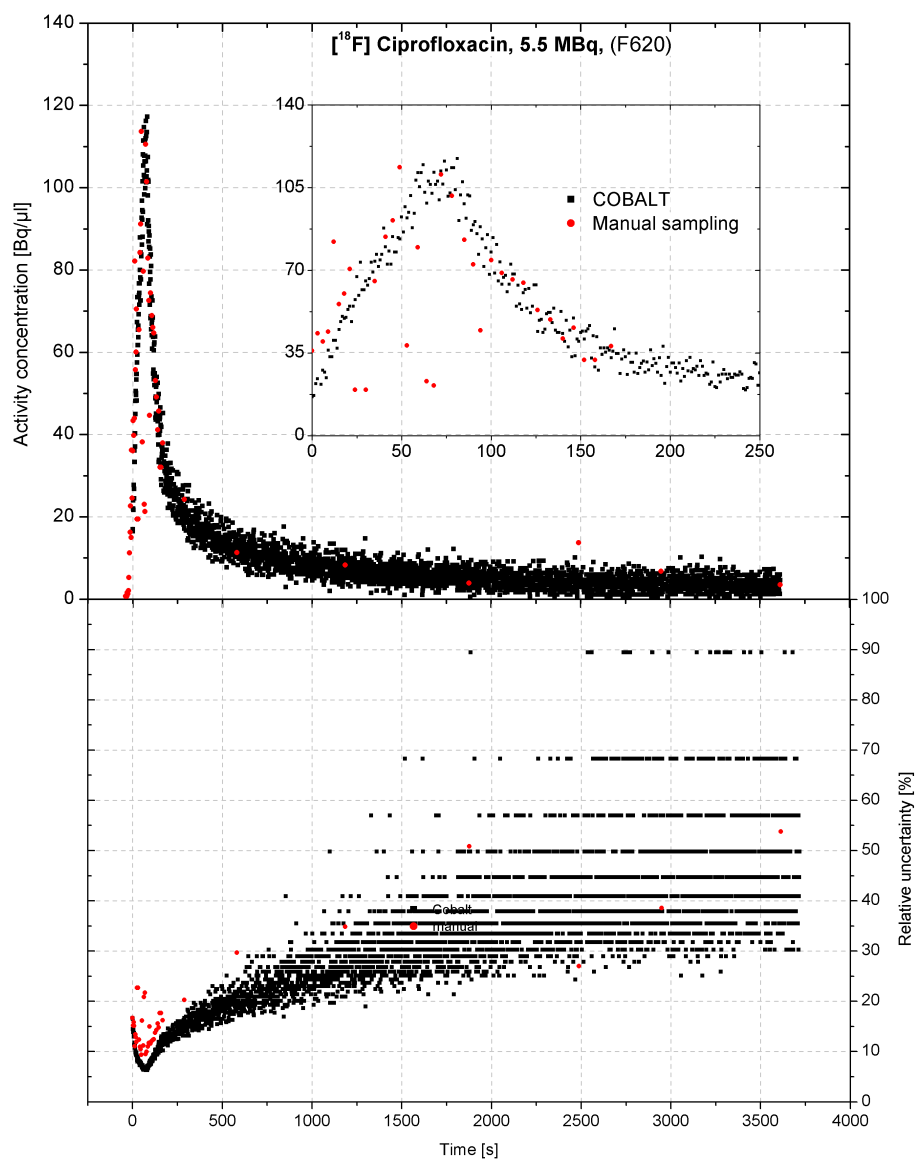
Figure 5.17: Arterial input function of the radiotracer [^{18}F]ciprofloxacin.
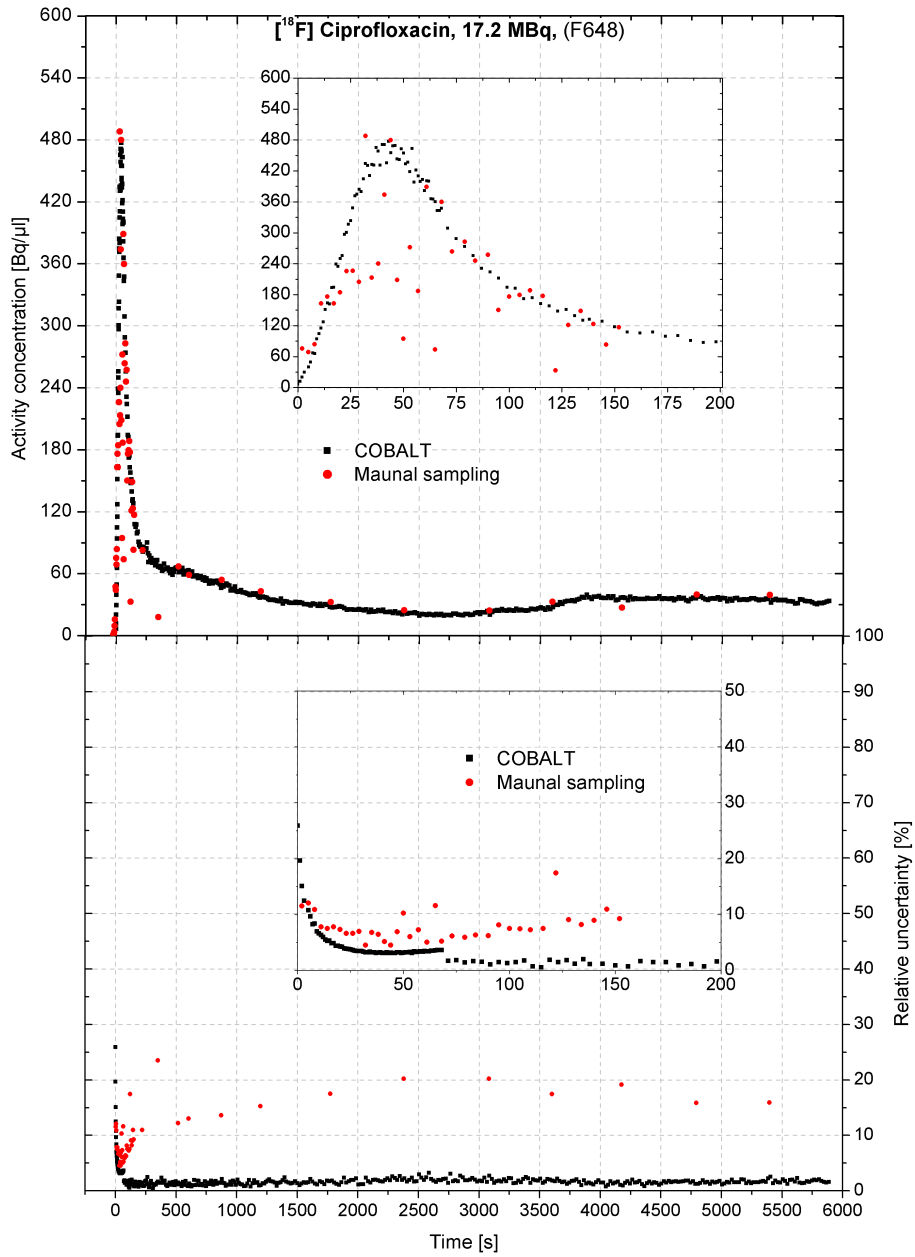
Figure 5.18: Arterial input function of the radiotracer [^{18}F]ciprofloxacin.

Chapter 6

Alternative Detector Systems

To compare the performance of the COBALT system with other detectors
and instruments further methods to acquire the input function had been
investigated. One alternative system is similar, however, instead of LYSO
crystals two plastic scintillators are used. PMT and electronics were also
changed in order to provide optimised signal production and treatment. The
other alternative method was to detect the positrons directly using a semi-
conductor detector. Both detectors, however, were analysed only just to get
an idea if it is worth to consider any further tests.

6.1 Plastic Scintillator

The setup of this system is similar to that using LYSO crystals to detect
both annihilation photons. However, instead of 1 inch $\times$ 1 inch LYSO crys-
tals two 2 inch $\times$ 2 inch plastic scintillators are used to produce scintillation
light. One is self assembled using PMT and base by *Hamamatsu* while the
latter one is a *Scionix* 51RB100/2M-HV-P-X-N. Compared to LYSO crys-
tals plastic scintillators have two advantages: Their decay time is shorter
and they are not self-active. However, as the results show, the disadvan-
tage of very low stopping power due to the low electron density can not be
compensated. Because the probability for a gamma quantum to interact
with material via the photo effect decreases rapidly with decreasing atomic
number only Compton scattering occurs. Consequently, the analogue output
signal of the detector does not contain any information about the energy of
the detected radiation. Moreover, a large part of the gamma radiation does
not interact with the scintillation material at all. The efficiency is therefore
much smaller than for scintillation crystals. For a point like source placed in
the center of the measurement volume a coincidence efficiency of 2.3 % was
measured (figure 6.1). In contrast, the same geometry using LYSO detectors
offers a coincidence efficiency of 7.9 %. The effective coincidence efficiency
was determined to be 2.2% using $[^{18}F]$FDG dissolved in a NaCl solution. Al-
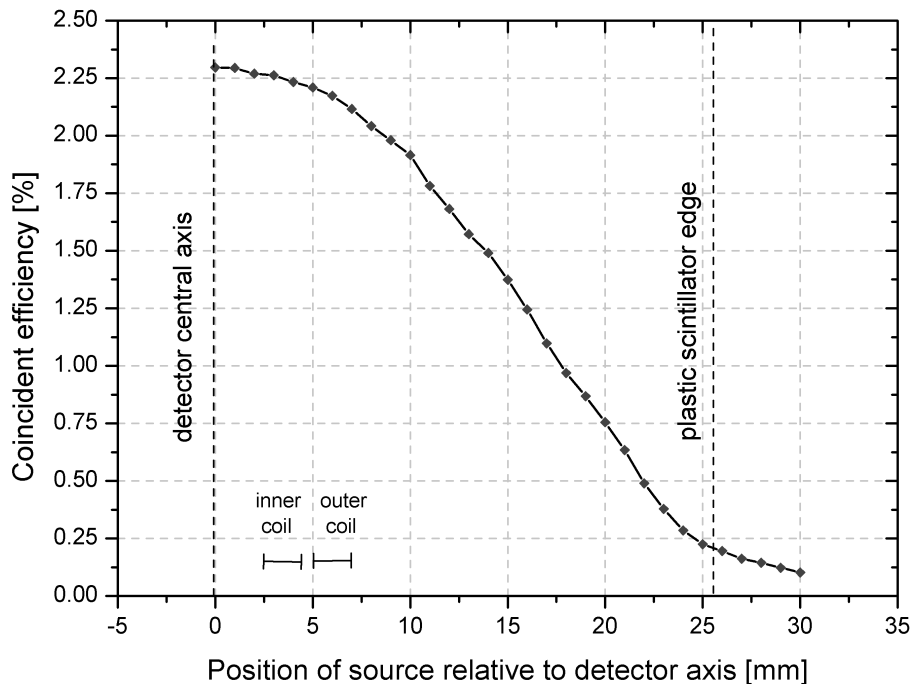
Figure 6.1: Coincident efficiency of a point like source depending on its position relative to the detector axis.

though the plastic scintillators are much larger, the efficiency is only one third compared the the LYSO system. Even if the plastic detectors are shielded in the same way as the LYSO detectors are, their sensitivity to interference by external sources (e.g. the animal) is much larger (compare figure 6.2 with figure 4.1). Besides their larger cross section, this fact is caused by Compton scattered gamma radiation in the lead and steel shielding. These photons lost a part of their energy due to Compton scattering and deposit at most the rest of their energy, which is always much less than 511 keV. This lower energy would be filtered in the signal treatment of the LYSO detectors. However, as described before, all signals of plastic detectors above noise have to be taken into account including those caused by perturbation source. Finally, the weight of the larger plastic detectors shielded as effectively as the LYSO detectors are would be approximately 30 kg each. The total weight of the detector system would therefore be over 60 kg. Since for easy handling it is necessary to place the measurement volume in the detector center and therefore the center of mass at about 150 cm above ground. However, the space of the trolley onto which both detectors have to be mounted is limited to 50 × 70 cm. This small base area combined with the heavy weight and the high center of mass would lead to a dangerous setup.

It was due to these three major problems why this measurement system was tested only briefly. No useful system was ever setup and no applications
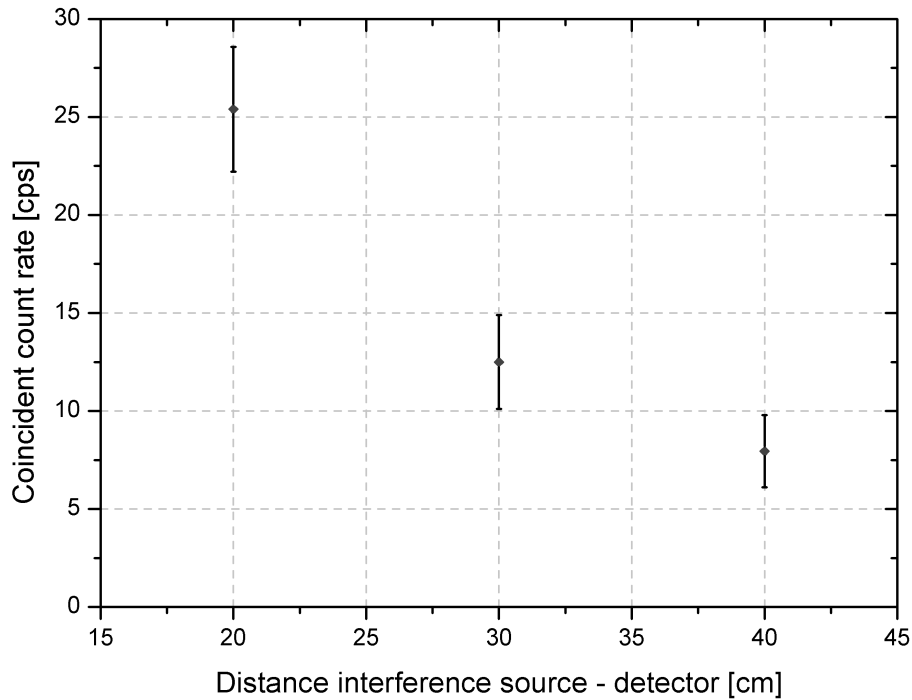
Figure 6.2: Error count rate due to a 185 MBq external interference source like the animal would be for example.

such as in-vitro and in-vivo tests were ever carried out.

6.2   Positron Detector

The measurement of the arterial input function via arterio-venous shunt requires a surgical procedure. In order to avoid this comprehensive prearrangement a method for direct and external detection of the positrons would be needed. This requires a positron sensitive detector with very thin detection surface being fixed onto the animal's skin. Furthermore, the detector should offer low sensitivity for gamma radiation, light and mechanical stress. To make sure enough positrons can be detected, an appropriate place has to be selected where an artery is next to the skin. In order to meet those requirements a recently developed *PIPS Detector* manufactured by *Canberra* was fixed at the upper end of the animal's tail. The signal treatment was performed using a Peltier cooled preamplifier (*CoolFet*) together with a digital Spectrometer (*DSPEC+, Ortec*). The signals were recorded by a special VBA based Excel application.

Although the measurement worked from the technical point of view, the enrichment of the tracer in the animal's tissue caused too much interference as is shown in figure 6.3. The arterial input function is superimposed by the
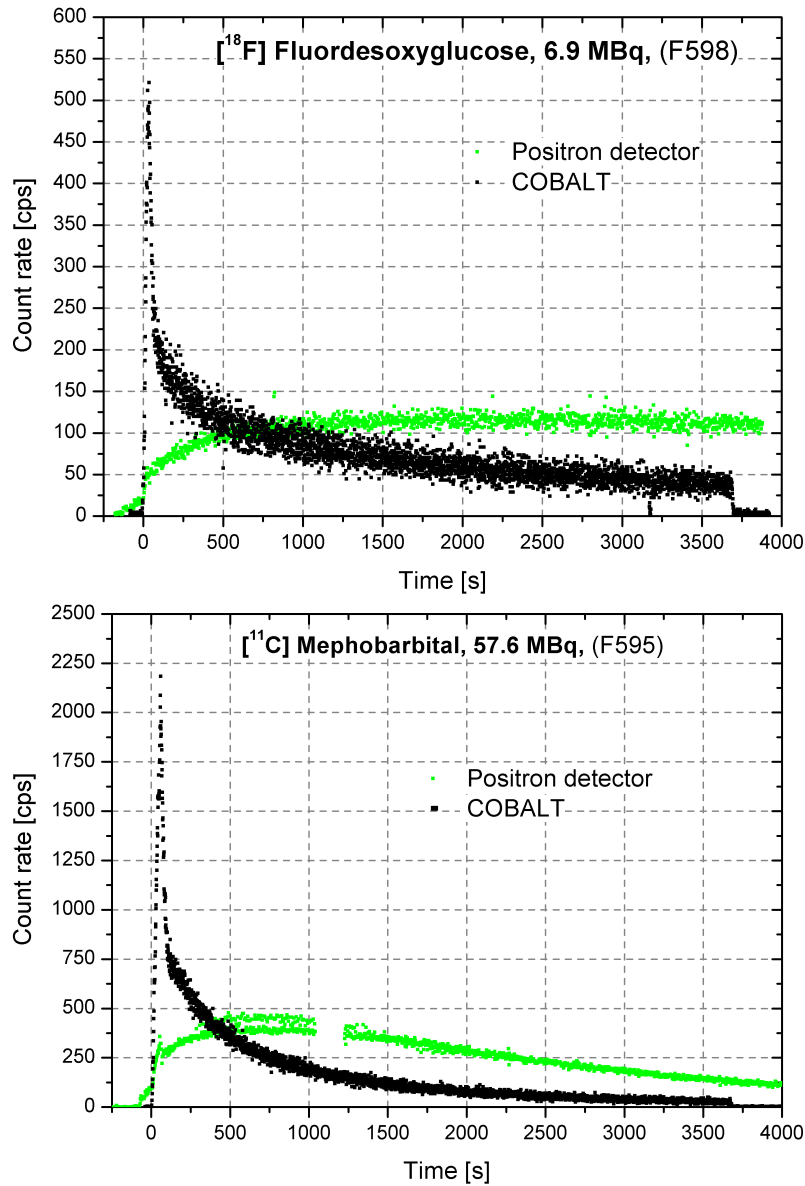
Figure 6.3: The comparison between the TACs recorded by direct positron detection and via flow through measurement. Obviously, both tracers are absorbed by the tissue leading to an enrichment of the activity which causes a strong interference.

Figure 6.4: Setup for direct detection of the positrons.

activity of the tissue right from the beginning of the measurement. Because this interference depends on the tissue which is different for each animal it will be very difficult to derive a function via which the measured TAC can be corrected to obtain an arterial input function.

Chapter 7

Discussion and Conclusion

This thesis describes the successful development of an online flow-through detector to record the arterial input function during PET investigations. The systems was named COBALT (Coincidence Online Blood Activity Level Tool) and offers high sensitivity as well as low background and is almost insusceptible to perturbation due to the animal. Due to the shielding by lead and steel and because the analogue detector signals are filtered by their energy and timing correlation the error count rate is reduced to 0.2 cps if the detector is exposed to an external 185 MBq ^{68}Ge source. The background count rate of 1.3 cps is almost exclusively caused by the intrinsic activity of the LYSO crystals. This fact limits the detection capability to a level between 0.4 and 3.1 Bq/μl depending on the isotope used for the investigation and the integration time. The efficiency of 6.5% agrees well to similar flow-through systems such as the pico-count method which offers 6.9% [Votaw and Shulman, 1998]. In order to smoothen the TAC as the count rate gets lower due to the absorption of the active tracer by the animal the system offers a variable integration time. It starts after the peak when the count rate does not decrease strongly anymore and integrates between 4 and 20 measurement values. How many values are used depends on their statistical fluctuations. This smoothes the TAC after the peak and improves the detection capability. This variable integration time is controlled by a software especially written for this instrument. Besides this feature, it offers control of the recording of the data as well as the calculation of the input function based on these data and the settings chosen by the user. It furthermore displays and stores the TAC.

Because this system measures the activity concentration via an arterio-venous shunt the blood losses can be reduced to a minimum and is only due to the collection of blood samples for metabolite analysis. The external blood volume remains below 250 μl if the detector is placed not more than 50 cm away from the animal. This is much less than the losses were when the measurement was carried out by manual sampling (approximately

1.8 ml). The influence of the measurement to the animal is therefore kept to a minimum. The animal did not exhibit any adverse effects during the measurements. The arterio-venous shunt also offers easy access to the animal blood circuit to collect blood samples for chemical or biological analysis.

In order to provide accurate and reproducible results a measurement geometry was developed optimised for Teflon tubes. The tube is fixed in two coils each consisting of three layers. Since the tube can only be placed in one way within this tube fixture and because this fixture as well as the tube in this fixture cannot move, the geometry is stable during a measurement and can be reproduced for each new measurement. The small coils in the center of the detection system offer sufficient efficiency to provide large count rates to keep the statistical uncertainty low. On the other hand, the measurement volume is small enough to be filled quickly within a few seconds. This leads to detailed timing information within the peak of the time activity curve.

As is shown in chapter 5 and in contrast to other systems [Ingvar et al., 1991; Weber et al., 2002] COBALT works well for different tracers and over a wide range of activity administered to the animal. The lowest activity administered to the animal was 5.5 MBq while the highest one was almost 100 MBq. Four different ^{11}C tracers ([^{11}C]verapamil, [^{11}C]tariquidar, [^{11}C]mephobarbital and [^{11}C]MC113) as well as two ^{18}F tracers ([^{18}F]fluorodeoxyglucose and [^{18}F]ciprofloxacin) were used for the measurements. In order to solve the adhesive problems at the inner tube walls with lipophilic tracers a combination of pump and Teflon tubes was used. However, even this combination has to be primed with the corresponding inactive substance and flushed thoroughly prior to each measurement to avoid any tracer from adhering to the tube walls.

The system was evaluated by measuring the TAC simultaneously with the reference method of manual sampling. The results of the online flow-through detector accorded well to those recorded by manual sampling for all tracers and activities. Apart from the almost identical TACs the values for the AUC and peak height agreed well between both methods. The mean of the relative differences of the AUC values is $-7.9 \pm 8.0\%$ and that of the peak values is $0.9 \pm 7.1\%$, respectively. Furthermore, the Pearson correlation coefficients between both systems are close to 1 for both values. All these facts together prove, that this newly development offers results corresponding well to those measured by the former method of manual sampling. Besides the advantages already mentioned COBALT also causes less radiation dose for the experimentalists as no manual sampling is required.

Appendix A

Pump Performance

Figure A.1: Performance of the peristaltic pump using a pump tube with an inner diameter of 0.51 mm depending on the settings.
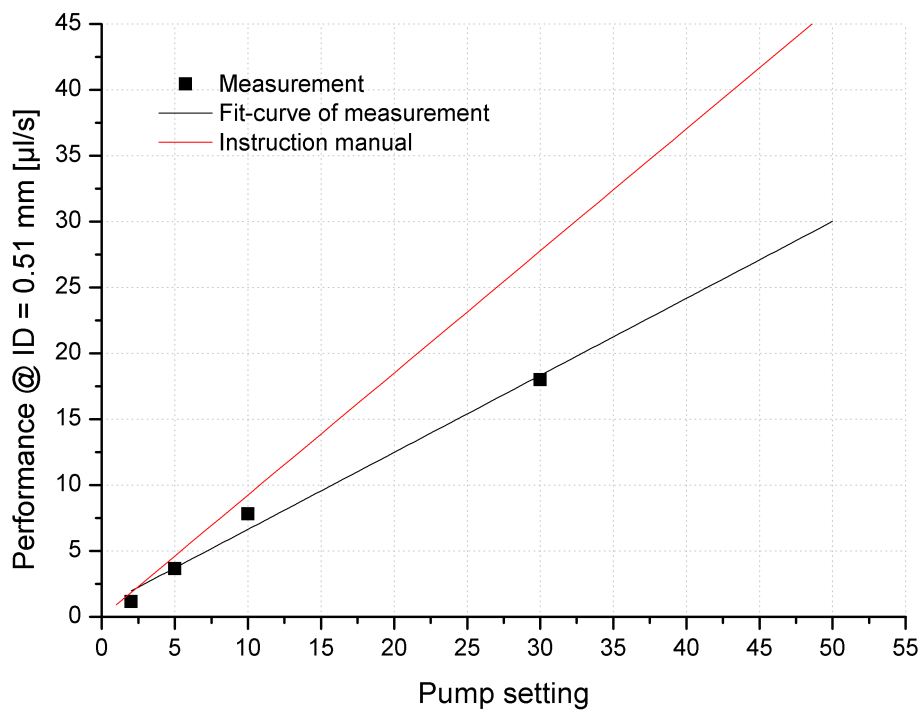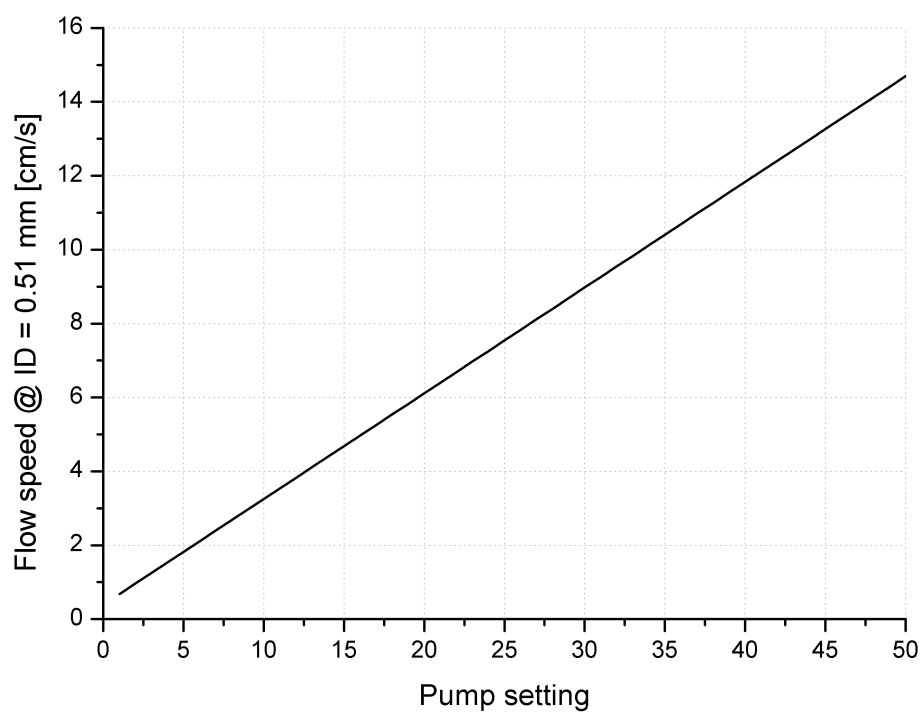
Figure A.2: Flow speed of the peristaltic pump using a pump tube with an inner diameter of 0.51 mm depending on the settings.

Appendix B

Software

The whole source code of the program covers over 3000 lines. Hence, only
the configuration file, a flow diagram and the two most important functions
are displayed.
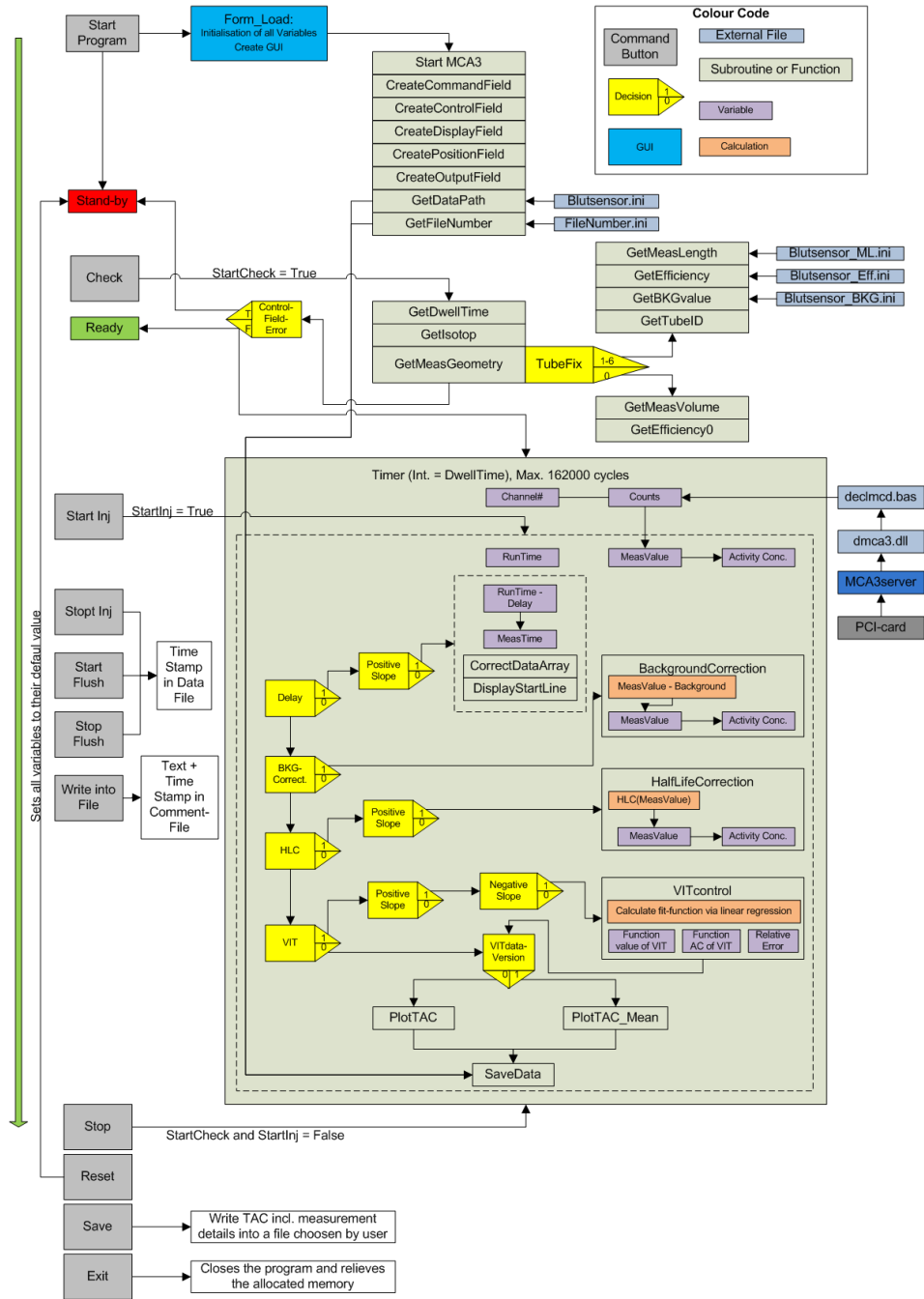
Figure B.1: Flowdiagram of the software.

B.1 Configuration File for the MCA3-Server Program

```
;Settings used by MCA3-Server to acquire the TAC
;================================================
;System-settings
;---------------
;sysdef=0
;gate=0
;coin=0
;diguse=8
;digval=0
;cycles=128
;sequences=1
;mempart=0

;MCS-Settings (Range, Preset):
;-----------------------------
range=162000 ;number of channels (total measurement time = range x dwelltime)
prena=0 ;preset enable: 0=disable, 1=enable / bit0
;rtpreset=1000 ;realtime preset in seconds
;mcsmode=1
;roimin=0
;roimax=1024
;evpreset=0
;swpreset=1
;rampmode=0
;rampstart=1024
;rampstep=1
;rampbin=1
;ramplen=1024
;qdacuse=0
;qdac=2048
;dac1use=0
;dac1val=0
;impsel=f
;thrstart=1716
;thr1=1716
;thr2=1716
;thrclk=2482

dwelltime=39999999 ;t[ns]=(N+1)x25[ns] with N = value displayed and t as the dwelltime --> N[s]=t[s]*10^9/25-1
dwellunit=3 ;0=ns, 1=usec, 2=msec, 3=sec
;Attention: changing the unit will lead to change in the value displayed under "Options/Range,Preset/DwellTime
;But has no influence on the Dwell-Time itself.

syncout=907 ;syntax:x0y with x=TTL and y=NIM, values: 0=clk, 1=gate/abort/adv, 2=trg/sample, 3=count1, 4=count2
;5=live_int, 6=live_ext, 7=1kHz, 8=sca, 9=on, 10=EoBin, 11=bin_div, 12=step_cnt, 13=go, 14=ramp_down, 15="1"
histlen=0

;Data Operations:
;----------------
autoinc=1 ;auto increment of filename, 0=disable, 1=enable
datname=Cobalt73files\Cobalt73MPA3messfile.csv
savedata=1 ;0=do nothing, 1=save at halt, 2=write listfile, 3=no histogram
fmt=4 ;format of datafile: 0=asc, 1=dat, 2=spe, 3=txt, 4=csv, 5=da2
smoothpts=5

;Calibration:
;------------
caluse=1 ;0=no calibration / 1=use formula p0+p1x / 2=use formula p0+p1x+p2x^2 / and so on...
caloff=0.000000 ;offset=p0
calfact=1.000000 ;factor=p1
calfact2=0 ;factor=p2
calfact3=0 ;factor=p3
calunit=sec
```

B.2 Main Function

```
Private Sub Timer1_Timer()
'*********************************************************************************************
'* This is the basic function of the whole program. It controls the timing and calculates most of
'* the necessary values. Its intervall is set in the function cmdCheck.
'*********************************************************************************************

    Dim response As Boolean

    If StartCheck = True Then
        '-- Get counts of the current channel from the PCI-card and display them in the output field
```

```
Call GetBlock(Counts, ChannelNo, ChannelNo + 1, 1, MCAno)

If Counts <= 1 Then
    Counts = 1
End If

lblChannelNo.Caption = ChannelNo
lblCountsDT.Caption = Counts

If StartInj = True Then 'Injection started

    VarCoeff = Sqr(Counts + BKGvalue) / Counts
    DataArray(currentMeasPoint, 12) = VarCoeff

    '-- calculate measurement time and activity concentration -----------------------------
    currentRunTime = currentMeasPoint * Dwelltime
    currentMeasValue = Counts
    currentAC = currentMeasValue / Dwelltime / (MeasVolume * Efficiency / 100)

    InjFlushClickCheck
    RefreshRunTime

    DataArray(currentMeasPoint, 0) = ChannelNo          'Channel number
    DataArray(currentMeasPoint, 1) = Counts             'Counts in this channel
    DataArray(currentMeasPoint, 2) = currentRunTime     'Runtime [s] = time elapsed since "Start/Inj"
    DataArray(currentMeasPoint, 3) = RunTime_hh         'Runtime - hour
    DataArray(currentMeasPoint, 4) = RunTime_mm         'Runtime - minute
    DataArray(currentMeasPoint, 5) = RunTime_ss         'Runtime - second

        '------------------------------------------------------------------------------------------
        '----------------------------------- DELAY TIME -------------------------------------------
        '------------------------------------------------------------------------------------------
        '-- It takes some time until the activity reaches the detector (=delay time). This depends
        '-- on several
        '-- parameters (tracer, weight of the animal, pump speed, tube length, connectors). Since
        '-- this might vary each measurement the program checks, when the activity reaches the
        '-- detector due to the increasing count rate. The point at which the count rate starts
        '-- to increase is then set to be 0 for the measurement time.
        If chkDelayTime.Value = 1 Then
            If PosSlopeCheck = False Then
                If currentMeasPoint > (NoPosSlopeValues + 5) Then
                    PosSlopeControl
                    If PosSlopeCheck = True Then
                        'calculate and display time delay =
                        'time between injection and activity reaches detector
                        DelayTime = currentRunTime - NoPosSlopeValues * Dwelltime
                        lblDelayTime.Caption = DelayTime
                        currentMeasTime = currentRunTime - DelayTime
                        CorrectDataArray
                        DisplayStartLine
                    End If
                End If
            Else 'PosSlopeCheck = True
                currentMeasTime = currentRunTime - DelayTime
                RefreshMeasTime
            End If
        Else 'chkDelayTime.Value = 0
            currentMeasTime = currentRunTime
            RefreshMeasTime
        End If
        DataArray(currentMeasPoint, 6) = currentMeasTime    'Measurement Time [s] = time since
                                                            'activity reached detector
        DataArray(currentMeasPoint, 7) = MeasTime_hh        'Measurement time - hour
        DataArray(currentMeasPoint, 8) = MeasTime_mm        'Measurement time - minute
        DataArray(currentMeasPoint, 9) = MeasTime_ss        'Measurement time - second
        lblCurrentMeasTime.Caption = currentMeasTime        'display Meas. time in output field

        DataArray(StartLinePlotPoint + NoPosSlopeValues - 1, 9) = NoPosSlopeValues
        '------------------------------------------------------------------------------------------


        '------------------------------------------------------------------------------------------
        '------------------------- BACKGROUND AND HALF-LIFE CORRECTION ------------------------
        '------------------------------------------------------------------------------------------
        '-- Subtract the (tube fix depending) background value from each measurement value and
        '-- correct this result for the half-life of the choosen isotop.
        If chkBackgroundCorr.Value = 1 Then
            BackgroundCorrection
        End If
        If chkHalfLifeCorr.Value = 1 Then
            If PosSlopeCheck = False Then
                If currentMeasPoint > (NoPosSlopeValues + 5) Then
                    PosSlopeControl
                End If
```

```
        End If
        If PosSlopeCheck = True Then
            HalfLifeCorrection
            EmissionProbCorrection
        End If
    End If
    DataArray(currentMeasPoint, 10) = currentMeasValue   'Measurement value
    DataArray(currentMeasPoint, 11) = currentAC          'Activity concentration
    lblCurrentMeasValue.Caption = CLng(currentMeasValue) 'Display measurement value in output field
    lblCurrentAC.Caption = CLng(currentAC)                        'Display activity conc. in output field
    '-----------------------------------------------------------------------------------


    '-----------------------------------------------------------------------------------
    '---------------------------- VARIABLE INTEGRATION TIME   ---------------------------
    '-----------------------------------------------------------------------------------
    '-- Since the count rate after the peak will be very low, the noise becomes a problem.
    '-- In order to smothen the data curve the integration time is increased depending
    '-- on the distribution of the values.
    If chkVarIntTime.Value = 1 Then
        If PosSlopeCheck = True Then
            If NegSlopeCheck = False Then
                If currentMeasPoint > (NoNegSlopeValues + 1) Then
                    NegSlopeControl
                End If
            End If
        End If
        If NegSlopeCheck = True Then
            VITdataCount = VITdataCount + 1
            If VITdataCount = NoLinRegValues Then
                VITcontrol
                VITdataCount = 0     '0=LinRegArray is full
            End If
        End If
    Else
        VITdataVersion = 0
        lblVITonoff.BackColor = &HFF&
        lblVITonoff.Caption = "OFF"
    End If
    '-----------------------------------------------------------------------------------


    '-----------------------------------------------------------------------------------
    '------------------------------- PLOT AND SAVE DATA   -------------------------------
    '-----------------------------------------------------------------------------------
    '-- Depending on the distribution of the count rates (=noise) either each measurement value
    '-- is plotted or the mean value of the integration time.
    Select Case VITdataVersion
        Case 0
            'No VIT at all - values are not changed
            If currentMeasValue > MaxPlotValue Then
                'New values are larger then the scale of the display --> new scale necessary
                '--> display and axis need to be refreshed.
                MaxPlotValue = currentMeasValue + 10
                RefreshCountValueAxis
                RefreshACValueAxis
                RefreshTACdisplay
            Else
                'Values are plotted as they are
                PlotTAC
            End If
        Case 1
            'Distribution of the measurement values (=noise) too large --> only mean values
            'of the integration time choosen by the function VITcontrol are plotted.
            DataArray(currentMeasPoint, 17) = 1 'signal flag in data array for active VIT

            'Only the mean values of the integration time choosen by VITcontrol are plotted and
            'stored in the data array:
            If VITdataCount = 0 Then
                If FirstVITcheck = False Then
                    DataArray(currentMeasPoint - CLng((NoLinRegValues + 0.2) / 2), 14) = AverExpFunctionValue
                    DataArray(currentMeasPoint - CLng((NoLinRegValues + 0.2) / 2), 15) = AverExpFunctionAC
                    DataArray(currentMeasPoint - CLng((NoLinRegValues + 0.2) / 2), 16) = RelError
                    PlotTAC_Mean
                End If
            End If
    End Select
    '-----------------------------------------------------------------------------------

    SaveData

    currentMeasPoint = currentMeasPoint + 1

End If   'StartInj
```

```
        ChannelNo = ChannelNo + 1

        'Stops the measurement at the number of maximum measurement points (=channels).
        If ChannelNo = MaxMeasPoint - 1 Then
            StartCheck = False
            Halt (SYSno)
            response = MsgBox("Maximum number of measurement points reached!", vbOKOnly, "Cobalt73")
        End If

    End If 'StartCheck

End Sub
```

B.3   Variable Integration Time

```
Function VITcontrol()

'********************************************************************************************
'* As the count rate becomes low due to the animals metabolism the noise causes a larger distribution
'* of the measurement values. In order to reduce this problem, the integration time is increased. The
'* factor of increasing is determined by the distribution of the measurement values. The larger this
'* distribution is, the longer the integration time will be.
'* This is done via fitting a calculated function based on the linear regression methode
'*
'* VITdataVersion = 0:  distribution of measurement values not large enough for larger integration time
'*                      Data are plotted and saved as they are collected (incl. HLC, BKG and delay but
'*                      no VIT)
'* VITdataVersion = 1:  No the measured values are plotted and saved but the average value of the calculated
'*                      exponential function.
'********************************************************************************************

    Dim Dummy1 As Double
    Dim Dummy2 As Double
    Dim I As Long
    Dim AverLogMeasValue As Double
    Dim AverLinFunctionValue As Double
    Dim AverMeasTime As Long
    Dim Variance As Double
    Dim StandardDeviation As Double
    Dim ConfidenceInterval As Long
    Dim LinFunctionValue As Double
    Dim SingleDiffSqr As Double
    Dim a As Double
    Dim b As Double
    Dim numerator As Double
    Dim denumerator As Double
    Dim MaxRelError As Double
    Dim IncrNoLinRegValues As Long
    Dim LinRegArray() As Double

    MaxRelError = 0.02        'Error of the value calculated by VIT in relation to the measurement
                             'values. Increase this value if the VITcontrol-function should react
                             'more passive, decrease it if VITcontrol-function should react more
                             'sensitive.

    ConfidenceInterval = 2   '1 = 68%, 2 = 95,4%, 3 = 99,7%

    IncrNoLinRegValues = 2   'Number of measurement points by which the VIT is increased if the
                             'relative error calculated in the function-call before is larger
                             'than the maximum error.

    FirstVITcheck = False    'Boolean for preventing the program to write data into DataArray too early

    '-------------------------------------------------------------------------------------
    '--------------------------- INCREASE INTEGRATION TIME   ----------------------------
    '-------------------------------------------------------------------------------------
    '-- Each time the relative error is larger than the maximum relative error defined above
    '-- the integration time is increased by IncrNoLinRegValues.
    If VITdataVersion = 1 Then
        If RelError > MaxRelError Then
            NoLinRegValues = NoLinRegValues + IncrNoLinRegValues
            If NoLinRegValues > MaxNoLinRegValues Then
                NoLinRegValues = MaxNoLinRegValues
            End If
        End If
    End If
    '-------------------------------------------------------------------------------------

    ReDim LinRegArray(1 To NoLinRegValues, 0 To 3)
```

```
'----------------------------------------------------------------------------------------
'------------------------ FILL ARRAY FOR LINEAR REGRESSION   ------------------------
'----------------------------------------------------------------------------------------
For I = 1 To NoLinRegValues
    LinRegArray(I, 0) = DataArray(currentMeasPoint - NoLinRegValues + I, 6)
    LinRegArray(I, 1) = DataArray(currentMeasPoint - NoLinRegValues + I, 10)
    LinRegArray(I, 2) = Log(DataArray(currentMeasPoint - NoLinRegValues + I, 10))
Next I
'----------------------------------------------------------------------------------------



'----------------------------------------------------------------------------------------
'----------------------------- CALCULATE LINEAR FIT-FUNCTION   -----------------------
'----------------------------------------------------------------------------------------
'Get average measurement time = x_bar
AverMeasTime = LinRegArray(CLng(NoLinRegValues / 2) + 1, 0)

'Calculate the mean value of the logarithmic measurement values of the last
' "NoLinRegValues"-Points = y_bar
Dummy1 = 0
For I = 1 To NoLinRegValues
    Dummy1 = Dummy1 + LinRegArray(I, 2)
Next I
AverLogMeasValue = Dummy1 / NoLinRegValues

'Calculate parameter a
Dummy1 = 0
Dummy2 = 0
For I = 1 To NoLinRegValues
    Dummy1 = Dummy1 + LinRegArray(I, 0) * LinRegArray(I, 2)
    Dummy2 = Dummy2 + (LinRegArray(I, 0) * LinRegArray(I, 0))
Next I
numerator = Dummy1 - NoLinRegValues * AverMeasTime * AverLogMeasValue
denumerator = Dummy2 - NoLinRegValues * AverMeasTime * AverMeasTime

a = numerator / denumerator

'calculate parameter b
b = AverLogMeasValue - AverMeasTime * numerator / denumerator

'Fill Function Values into LinRegArray
For I = 1 To NoLinRegValues
    LinRegArray(I, 3) = a * LinRegArray(I, 0) + b    'y=ax+b
Next I
'----------------------------------------------------------------------------------------



'----------------------------------------------------------------------------------------
'----------------------------- CALCULATE RELATIVE ERROR -----------------------------
'----------------------------------------------------------------------------------------
Dummy1 = 0
Dummy2 = 0
For I = 1 To NoLinRegValues
    Dummy1 = Dummy1 + (LinRegArray(I, 3) - LinRegArray(I, 2)) * (LinRegArray(I, 3) - LinRegArray(I, 2))
    Dummy2 = Dummy2 + LinRegArray(I, 3)
Next I
AverLinFunctionValue = Dummy2 / NoLinRegValues
Variance = Dummy1 / ((NoLinRegValues - 2) * NoLinRegValues)
StandardDeviation = Sqr(Variance)
RelError = ConfidenceInterval * StandardDeviation / AverLinFunctionValue
AverExpFunctionValue = Exp(AverLinFunctionValue)
AverExpFunctionAC = AverExpFunctionValue / Dwelltime / (MeasVolume * Efficiency / 100)
'----------------------------------------------------------------------------------------



'----------------------------------------------------------------------------------------
'------------------------------- VERSION CONTROL -----------------------------------
'----------------------------------------------------------------------------------------
'-- Choosing the version what data will be plotted and saved depending on the relative error
If VITdataVersion = 0 Then
    'If RelError > MaxRelError Then
    If RelError < VarCoeff Then
        VITdataVersion = 1
        FirstVITcheck = True
        lblVITonoff.Caption = "ON"
        lblVITonoff.BackColor = &HFF00&
        lblVIT.Caption = NoLinRegValues
    End If
Else
    lblVIT.Caption = NoLinRegValues
End If
'----------------------------------------------------------------------------------------
Erase LinRegArray
End Function
```

Appendix C

Summary of Settings, Parameters and Characteristics

C.1 Szintillation Crystal LYSO

Chemical Formula: $(Lu-Y)_2SiO_5 : Ce$
Z_{eff}: 60
Density: 7.1 g/cm^3
Light yield: 32 photons/keV
Energy resolution: 8% @ 511 keV
Wave length at emission maximum: 420 nm
1/e-decay time: 41 ns
Refractive index at emission maximum: 1.81
Attenuation length for 511 keV: 1.2 cm

Self Activity

Radioactive isotope: ^{176}Lu
Gamma lines at: 88.3, 201.8 and 306.8 keV
Maximum energy of beta emission: 593.2 keV
Half-life: $3.8 \cdot 10^{10}$
Count rate: 39 cps/g

C.2 Photo Multiplier Tube

Detailed notation: Photonis XP20D0, 8-stage, 51mm, Round tube
Window material: Borosilicate glass
Refr. Index at 420nm: 1.48
Voltage supply detector A: 1165 V
Voltage supply detector B: 985 V
Gain at 1000 V supply voltage: $2.4 \cdot 10^5$

Photocathode

Photocathode: Bi-alkali
Spectral range: 270 - 650 nm
Maximum sensitivity at: 420 nm
Quantum efficiency @ 420 nm: 25%

C.3   Detector Characteristics

Energy resolution: 23 %

Output Signal

Rise time (10/90): 6 ns
Peak voltage (into 50Ω): -50 mV
1/e decay time: 60 ns
Maximum count rate: $2.5 \cdot 10^6$ cps = 300 kBq/μl

C.4   NI-Modules Settings

CFD

Threshold: $1.0 = -180$ mV = 225 keV
LLD: $2.2 = -360$ mV = 415 kev
ULD: $4.0 = -630$ mV = 680 keV
CFD-delay: 5 ns (incl. 1 ns internal delay) = 80 cm BNC cable
Operation mode: CF
Dead time mode: N

Majority Logic

Channel 2 (A): Coinc-Level = 1 (=OR), Output-Signal: -1.6 V, 8 ns
Channel 4 (B): Coinc-Level = 1 (=OR), Output-Signal: -1.6 V, 4 ns
Channel 3 (Coinc): Coinc-Level = 2 (=AND), Output-Signal: -1.6 V, 5 ns

C.5   Instrument Characteristics

Time resolution: 550 ps
Background count rate: 1.3 cps (without interference due to animal)
Efficiency for TubeFix 3: 6.5%
Measurement volume for TubeFix 3: 33.4 μl
Time to pass measurement volume in TubeFix 3: 2.4 s
Coincidence time window: 12 ns
Coincidence delay: 2 ns

C.6   Software

Variable integration time: 4 - 20 times of the dwell time
Trigger slope at which the arrival of radioactive tracer is accepted: 0.7
Trigger slope at which the decrease of the tracer concentration is accepted: 0.8

C.7   Pump and Tubes

Catheder tubes: S-54-HL made of tygon, ID = 0.508 mm and OD = 1.524 mm
Pump withdrawal: 14 μls^{-1}
Pump tube: PharMed BPT by Saint Gobain, ID = 0.51 mm, OD = 2.33 mm
Teflon tube: ID = 0.5 mm, OD = 1.55 mm
Tube connector: hollow needle with ID = 0.5 mm, OD = 0.55 mm

List of Figures

List of Tables

Bibliography

M. Bedwell and T. Paulus. A constant fraction differential discriminator for use in fast timing coincidence systems. *IEEE Transitions on Nuclear Science*, NS-26:422 – 427, 1979.

J. Breuer, R. Grazioso, N. Zhang, M. Schmand, and K. Wienhard. Evaluation of an mr-compatible blood sampler for pet. *Physics in Medicin and Biology*, 55:5883–93, 2010.

L. Convert, G. Morin-Brassard, J. Cadorette, D. Rouleau, Croteau, M. Archambault, R. Fontaine, and R. Lecomte. A microvolumetric β blood counter for pharmacokinetic pet studies in small animals. *IEEE Transactions on Nuclear Science*, 54:173–80, 2007.

L. Currie. Limits for qualitative detection and quantitative determination. *Analytical Chemistry*, 40:586–593, 1968.

H. Derendorf, T. Gramatte, and H. Schäfer. *Pharmakokinetik.* Wissenschaftliche Verlagsgesellschaft, Stuttgart, 2 edition, 2002.

S. Eberl, A. Anayat, R. Fulton, P. Hooper, and M. Fulham. Evaluation of two population-based input functions for quantitative neurological fdg pet studies. *European Journal of Nuclear Medicine*, 24:299–304, 1997.

L. Eriksson, S. Holte, C. Bohm, M. Kesselberg, and B. Hovander. Automated blood sampling systems for positron emission tomography. *IEEE Transactions on Nuclear Science*, 35:703–707, 1988.

L. Eriksson, M. Ingvar, G. Rosenqvist, S. Stone-Elander, T. Ekdahl, and P. Kappel. Characteristics of a new automated blood sampling system for positron emission tomography. *IEEE Transactions on Nuclear Science*, 42:1007–11, 1995.

G. Ferl, X. Zhang, H. Wu, M. Kreissl, and S. Huang. Estimation of the 18f-fdg input function in mice by use of dynamic small-animal pet and minimal blood sample data. *Journal of Nuclear Medicine*, 48:2037–45, 2007.

D. Gedcke and W. McDonald. Design of the constant fraction of pulse height trigger for optimum time resolution. *Nuclear Instruments and Methods*, 58:253–260, 1968.

G. Hutchins, R. Hichwa, and R. Koeppe. A continuous flow input function detector for h2 15o blood flow studies in positron emission tomography. *IEEE Transactions on Nuclear Science*, 33:546–549, 1986.

M. Ingvar, L. Eriksson, G. Rogers, S. Stone-Elander, and L. Widen. Rapid feasibility studies of tracers for positron emission tomography: high-resolution pet in small animals with kinetic analysis. *Journal of Cerebral Blood Flow and Metabolism*, 11:926–931, 1991.

I. Kanno, H. Iida, S. Miura, M. Murakami, K. Takahashi, H. Sasaki, A. Inugami, F. Shishido, and K. Uemura. A system for cerebral blood flow measurement using an h215o autoradiographic method and positron emission tomography. *Journal of Cerebral Blood Flow and Metabolism*, 7:143–153, 1987.

J. Kim, P. Herrero, T. Sharp, R. Laforest, D. Rowland, Y. Tai, J. Lewis, and M. Welch. Minimally invasive method of determining blood input function from pet images in rodents. *Journal of Nuclear Medicine*, 47:330–336, 2006.

G. Knoll. *Radiation Detection and Measurement*. Wiley, 2010.

N. Kudomi, C. Eunjoo, S. Yamamoto, H. Watabe, K. K. Min, M. Shidahara, M. Ogawa, N. Teramoto, E. Sakamoto, and H. Iida. Development of a gso detector assembly for a continuous blood sampling system. *IEEE Transitions on Nuclear Science*, 50:70–73, 2003.

W. Leo. *Techniques for Nuclear and Particle Physics*. Springer, 1994.

J. Litton and L. Eriksson. Transcutaneous measurement of the arterial input function in positron emission tomography. *IEEE Transaction on Nuclear Science*, 37:627–628, 1990.

S. Maramraju, S. Stoll, C. Woody, D. Schlyer, W. Schiffer, D. Lee, S. Dewey, and V. P. A lso beta microprobe for measuring input functions for quantitative small animal pet. *IEEE Nuclear Science Symposium Conference Record*, 1-6:2713–2716, 2006.

M. McGuill and A. Rowan. Biological effects of blood loss: Implications for sampling volumes and techniques. *ILAR News*, 31:5–18, 1989.

C. Melcher and J. Schweitzer. Cerium-doped lutetium oxyorthosilicate: a fast, efficient new scintillator. *IEEE Transaction on Nuclear Science*, 39:502–505, 1992.

National Nuclear Data Center, 2011. URL `http://www.nndc.bnl.gov/`.

A. Ranicar, C. Williams, L. Schnorr, J. Clark, C. Rhodes, P. Bloomfield, and T. Jones. The on-line monitoring of continuously withdrawn arterial blood during pet studies using a single bgo/photomultiplier assembly and non-stick tubing. *Medical Progress Through Technology*, 17:259–264, 1991.

L. Sachs and J. Hedderich. *Angewandte Statistik*. Springer, 13 edition, 2009.

Saint-Gobain Ceramics and Plastics Inc. 104 Route de Larchant BP 521, 77754 Nemours Cedex, France. URL `http://www.detectors.saint-gobain.com/`.

J. Votaw and S. Shulman. Performance evaluation of the pico-count flow-through detector for use in cerebral blood flow pet studies. *Journal of Nuclear Medicine*, 39:509–515, 1998.

G. Walsh, R. Ferrone, M. Tsuchiya, E. Woods, and E. Deland. Hemodynamic and metabolic responses to repeated blood sampling in the rat. *The American Journal of Physiology*, 239:H805–9, 1980.

H. Watabe, Y. Ikoma, Y. Kimura, M. Naganawa, and M. Shidahara. Pet kinetic analysis - compartment model. *Annals of Nuclear Medicine*, 20: 583–588, 2006.

S. Webb, editor. *The Physics of Medical Imaging*. IOP Publishing, 1988.

B. Weber, C. Burger, P. Biro, and A. Buck. A femoral arteriovenous shunt facilitates arterial whole blood sampling in animals. *European Journal of Nuclear Medicine*, 29:319–323, 2002.

S. Yamamoto, M. Imaizumi, E. Shimosegawa, Y. Kanai, Y. Sakamoto, K. Minato, K. Shimizu, M. Senda, and J. Hatazawa. A compact and high sensitivity positron detector using dual-layer thin gso scintillators for a small animal pet blood sampling system. *Physics in Medicine and Biology*, 55: 3813–3826, 2010.

Curriculum Vitae

Personal Data

Born:	August 2, 1973 in Vienna, Austria
Nationality:	Austria

Education

1997–2007	University studies in Physics ("Technische Physik"), Vienna University of Technology
2001	ERASMUS exchange programme at the Royal Institute of Technology, Stockholm (6 months)
since 05/2008	Ph.D. Studies in Physics, Vienna University of Technology

Career History & Work Experience

10/2004–02/2005	Tutor, Institute for Physics and Material Sciences, Physics, University of Natural Resources and Life Sciences, Vienna
05/2008–12/2011	PhD-Student, System Development, Seibersdorf Labor GmbH, Seibersdorf
since 01/2012	Engineer for research and development, System Development, Seibersdorf Labor GmbH, Seibersdorf